Electric Field Driven Manipulation of Nanostructured Metal Oxide Thin Films: Applications in Chromic Devices

David Di Yao

BEng (Electronics)

2014

RMIT

Electric Field Driven Manipulation of Nanostructured Metal Oxide Thin Films: Applications in Chromic Devices

A thesis submitted in fulfilment of the requirements for the degree of

Doctor of Philosophy

David Di Yao

BEng (Electronics)

School of Electrical and Computer Engineering

RMIT University

February 2014

Declaration

I certify that except where due acknowledgement has been made, the work is that of the author alone; the work has not been submitted previously, in whole or in part, to qualify for any other academic award; the content of this thesis is the result of work which has been carried out since the official commencement date of the approved research program; any editorial work, paid or unpaid, carried out by a third party is acknowledged; and, ethics procedures and guidelines have been followed.

……

David Yao

February, 2014

Acknowledgements

There have been many people whose help has ensured the completion of this dissertation. First and foremost, I would like to thank my senior supervisor Prof. Kourosh Kalantar-zadeh for his guidance, encouragement and supervision during my PhD candidature. His persistent assistance on my experiments and research papers were of great help. Certainly, his passion for research was a great motivation for me throughout my PhD candidature. I would also like to thank my second supervisor Dr. Anthony Holland for his valuable knowledge and input on areas of micro-fabrication towards my candidature and Dr. Anthony O'Mullane for his valuable ideas and discussions on my research work.

I would also like to thank current and former researchers and students within the School of Electrical and Computer Engineering: Dr. Haidong Zheng, Dr. Jian Zhen Ou, Dr. Michael Breedon, Dr. Haneef Yacoob, Dr. Jerry Yu, Dr Sivacarendran Balendhran, Dr Sumeet Walia, Dr Adam Chrimes, Dr. Charan Shah, Dr. Ahmad Sabirin. Mrs Rozina Abdul Rani, Mr Majid Nour, Mr. Kyle Berean, Dr Jos Campbell. Mrs Rosemalini Ab Kadir, Dr. Leith Johns, Ms. Pyshar Yi, Mr. Daniel Oppedisano. Dr Blake Plowman, Ms Manika Mahajan for their assistance and for providing an excellent research environment.

My work would not have been possible without access to state-of-the-art equipment and facilities and I would like to thank the people and technical staff who work hard to keep these facilities operational. Specifically, Mr. Yuxun Cao, Mr. Paul Jones of the Microelectronics and Materials Technology Centre, RMIT University and Mr. Philip Francis and Dr. Matthew Field from the RMIT Microscopy and Microanalysis facility for their assistance and advise throughout the duration of my candidature.

My research would not have been possible without the financial support from the School of Electrical and Computer Engineering.

I am also very grateful to my parents and grandparents for their continuous support and encouragement.

Abstract

Chromism by definition is the process that induces coloration change in a material and is generally favourable for many applications when it is reversible. Many modern applications such as optical modulators, smart windows and optical displays are based on the chromic effect. This chromic effect is always aided with a compatible stimulus. In semiconductors, particularly those made of thin films, an induced coloration is often initiated by the intercalation of positive ions such as Li^+ or H^+ into the exposed active sites of the material's structure.

Nanostructure synthesis of semiconducting crystals continues to expand and evolve. Each synthesis method offers unique prospects that affect morphology, stoichiometry, crystallinity, dopant behaviour and eventually performance of the semiconducting crystals. Electric field driven methods such as anodization and electrodeposition are especially applicable since they are often carried out under ambient conditions with non-toxic electrolytes. In addition, manipulation of anodization and electrodeposition parameters is simple, depending upon facile changes of parameters such as voltage, current and electrolytes while delivering astounding results.

In this PhD thesis, the author focuses on the electric field deposited and manipulated transition metal oxides (TMOs). The target TMOs are molybdenum trioxide (MoO_3), titanium dioxide (TiO_2) and niobium pentoxide (Nb_2O_5) which have suitable band energy diagrams and crystal structure for chromic devices. The author shows that these TMOs can be synthesised into high surface area, highly crystalline and homogenous nanostructures using the two aforementioned techniques. However, these potential candidates also experience inherent limitations that restrict their chromic performances. Therefore the author of this thesis intended to seek out solutions in overcoming these limitations.

In order to achieve the goals of this PhD research program, the author comprehensively investigated chromic properties of nanostructured MoO_3, TiO_2 and Nb_2O_5 and assessed their chromic performance and potential strategies to enhance them. Based on the strategies and investigations by the author, the PhD project was conducted in four distinct stages that each resulted in novel outcomes.

In the first stage, the author demonstrated gasochromic devices based on MoO_3. MoO_3 was implemented due to its well-known chromic capabilities. The author developed a novel method to fabricate chromic devices based on selective electrodeposition of α- and β-MoO_3. The α-MoO_3 based devices exhibited significantly better optical modulation (20%) in comparison to β-MoO_3 (5%) that was associated with the layered nature of α-MoO_3. It was also revealed that porous α-MoO_3 shown higher optical modulation than compact layered α-MoO_3. However the deposited films exhibited poor adhesion to the substrates, rendering it unsuitable for electrochromic (EC) measurements.

In the second stage, the author carried out a novel combination of anodised TiO_2 ordered nanotubular template and electrodeposited α-MoO_3 chromic interface as complimentary binary EC semiconducting materials in order to overcome the chromic limitations of each of these individual TMO. The binary EC devices performed significantly better than the bare TiO_2 template in terms of change of optical modulation (ΔOD of 0.08 and 0.02 respectively). A comprehensive characterisation and theoretical analysis were carried out, and they revealed some of the benefits and merits of the developed binary EC system, including faster charge carrier transfer, better cyclic stability and high capacity of ion accommodation. As a result, the electric field driven methods together with the concept of binary chromic systems provide validation for the core concept of this thesis.

In the third stage, the author investigated Nb_2O_5, which is a TMO known for exhibiting great potential for chromic applications but is limited due to its relatively large bandgap. The author demonstrated EC devices based on ordered anodized Nb_2O_5, where a

coloration efficiency (CE) value of 47.0 cm^2 C^{-1} was calculated. The calculated CE value was the highest in comparison to all other Nb_2O_5 based EC devices at the time. The author provided theoretical and experimental insight into the enhanced EC performance in comparison to compact Nb_2O_5 and non-ordered nanostructures. It was shown that a combination of large surface to volume ratio, high order and low embedded impurities were the reason for the enhanced chromic performance. However due to the relatively large electronic bandgap, the performance of Nb_2O_5 was limited to high applied voltages and still relatively small CE in comparison to conventional EC materials.

In the final stage, to overcome the limitations Nb_2O_5, the author applied the concept of binary complimentary TMO system incorporating MoO_3 as the chromic layer while the ordered Nb_2O_5 nanostructure functions as the template. As a result, the EC performance of the binary device exceeded that of each individual incorporated TMO with a significantly high CE value of 149.0 cm^2 C^{-1}. In addition, the electronic bandgap of the binary device was reduced to closer to that of MoO_3 electronic bandgap, which allowed for operation in low applied voltages. The author provided a comprehensive characterization of the fabrication procedures and EC measurements for this binary system to associate these enhancements to the properties that were offered by each TMO.

In summary, the author believes that the outcomes of this PhD research provide an in-depth analysis of chromic devices based on TMOs including MoO_3, TiO_2, Nb_2O_5 and their selected binary systems synthesised using electric field driven techniques. The author also believes that this study has contributed significantly towards improving TMO capabilities for chromic applications.

List of figures

List of tables

Table of contents

Chapter 1

Introduction and Literature Review

1.1 Motivation

The constant pursuit for better methods and materials for creating chromic devices is one of the major fields of research of our time. Experiments carried out under investigation of materials for more efficient morphologies, crystalline phases and stoichiometries as well as optical and electronic properties are vital for future advancement in the development of higher quality chromic systems.

Nowadays, chromic systems are the core of many systems and devices such as smart windows for architectural and automotive industries, optical modulators and solar cells as well as optical devices and displays. These chromic systems can be fabricated using thin films in the thicknesses of nanometer to micrometer range and coated on surfaces of flat or irregular dimensions. The focus is on thin films with high transparency, large optical modulation, while maintaining excellent coloration efficiency. In addition, the fabrication process should pose low harm to the environment, requiring low energies to produce and at the same time is easy to control.

Many materials have shown excellent potential over the past years of intense research on chromic systems. Nanostructured transition metal oxides (TMOs) such as titanium dioxide (TiO_2), tungsten trioxide (WO_3), molybdenum trioxide (MoO_3), zinc oxide (ZnO), vanadium pentoxide (V_2O_5) and niobium pentoxide (Nb_2O_5) have received significant attention in recent years for the application of chromic devices.[1-7] Their unique features such as high optical transparency, large surface to volume ratio, large capacity for accommodating intercalating ions, and the possibility of uniform interaction across the whole volume are

largely attributed to the merits of ordered zero- one- and two-dimensional (0D, 1D and 2D) nanostructures.[8-13] Additionally, combining TMOs with complementary features have been shown to promote enhanced charge separation, surface absorption and structure stability as well as bandgap engineering.[8, 13-15] These features provide pivotal aspects chromic systems.

In this PhD research, the author has made an informed decision to focus on MoO_3 as core material of the investigation. MoO_3 is very similar to WO_3 in many semiconducting and chromic aspects. As a result, it has been shown to be widely investigated in chromic devices, electronic systems and batteries.[16-20] Similar to WO_3, MoO_3 performs remarkably for ion and electron intercalation.[4, 21-23] However, it is known that MoO_3 is not stable for any long term chromic applications. The possibility of incorporating this material into frameworks that can enhance its longevity will greatly improve the performance and stability of MoO_3 based chromic systems. An important aspect in developing chromic systems based on MoO_3 is to choose fabrication methods that are easy to control and compatible with electronic and optical industrial standards. As such, an electric field driven technique, electrochemical deposition method, will be the primary focus for the deposition of MoO_3 in this PhD research as it is one of the least energy hungry methods, which is compatible with many industrial processes and can be widely controlled.

The investigation of compatible chromic frameworks for MoO_3 is the other goal of this PhD research. The author of this thesis chose TiO_2 and Nb_2O_5 as the possible frameworks as they are capable to be used in chromic devices themselves. They are in general more durable materials than MoO_3, which also potentially increase the longevity of the developed chromic systems. As the focus of this PhD study is the implementation of electric field driven electrochemical methods, anodization is used as the primary technique for the development of highly porous and stable TiO_2 and Nb_2O_5 templates. Anodization is chosen by the author of this thesis as it has shown to produce highly ordered nanostructured films of such TMOs that exhibit strong stability and large surface to volume

ratio.[3, 24-28] The author of this thesis hypothesized that MoO_3 can be potentially electrodeposited conformally into these template nanostructures to incorporate such advantages for possible enhanced charge carrier transfer, efficient ionic intercalation, high stability and, as such, better chromic performance.

According to the aforementioned justifications and motivations, the objectives of this PhD work are planned which are presented in the following section.

1.2 Objectives

1.2.1 Investigation of Electrodeposited MoO_3 for Gasochromic Systems

Amongst TMOs, MoO_3 in various nanostructure morphologies such as wires, rods, belts, particles, flowers and tubes[29-38], has presented great potential in a wide range of applications, such as photochromic and electrochromic devices,[39-41] catalysts,[42] gas sensors,[30, 43] photovoltaic cells[40] and batteries.[22]

The two most common crystal phases of MoO_3 are the thermodynamically stable orthorhombic α-phase MoO_3 and the metastable monoclinic β-phase MoO_3.[44-45] These two phases have very different crystal structures (Figure 1.1). Transition of β-MoO_3 to α-MoO_3 has been reported as a result of thermal treatments at temperatures of 350°C and above.[45]

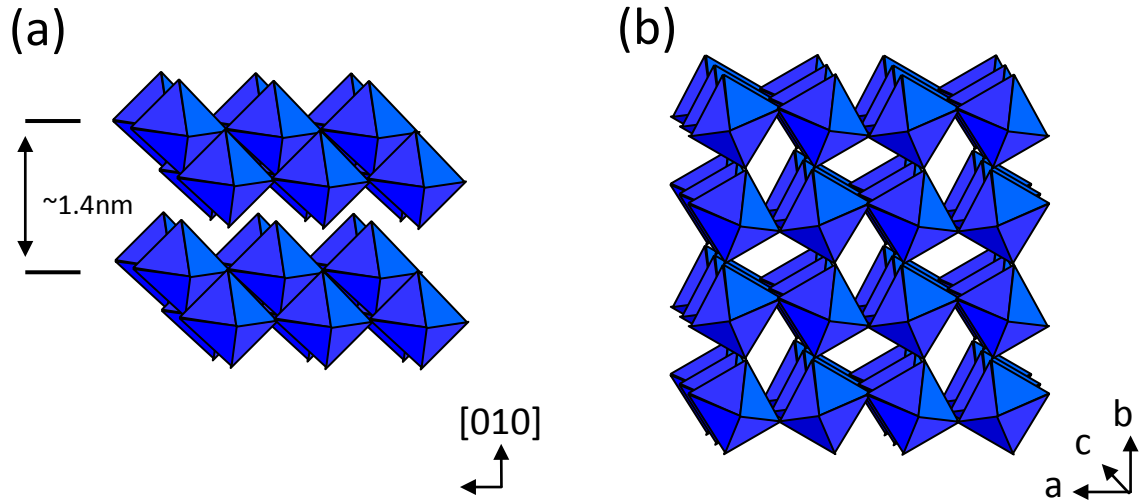

Figure 1.1 (a) Thermodynamically stable orthorhombic α-MoO_3, which are structured in compact overlapping double layers of 0.7 nm thickness and (b) metastable monoclinic β-MoO_3, which is structured in zigzagging arrays.

α-MoO_3 is of particular interest for its unique layered structure. The layers are made of atomically thin layers that have a thickness of ~0.7 nm, and exist in double-planes of link distorted MoO_6 octahedra, which then stack up to form secondary layers of several tens of nanometers.[10] In each double-layer, MoO_6 octahedra form corner sharing rows along the [100] plane and edge-sharing zigzag rows along the [001] plane (Figure 1 (a)). Lamellar formation is made by linking the adjacent layers along the [010] plane only through weak van der Waals forces[46], while the internal interactions between atoms within the double-layers are dominated by strong covalent and ionic bonding. Knowing that the lamellar formation of the secondary layers is bonded together by weak van der Waal's forces, it is possible to reduce the thickness of the layered structure through techniques such as mechanical exfoliation.[10] It has been shown that the reduction in the number of layers can increase the carrier mobility of the material, as also demonstrated for structurally similar materials such as MoS_2,[47] so it is highly probable that a similar procedure can be adopted for obtaining thin layers of MoO_3 with high carrier mobility.

The MoO_6 octahedra that form the β-MoO_3 structure do not exist in zigzag rows along the [001] plane, and do not form double-layers like α-MoO_3 (Figure 1 (b)). There are no van

der Waal forces, because adjacent MoO_6 octahedra share corners in three dimensions to produce a monoclinic structure.[44, 48] There are some suggestions that β-MoO_3 has better catalytic properties than α-MoO_3 for special applications.[49-50] However, it is possible that such observations are due to the size of the grains rather than their crystal phase, as these reports have not compared films with α- and β- MoO_3 phases of the same morphologies and grain dimensions.

Numerous synthetic techniques have been reported for the formation of MoO_3, including pulsed laser deposition[51], sol-gel[52], sputtering[53], spray pyrolysis[54], chemical vapor deposition[20], thermal evaporation[55-56], hydrothermal[57], anodization[58] and electrodeposition.[45, 59-61] Amongst these techniques, electrochemical methods are advantageous, as they are generally easy to perform and can be readily used for engineering films' physical and chemical properties.[62] They offer facile control over thickness, morphology, extent of oxidation and doping, at room temperature under ambient conditions, which makes the process versatile and compatible with electronic device industry standards.

The focus of this PhD research is only gasochromic MoO_3 as for electrochromic systems based on MoO_3, as the sole chromic component, have not shown to provide any great long term stability. MoO_3 is a widely reported chromic material and hydrogen interaction has been widely studied with respect to chromic properties of MoO_3. It has been reported that through electrochemical reactions, the injection of H^+ ions causes a transformation of the original MoO_3 crystal structure into hydrogen molybdenum bronze.[21, 63] However for the gasochromic experiments, the hydrogen molybdenum bronze is not the sole product, as part of the material appears as MoO_{3-x}, and this leads to the formation of water and oxygen vacancies. Additionally, the MoO_{3-x} exposure to air does not allow the full transformation of the crystal structure back into MoO_3.[64] Such studies are more focused on the physical vapor deposited type MoO_3 and the effect of different crystal phases in electrodeposited MoO_3 on its gasochromic properties has yet to be explored.

In this thesis, the author attempts to electrodeposit MoO_3 by carrying out potential cycling deposition. Through the tuned control of electrodeposition, the author demonstrates selective deposition of α and β phase MoO_3 onto transparent fluorine-doped tin oxide (FTO) substrates. Comprehensive characterization will be carried out to assess the morphology and crystal structure of the electrodeposited films before and after annealing. Gasochromic devices based on α and β phase MoO_3 will be fabricated to evaluate the influence that each crystalline structure will have on the gasochromic performance.

1.2.2 Investigation of Anodized TiO_2 with Electrodeposited MoO_3 Coating for Electrochromic Applications

As described in the previous sections, ordered 1D and 2D nanostructures of TMOs have received significant attention for chromic applications.[15, 65] Adding thin coatings of another TMO onto such 1D and 2D nanostructures, can potentially promote enhanced charge separation, surface absorption and structural stability as well as the possibility of tuning electronic features such as their bandgap.[12, 66] These distinctive characteristics provide opportunities in augmenting the properties of nanotechnology enabled systems incorporating binary TMOs.

TiO_2 nanotubes (TNT) are one of the most extensively studied nanostructured TMOs.[26, 67-68] It has been shown that their highly ordered structure provides many opportunities for creating electronic, mechanical and optical devices and systems with remarkable properties. The ordered structure and highly tunable electronics of TNT can also be potentially used for facilitating electrochromic activities. However its weak ion accommodation ability,[14] unfavorable band structures[69] and the newly discovered issues with charge carrier mobility[70] within the tubes lead to mediocre electrochromic responses.[69] This has thus far excluded TNT as a prominent choice for electrochromic applications. It has been reported that coating or decorating TNT with complimentary electrochromic TMOs such as WO_3 significantly improves its electrochromic properties.[2, 71]

However, comprehensive studies on MoO_3 complimentary electrochromic TMOs are rarely available.[72-74]

If α-MoO_3 is used as a coating material, its peculiar properties such as the high capacity for accepting intercalating ions due to its stratified structure as well as many free charge carrier within these planes will potentially offer opportunities for adjusting the band structure of TNT thereby enhancing ion intercalation that can improve the electrochromic properties of TNT's. Additionally, implementing electron scavenging materials with the proper electronic structures, with reference to the electronic structure of MoO_3, can improve the charge transfer and subsequently augment the electrochromic performance. So far, previous research on decorating TiO_2 with MoO_3 and developing composites of MoO_3 and TiO_2 has resulted in limited success for practical applications. This is largely due to the fact that in those reports metal or alloy sheets were used as the substrates,[73-74] which are non-transparent. As a result, the outcomes are not feasible for the fabrication of many types of optical devices or displays. Furthermore, there is a lack of fine control over synthesis and insufficient analysis of the incorporated MoO_3 that influences the system.

Various liquid and vapor synthesis techniques have been used for synthesizing MoO_3 in different morphologies.[8, 75-76] However, there is rarely any report on methods that result in a uniform and conformal coating of MoO_3 onto templating substrates. Access to such a method is critical for forming a homogenous coverage on a nanostructured substrate such as TNT. In this regard, electrochemical deposition is an attractive synthesis technique as it offers facile control over film growth, where the experimental parameters can in principle be tuned for depositing very thin layers of MoO_3. The electrodeposition of MoO_3 can be carried out under ambient conditions and relatively mild environments, making it a suitable approach to be implemented onto TNT platforms.[77]

In this PhD research, the author attempts to electrodeposit MoO_3 onto transparent conductive substrates to achieve a uniform coverage over a large area. The author hypothesises that adhesion of electrodeposited MoO_3 to conductive substrates may not be

strong enough to withstand the conditions for electrochromic measurements, posing a stability issue for possible applications in electrochromic devices. In such devices a potential is applied against a reference electrode that could result in peeling the loosely adhered MoO_3 layers, rendering it inefficient for industrial applications that require durability. Therefore the author theorize that by increasing the roughness of the substrate surface the adhesion of MoO_3 can be substantially increased, which would enhance the stability and durability of an electrochromic device. In this case TNT, with its large surface to volume ratio is a promising template.

In this thesis, the author will demonstrate the coating of TNT films with electrodeposited MoO_3 and comprehensively investigates their composition and electrochromic properties. The EC performance of the MoO_3 coated TiO_2 devices will be assessed and compared with the bare TiO_2 devices. Thorough characterization of each set of devices will be carried out to examine the TiO_2 nanostructure template as well as the strucutural impact and EC performance the MoO_3 augmentation will cause.

1.2.3 Investigation of Chromic Anodized Nb_2O_5

Within the TMO family, Nb_2O_5 is one of the emerging but less studied oxides. Nb_2O_5 has an excellent potential as an EC material. Its merits include multicolor capabilities[78] and long term cyclic stability.[79] Compact crystalline Nb_2O_5 has been reported to show a coloration efficiency (CE) of less than 10 $cm^2\ C^{-1}$ and therefore many studies have been conducted to improve the EC performance by employing nanostructured Nb_2O_5.[80] Previously investigated morphologies of Nb_2O_5 such as nano-nuggets and nano-fibers have demonstrated increased active surface areas, which have improved CE efficiency to 13 and 26 $cm^2\ C^{-1}$, respectively.[7, 81] However these nano-morphologies lack the necessary structural fundamentals such as optimum active sites and efficient electron transportation to utilize the potentials Nb_2O_5 have for the EC industry, as for practical applications higher CEs and better than reported long term stabilities are required.

Many Nb_2O_5 morphologies have been reported, which have been employed in applications including dye-sensitized solar cells (DSSC)[24, 27, 82] and vapor sensors.[83] Amongst them, ordered nano morphologies such as nano-rods,[83] nano-forest,[27] nanotubes[84] and ordered nanopores[24] structures have the potential to provide adequate active sites, large surface area and structured electron transportation for enhanced EC applications. A variety of synthesis techniques such as anodization,[24] spray pyrolysis,[7] sputtering[85] and pulse-laser deposition[86] have been reported in recent years to facilitate ordered Nb_2O_5 deposition. However, it is preferable that the synthesis technique to be carried out in ambient conditions, low cost and with minimal use of harmful substances in order to accommodate electronic and manufacturing industries standards.

To date, dense and well-ordered nanoporous Nb_2O_5 films, with a high degree of purity, which facilitate directional electron transfer, have been successfully synthesized using the anodization of niobium (Nb) thin films and foil.[24] The application of such thin films for DSSC has been demonstrated, showing their improved efficiency as a result of directional and low scattering paths for free electrons as well as increased-active surface sites for substantial enhancement in electron scavenging. As such, the author hypothesizes that such nanostructured Nb_2O_5 thin films will also be of great value for EC applications.

In this PhD research, the author will comprehensively study anodized nanoporous Nb_2O_5 films which are formed on FTO substrates. The work is conducted with the aim to demonstrate that these films can potentially show impressive EC properties due to the abovementioned hypothesis.

1.2.4 Investigation of Anodized Nb_2O_5 with Electrodeposited MoO_3 coating for Chromic Applications

Due to Nb_2O_5 innately possessing a relatively wide bandgap of ~3.8 eV,[87] EC devices operated at low applied voltages cannot be realized using this TMO. This is in contrast with TMOs such as anodized WO_3, which has been shown to have an impressive CE of

141.7 cm^2 C^{-1} obtained at a low applied potential of −0.25 V.[3] In order to lift the restrictions placed on wide bandgap TMOs as an EC material, binary devices made up of complimentary TMOs have been investigated. Methods such as coating and composites have shown great improvement upon existing mono-systems.[88-89]

In this thesis, the author attempts to combine highly ordered nanochannelled anodized Nb_2O_5 with a stratified electrodeposited α-phase MoO_3, using which the author theorizes will enhance the EC performance. Nanochanelled Nb_2O_5 will be used to provide low defect pathways for charge transfer[28] while also increasing the surface to volume ratio. Stratified α-MoO_3 will potentially enhance the intercalation capacity and help in reducing the operation voltage due to its relatively narrow bandgap. The morphology and crystalline structures of the developed materials and the EC performance of such films will be comprehensively investigated in this PhD research.

1.3 Thesis Organisation

This thesis is primarily dedicated to the investigation and development of thin film chromic devices based on TMOs using electric field driven methods using selected electrolytes. The aim is to achieve high transparency, optical modulation, coloration efficiency, device operational stability and physical stability using such electrochemically deposited or manipulated methods. The major sections of this thesis are as follows: In Chapter 2, the author will demonstrate his investigation of MoO_3 based gasochromic devices. In this chapter the author will investigate the gasochromic performance of devices fabricated from electrodeposition of MoO_3 onto FTO transparent substrates. The processes for the deposition of α and β-MoO_3 are presented. The investigation on gasochromic devices due to different morphologies and crystalline structures will be demonstrated. In Chapter 3, the author will investigate the electrochromic performance of ordered anodized TiO_2 nanotube arrays and the influence of electrodeposited MoO_3 coating over the TiO_2 template. The

characterizations and analysis of these combined systems will be shown and the EC performance of the MoO_3 coated TiO_2 devices will be presented. The author will also provide a theoretical analysis of the combined system. In Chapter 4, the author will present electrochromic devices based on ordered anodized Nb_2O_5. The investigation of these devices in terms of their transparency, optical modulation, CE and cyclic stability will be fully demonstrated. In Chapter 5, the author will demonstrate the electrochromic devices based on electrodeposited MoO_3 coated ordered nanochannelled Nb_2O_5. The author will provide characterization of the MoO_3 coated Nb_2O_5 devices and theoretical analysis of the performance augmentation of such systems. Finally, in Chapter 6, the author will present concluding remarks and suggest possible future works.

Reference

1. Wang, D.; Choi, D.; Li, J.; Yang, Z.; Nie, Z.; Kou, R.; Hu, D.; Wang, C.; Saraf, L. V.; Zhang, J.; Aksay, I. A.; Liu, J., Self-Assembled TiO_2–Graphene Hybrid Nanostructures for Enhanced Li-Ion Insertion. *ACS Nano* 2009, *3*, 907-914.

2. Song, Y. Y.; Gao, Z. D.; Wang, J. H.; Xia, X. H.; Lynch, R., Multistage Coloring Electrochromic Device Based on TiO_2 Nanotube Arrays Modified with Wo3 Nanoparticles. *Adv. Funct. Mater.* 2011, *21*, 1941-1946.

3. Ou, J. Z.; Balendhran, S.; Field, M. R.; McCulloch, D. G.; Zoolfakar, A. S.; Rani, R. A.; Zhuiykov, S.; O'Mullane, A. P.; Kalantar-zadeh, K., The Anodized Crystalline WO_3 Nanoporous Network with Enhanced Electrochromic Properties. *Nanoscale* 2012, *4*, 5980-5988.

4. Ou, J. Z.; Campbell, J. L.; Yao, D.; Wlodarski, W.; Kalantar-zadeh, K., In Situ Raman Spectroscopy of H_2 Gas Interaction with Layered MoO_3. *The Journal of Physical Chemistry C* 2011, *115*, 10757-10763.

5. Faughnan, B. W.; Crandall, R. S., Optical Properties of Mixed-Oxide WO_3/MoO_3 Electrochromic Films. *Appl. Phys. Lett.* 1977, *31*, 834-836.

6. Bueno, P. R.; Gabrielli, C.; Perrot, H., Coloring Ionic Trapping States in WO_3 and Nb_2O_5 Electrochromic Materials. *Electrochim. Acta* 2008, *53*, 5533-5539.

7. Romero, R.; Dalchiele, E. A.; Martín, F.; Leinen, D.; Ramos-Barrado, J. R., Electrochromic Behaviour of Nb_2O_5 Thin Films with Different Morphologies Obtained by Spray Pyrolysis. *Sol. Energy Mater. Sol. Cells* 2009, *93*, 222-229.

8. Balendhran, S.; Deng, J.; Ou, J. Z.; Walia, S.; Scott, J.; Tang, J.; Wang, K. L.; Field, M. R.; Russo, S.; Zhuiykov, S.; Strano, M. S.; Medhekar, N.; Sriram, S.; Bhaskaran, M.; Kalantar-zadeh, K., Enhanced Charge Carrier Mobility in Two-Dimensional High Dielectric Molybdenum Oxide *Adv. Mater.* 2013, *25*, 109-114.

9. Chu, C.-W.; Li, S.-H.; Chen, C.-W.; Shrotriya, V.; Yang, Y., High-Performance Organic Thin-Film Transistors with Metal Oxide/Metal Bilayer Electrode. *Appl. Phys. Lett.* 2005, *87*, 193508.

10. Kalantar-zadeh, K.; Tang, J. S.; Wang, M. S.; Wang, K. L.; Shailos, A.; Galatsis, K.; Kojima, R.; Strong, V.; Lech, A.; Wlodarski, W.; Kaner, R. B., Synthesis of Nanometre-Thick MoO_3 Sheets. *Nanoscale* 2010, *2*, 429-433.

11. Kim, S.-S.; Yum, J.-H.; Sung, Y.-E., Flexible Dye-Sensitized Solar Cells Using ZnO Coated TiO_2 Nanoparticles. *Journal of Photochemistry and Photobiology A: Chemistry* 2005, *171*, 269-273.

12. Miyauchi, M.; Nakajima, A.; Watanabe, T.; Hashimoto, K., Photoinduced Hydrophilic Conversion of TiO_2/WO_3 Layered Thin Films. *Chem. Mater.* 2002, *14*, 4714-4720.

13. Zhou, L.; Wu, H. B.; Wang, Z.; Lou, X. W., Interconnected MoO_2 Nanocrystals with Carbon Nanocoating as High-Capacity Anode Materials for Lithium-ion Batteries. *ACS Appl. Mater. Interfaces* 2011, *3*, 4853-4857.

14. Shin, J.-Y.; Joo, J. H.; Samuelis, D.; Maier, J., Oxygen-Deficient $TiO_{2-\Delta}$ Nanoparticles Via Hydrogen Reduction for High Rate Capability Lithium Batteries. *Chem. Mater.* 2011, *24*, 543-551.

15. Ramasubramaniam, A.; Naveh, D.; Towe, E., Tunable Band Gaps in Bilayer Transition-Metal Dichalcogenides. *Phys. Rev. B* 2011, *84*, 205325.

16. Wang, Z.; Madhavi, S.; Lou, X. W., Ultralong A-MoO_3 Nanobelts: Synthesis and Effect of Binder Choice on Their Lithium Storage Properties. *The Journal of Physical Chemistry C* 2012, *116*, 12508-12513.

17. Mariotti, D.; Lindstrom, H.; Bose, A. C.; Ostrikov, K., Monoclinic Beta-MoO_3 Nanosheets Produced by Atmospheric Microplasma: Application to Lithium-Ion Batteries. *Nanotechnology* 2008, *19*. 495302.

18. Chen, J. S.; Cheah, Y. L.; Madhavi, S.; Lou, X. W., Fast Synthesis of A-MoO_3 Nanorods with Controlled Aspect Ratios and Their Enhanced Lithium Storage Capabilities. *The Journal of Physical Chemistry C* 2010, *114*, 8675-8678.

19. Zhao, Y.; Liu, J. G.; Zhou, Y.; Zhang, Z. J.; Xu, Y. H.; Naramoto, H.; Yamamoto, S., Preparation of MoO_3 Nanostructures and Their Optical Properties. *Journal of Physics-Condensed Matter* 2003, *15*, L547-L552.

20. Young Jung, L.; William, T. N.; Dae-Gun, K.; Young Do, K., Chemical Vapour Transport Synthesis and Optical Characterization of MoO_3 Thin Films. *J. Phys. D: Appl. Phys.* 2009, *42*, 115419.

21. Yang, Y. A.; Cao, Y. W.; Loo, B. H.; Yao, J. N., Microstructures of Electrochromic MoO_3 Thin Films Colored by Injection of Different Cations. *J. Phys. Chem. B* 1998, *102*, 9392-9396.

22. Riley, L. A.; Lee, S.-H.; Gedvilias, L.; Dillon, A. C., Optimization of MoO_3 Nanoparticles as Negative-Electrode Material in High-Energy Lithium Ion Batteries. *J. Power Sources* 2010, *195*, 588-592.

23. Ramana, C. V.; Atuchin, V. V.; Groult, H.; Julien, C. M., Electrochemical Properties of Sputter-Deposited MoO_3 Films in Lithium Microbatteries. *Journal of Vacuum Science & Technology A: Vacuum, Surfaces, and Films* 2012, *30*, 04D105.

24. Ou, J. Z.; Rani, R. A.; Ham, M. H.; Field, M. R.; Zhang, Y.; Zheng, H.; Reece, P.; Zhuiykov, S.; Sriram, S.; Bhaskaran, M.; Kanee, R. B.; Kalantar-Zadeh, K., Elevated Temperature Anodized Nb_2O_5: A Photoanode Material with Exceptionally Large Photoconversion Efficiencies. *ACS Nano* 2012, *6*, 4045-4053.

25. Zheng, H. D.; Sadek, A. Z.; Breedon, M.; Yao, D.; Latham, K.; du Plessis, J.; Kalantar-Zadeh, K., Fast Formation of Thick and Transparent Titania Nanotubular Films from Sputtered Ti. *Electrochem. Commun.* 2009, *11*, 1308-1311.

26. Chanmanee, W.; Watcharenwong, A.; Chenthamarakshan, C. R.; Kajitvichyanukul, P.; de Tacconi, N. R.; Rajeshwar, K., Formation and Characterization of Self-Organized TiO_2 Nanotube Arrays by Pulse Anodization. *J. Am. Chem. Soc.* 2008, *130*, 965-974.

27. Jeong, B.-Y.; Jung, E., Micro-Mountain and Nano-Forest Pancake Structure of Nb_2o_5 with Surface Nanowires for Dye-Sensitized Solar Cells. *Met. Mater.-Int.* 2013, *19*, 617-622.

28. Rani, R. A.; Zoolfakar, A. S.; Ou, J. Z.; Ab. Kadir, R.; Nili, H.; Latham, K.; Sriram, S.; Bhaskaran, M.; Zhuiykov, S.; Kaner, R. B.; Kalantar-zadeh, K., Reduced Impurity-Driven Defect States in Anodized Nanoporous Nb_2O_5: The Possibility of Improving Performance of Photoanodes. *Chem. Commun.* 2013, *49*, 6349-6351.

29. Chandrappa, G. T.; Livage, J., Synthesis and Characterization of Mo-Oxide Nanoribbons. *Synthesis and Reactivity in Inorganic Metal-Organic and Nano-Metal Chemistry* 2006, *36*, 23-28.

30. Comini, E.; Yubao, L.; Brando, Y.; Sberveglieri, G., Gas Sensing Properties of MoO_3 Nanorods to Co and CH_3OH. *Chem. Phys. Lett.* 2005, *407*, 368-371.

31. Ding, Q. P.; Huang, H. B.; Duan, J. H.; Gong, J. F.; Yang, S. G.; Zhao, X. N.; Du, Y. W., Molybdenum Trioxide Nanostructures Prepared by Thermal Oxidization of Molybdenum. *J. Cryst. Growth* 2006, *294*, 304-308.

32. Wei, G.; Qin, W.; Zhang, D.; Wang, G.; Kim, R.; Zheng, K.; Wang, L., Synthesis and Field Emission of MoO_3 Nanoflowers by a Microwave Hydrothermal Route. *J. Alloys Compd.* 2009, *481*, 417-421.

33. Lou, X. W.; Zeng, H. C., Hydrothermal Synthesis of Alpha-MoO_3 Nanorods Via Acidification of Ammonium Heptamolybdate Tetrahydrate. *Chem. Mater.* 2002, *14*, 4781-4789.

34. Lou, X. W.; Zeng, H. C., Complex Alpha-MoO_3 Nanostructures with External Bonding Capacity for Self-Assembly. *J. Am. Chem. Soc.* 2003, *125*, 2697-2704.

35. Niederberger, M.; Krumeich, F.; Muhr, H.-J.; Muller, M.; Nesper, R., Synthesis and Characterization of Novel Nanoscopic Molybdenum Oxide Fibers. *J. Mater. Chem.* 2001, *11*, 1941-1945.

36. Patzke, G. R.; Michailovski, A.; Krumeich, F.; Nesper, R.; Grunwaldt, J.-D.; Baiker, A., One-Step Synthesis of Submicrometer Fibers of MoO_3. *Chem. Mater.* 2004, *16*, 1126-1134.

37. Chen, J. S.; Cheah, Y. L.; Madhavi, S.; Lou, X. W., Fast Synthesis of α-MoO_3 Nanorods with Controlled Aspect Ratios and Their Enhanced Lithium Storage Capabilities. *J. Phys. Chem. C* 2010, *114*, 8675-8678.

38. Zhou, L.; Yang, L.; Yuan, P.; Zou, J.; Wu, Y.; Yu, C., A-MoO_3 Nanobelts: A High Performance Cathode Material for Lithium Ion Batteries. *J. Phys. Chem. C* 2010, *114*, 21868-21872.

39. Chernova, N. A.; Roppolo, M.; Dillon, A. C.; Whittingham, M. S., Layered Vanadium and Molybdenum Oxides: Batteries and Electrochromics. *J. Mater. Chem.* 2009, *19*, 2526-2552.

40. Gesheva, K.; Szekeres, A.; Ivanova, T., Optical Properties of Chemical Vapor Deposited Thin Films of Molybdenum and Tungsten Based Metal Oxides. *Sol. Energy Mater. Sol. Cells* 2003, *76*, 563-576.

41. Yao, J. N.; Hashimoto, K.; Fujishima, A., Photochromism Induced in an Electrolytically Pretreated MoO_3 Thin Film by Visible Light. *Nature* 1992, *355*, 624-626.

42. Ohler, N.; Bell, A. T., Selective Oxidation of Methane over MoO_x/SiO_2: Isolation of the Kinetics of Reactions Occurring in the Gas Phase and on the Surfaces of SiO_2 and MoO_x. *J. Catal.* 2005, *231*, 115-130.

43. Rahmani, M. B.; Keshmiri, S. H.; Yu, J.; Sadek, A. Z.; Al-Mashat, L.; Moafi, A.; Latham, K.; Li, Y. X.; Wlodarski, W.; Kalantar-zadeh, K., Gas Sensing Properties of Thermally Evaporated Lamellar MoO_3. *Sensor Actuat B-Chem* 2010, *145*, 13-19.

44. Carcia, P. F.; McCarron Iii, E. M., Synthesis and Properties of Thin Film Polymorphs of Molybdenum Trioxide. *Thin Solid Films* 1987, *155*, 53-63.

45. McEvoy, T. M.; Stevenson, K. J.; Hupp, J. T.; Dang, X., Electrochemical Preparation of Molybdenum Trioxide Thin Films: Effect of Sintering on Electrochromic and Electroinsertion Properties. *Langmuir* 2003, *19*, 4316-4326.

46. Sunu, S. S.; Prabhu, E.; Jayaraman, V.; Gnanasekar, K. I.; Gnanasekaran, T., Gas Sensing Properties of Pld Made MoO_3 Films. *Sensor Actuat B-Chem* 2003, *94*, 189-196.

47. Radisavljevic, B.; Radenovic, A.; Brivio, J.; Giacometti, V.; Kis, A., Single-Layer Mos(2) Transistors. *Nat. Nanotechnol.* 2011, *6*, 147-150.

48. Chang, W. C.; Qi, X. D.; Kuo, J. C.; Lee, S. C.; Ng, S. K.; Chen, D., Post-Deposition Annealing Control of Phase and Texture for the Sputtered $MoO_{(3)}$ Films. *Crystengcomm* 2011, *13*, 5125-5132.

49. Tanisaki, S., Crystal Structure of Monoclinic Tungsten Trioxide at Room Temperature. *J. Phys. Soc. Jpn.* 1960, *15*, 573-581.

50. Machiels, C. J.; Cheng, W. H.; Chowdhry, U.; Farneth, W. E.; Hong, F.; McCarron, E. M.; Sleight, A. W., The Effect of the Structure of Molybdenum Oxides on the Selective Oxidation of Methanol. *Appl. Catal.* 1986, *25*, 249-256.

51. Bhosle, V.; Tiwari, A.; Narayan, J., Epitaxial Growth and Properties of $MoO_{X\ (2 < X < 2.75)}$ Films. *J. Appl. Phys.* 2005, *97*, 083539.

52. Prasad, A. K.; Kubinski, D. J.; Gouma, P. I., Comparison of Sol-Gel and Ion Beam Deposited MoO_3 Thin Film Gas Sensors for Selective Ammonia Detection. *Sensor Actuat B-Chem* 2003, *93*, 25-30.

53. Navas, I.; Vinodkumar, R.; Lethy, K. J.; Detty, A. P.; Ganesan, V.; Sathe, V.; Pillai, V. P. M., Growth and Characterization of Molybdenum Oxide Nanorods by RF Magnetron Sputtering and Subsequent Annealing. *J. Phys. D: Appl. Phys.* 2009, *42*, 175305.

54. Bouzidi, A.; Benramdane, N.; Tabet-Derraz, H.; Mathieu, C.; Khelifa, B.; Desfeux, R., Effect of Substrate Temperature on the Structural and Optical Properties of MoO_3 Thin Films Prepared by Spray Pyrolysis Technique. *Mater. Sci. Eng., B* 2003, *97*, 5-8.

55. Siciliano, T.; Tepore, A.; Filippo, E.; Micocci, G.; Tepore, M., Characteristics of Molybdenum Trioxide Nanobelts Prepared by Thermal Evaporation Technique. *Mater. Chem. Phys.* 2009, *114*, 687-691.

56. Xie, Y. L.; Cheong, F. C.; Zhu, Y. W.; Varghese, B.; Tamang, R.; Bettiol, A. A.; Sow, C. H., Rainbow-Like MoO_3 Nanobelts Fashioned Via Afm Micromachining. *J. Phys. Chem. C* 2009, *114*, 120-124.

57. Wang, S.; Zhang, Y.; Ma, X.; Wang, W.; Li, X.; Zhang, Z.; Qian, Y., Hydrothermal Route to Single Crystalline [Alpha]-MoO_3 Nanobelts and Hierarchical Structures. *Solid State Commun.* 2005, *136*, 283-287.

58. Padmanab.Kr, Preparation of MoO_3 Films by Anodization. *Rev. Sci. Instrum.* 1974, *45*, 593-593.

59. Gacitua, M.; Boutaleb, Y.; Cattin, L.; Abe, S. Y.; Lare, Y.; Soto, G.; Louarn, G.; Morsli, M.; Rehamnia, R.; del Valle, M. A.; Drici, A.; Bernède, J. C., Electrochemical

Preparation of MoO_3 Buffer Layer Deposited onto the Anode in Organic Solar Cells. *physica status solidi (a)* 2010, *207*, 1905-1911.

60. Guerfi, A.; Paynter, R. W.; Dao, L. H., Characterization and Stability of Electrochromic MoO_3 Thin Films Prepared by Electrodeposition. *Journal of The Electrochemical Society* 1995, *142*, 3457-3464.

61. McEvoy, T. M.; Stevenson, K. J., Electrochemical Quartz Crystal Microbalance Study of the Electrodeposition Mechanism of Molybdenum Oxide Thin Films from Peroxo-Polymolybdate Solution. *Anal. Chim. Acta* 2003, *496*, 39-51.

62. Plowman, B. J.; Bhargava, S. K.; O'Mullane, A. P., Electrochemical Fabrication of Metallic Nanostructured Electrodes for Electroanalytical Applications. *Analyst* 2011, *136*, 5107-5119.

63. Hirata, T.; Ishioka, K.; Kitajima, M., Raman Spectra of MoO_3 Implanted with Protons. *Appl. Phys. Lett.* 1996, *68*, 458-460.

64. Ou, J. Z.; Campbell, J. L.; Yao, D.; Wlodarski, W.; Kalantar-zadeh, K., In Situ Raman Spectroscopy of H2 Gas Interaction with Layered MoO_3. *J. Phys. Chem. C* 2011, *115*, 10757-10763.

65. Kumar, A.; Ahluwalia, P. K., Electronic Structure of Transition Metal Dichalcogenides Monolayers 1H-Mx2 (M = Mo, W; X = S, Se, Te) from Ab-Initio Theory: New Direct Band Gap Semiconductors. *Eur. Phys. J. B* 2012, *85*, 1-7.

66. Tae Kwon, Y.; Yong Song, K.; In Lee, W.; Jin Choi, G.; Rag Do, Y., Photocatalytic Behavior of WO_3-Loaded TiO_2 in an Oxidation Reaction. *J. Catal.* 2000, *191*, 192-199.

67. Kawahara, T.; Konishi, Y.; Tada, H.; Tohge, N.; Ito, S., Patterned TiO_2/SnO_2 Bilayer Type Photocatalyst. 2. Efficient Dehydrogenation of Methanol. *Langmuir* 2001, *17*, 7442-7445.

68. Watcharenwong, A.; Chanmanee, W.; de Tacconi, N. R.; Chenthamarakshan, C. R.; Kajitvichyanukul, P.; Rajeshwar, K., Self-Organized TiO_2 Nanotube Arrays by Anodization of Ti Substrate: Effect of Anodization Time, Voltage and Medium Composition

on Oxide Morphology and Photoelectrochemical Response. *J. Mater. Res.* 2007, *22*, 3186-3195.

69. Baker, A. T.; Bosi, S. G.; Bell, J. M.; MacFarlane, D. R.; Monsma, B. G.; Skryabin, I.; Wang, J., Degradation Mechanisms in Electrochromic Devices Based on Sol-Gel Deposited Thin Films. *Sol. Energy Mater. Sol. Cells* 1995, *39*, 133-143.

70. Richter, C.; Schmuttenmaer, C. A., Exciton-Like Trap States Limit Electron Mobility in TiO_2 Nanotubes. *Nat. Nanotechnol.* 2010, *5*, 769-772.

71. Zheng, H. D.; Ou, J. Z.; Strano, M. S.; Kaner, R. B.; Mitchell, A.; Kalantar-Zadeh, K., Nanostructured Tungsten Oxide - Properties, Synthesis, and Applications. *Adv. Funct. Mater.* 2011, *21*, 2175-2196.

72. Natori, H.; Kobayashi, K.; Takahashi, M., Fabrication and Photocatalytic Activity of TiO_2/MoO_3 Particulate Films. *Journal of Oleo Science* 2009, *58*, 203-211.

73. Shrestha, N. K.; Nah, Y.-C.; Tsuchiya, H.; Schmuki, P., Self-Organized Nano-Tubes of TiO_2-MoO_3 with Enhanced Electrochromic Properties. *Chem. Commun.* 2009, *0*, 2008-2010.

74. Lorenz, K.; Bauer, S.; Gutbrod, K.; Guggenbichler, J.; Schmuki, P.; Zollfrank, C., Anodic TiO_2 Nanotube Layers Electrochemically Filled with MoO_3 and Their Antimicrobial Properties. *Biointerphases* 2011, *6*, 16-21.

75. Song, L. X.; Wang, M.; Pan, S. Z.; Yang, J.; Chen, J.; Yang, J., Molybdenum Oxide Nanoparticles: Preparation, Characterization, and Application in Heterogeneous Catalysis. *J. Mater. Chem.* 2011, *21*, 7982-7989.

76. Ramana, C. V.; Atuchin, V. V.; Kesler, V. G.; Kochubey, V. A.; Pokrovsky, L. D.; Shutthanandan, V.; Becker, U.; Ewing, R. C., Growth and Surface Characterization of Sputter-Deposited Molybdenum Oxide Thin Films. *Appl. Surf. Sci.* 2007, *253*, 5368-5374.

77. Yao, D. D.; Ou, J. Z.; Latham, K.; Zhuiykov, S.; O'Mullane, A. P.; Kalantar-zadeh, K., Electrodeposited α- and β-Phase MoO_3 Films and Investigation of Their Gasochromic Properties. *Cryst. Growth Des.* 2012, *12*, 1865-1870.

78. Heusing, S.; Sun, D. L.; Otero-Anaya, J.; Aegerter, M. A., Grey, Brown and Blue Coloring Sol–Gel Electrochromic Devices. *Thin Solid Films* 2006, *502*, 240-245.

79. Avellaneda, C. O.; Pawlicka, A.; Aegerter, M. A., Two Methods of Obtaining Sol–Gel Nb_2O_5 Thin Films for Electrochromic Devices. *J. Mater. Sci.* 1998, *33*, 2181-2185.

80. Maruyama, T.; Arai, S., Electrochromic Properties of Niobium Oxide Thin-Films Prepared by Radiofrequency Magnetron Sputtering Method. *Appl. Phys. Lett.* 1993, *63*, 869-870.

81. Mujawar, S. H.; Inamdar, A. I.; Betty, C. A.; Ganesan, V.; Patil, P. S., Effect of Post Annealing Treatment on Electrochromic Properties of Spray Deposited Niobium Oxide Thin Films. *Electrochim. Acta* 2007, *52*, 4899-4906.

82. Le Viet, A.; Jose, R.; Reddy, M. V.; Chowdari, B. V. R.; Ramakrishna, S., Nb_2O_5 Photoelectrodes for Dye-Sensitized Solar Cells: Choice of the Polymorph. *J. Phys. Chem. C* 2010, *114*, 21795-21800.

83. Fiz, R.; Hernandez-Ramirez, F.; Fischer, T.; Lopez-Conesa, L.; Estrade, S.; Peiro, F.; Mathur, S., Synthesis, Characterization, and Humidity Detection Properties of Nb_2O_5 Nanorods and Sno_2/Nb_2o_5 Heterostructures. *J. Phys. Chem. C* 2013, *117*, 10086-10094.

84. Yan, C.; Xue, D., Formation of Nb_2O_5 Nanotube Arrays through Phase Transformation**. *Adv. Mater.* 2008, *20*, 1055-1058.

85. Huang Yin-Song, Z. Y.-Z., Hu Xing-Fang, Electrochromic Properties of Niobium Oxide Thin Films Fabricated by RF Sputtering. *J. Inorg. Mater.* 2002, *17*, 632-636.

86. Fu, Z. W.; Kong, J. J.; Qin, Q. Z., Electrochemical and Electrochromic Properties of Niobium Oxide Thin Films Fabricated by Pulsed Laser Deposition. *J. Electrochem. Soc.* 1999, *146*, 3914-3918.

87. Liu, J.; Xue, D. F.; Li, K. Y., Single-Crystalline Nanoporous Nb_2O_5 Nanotubes. *Nanoscale Research Letters* 2011, *6*. 138.

88. Kim, S. S.; Yum, J. H.; Sung, Y. E., Improved Performance of a Dye-Sensitized Solar Cell Using a TiO_2/ZnO/Eosin Y Electrode. *Sol. Energy Mater. Sol. Cells* 2003, *79*, 495-505.

89. Yao, D. D.; Field, M. R.; O'Mullane, A. P.; Kalantar-zadeh, K.; Ou, J. Z., Electrochromic Properties of TiO_2 Nanotubes Coated with Electrodeposited Moo_3. *Nanoscale* 2013, *5*, 10353-10359.

Chapter 2

Electrodeposited α- and β-phase MoO_3 Films and Investigation of Their Gasochromic Properties

2.1 Introduction

In chapter 1, it was emphasized that the author has chosen to focus on chromic materials that held potentials to exceed current performance limits. This was carried out by searching and analysing the state-of-the-art materials presented in literature on transition metal oxides (TMOs),[48, 71, 90-91] which have excellent capacities for intercalation of ions and electrons for applications including chromic systems, catalysts,[42] sensors[43] and batteries.[22] In order to identify the capability of TMOs as chromic materials, the author reviewed the crystalline structures, morphologies and electronic properties of many TMOs.[29-31, 33-36, 38, 92] Base on the analysis carried out, the author of this thesis identified MoO_3 as one of the candidates due to its suitable electronic structure for chromic applications, suitable band energy diagram, high capacity to accommodate intercalation ions and versatile synthesis methods.[10, 21, 44-45, 49-59, 61-63, 93-94]

In this chapter, the author will present his work on the development of gasochromic devices based on electrochemical synthesis of α- and β-MoO_3. As preferential synthesis of different phases of MoO_3 is rarely reported, the author used this opportunity to investigate and demonstrate a facile electrodeposition method with the intent to selectively produce and tune different phases of MoO_3 onto transparent fluorine-doped tin oxide (FTO) substrates. The electrodeposition technique was chosen in line with the core concept of this thesis that emphasizes on the electric field driven methods for the formation and engineering of the chromic thin films.

In this chapter, the author presents the outcomes of the study on electrodeposited α- and β-phase MoO_3 films. A comprehensive characterization of the electrodeposited MoO_3 will be presented. The influence of the electrodeposition parameters on the crystal phase of MoO_3 films will be described. Eventually, the crystal phase and morphology of the synthesised MoO_3 films will be compared and evaluated for gasochromic performances. The work in this chapter was published as a full article in the journal Crystal Growth and Design.[77]

2.2 Experimental

2.2.1 Solution Preparation

Aqueous solutions of sodium molybdate (Thermo Fisher Scientific Australia) over a concentration range of 0.01 to 0.20 M were prepared with deionized water (resistivity of 18.2 MΩ cm) purified by use of a Milli-Q filtering system (Millipore). H_2SO_4 (95 – 98% analytical grade, Ajax Finechem) was added to each solution to adjust the pH levels to 1, 2, 4 and 6. The pH was measured using a pH meter from Hanna Instruments (pH211).

2.2.2 Electrodeposition

Electrodeposition experiments were carried out at room temperature (22 ± 2 °C) with a CH Instruments, Model CHI413A potentiostat using a 3 electrode configuration and employing a fluorine doped tin-oxide (FTO) glass substrate (0.2 cm^2 exposed area) working electrode, a graphite rod (6 mm diameter, Johnson Matthey Ultra “F” purity grade) counter electrode and a Ag/AgCl (3 M KCl) reference electrode. The electrodeposition protocol involved cycling the potential from defined upper limits to a negative potential value of −1.2 V at different sweep rates ranging from 3 to 10 mV s^{-1} for 1 to 50 cycles. After electrodeposition the samples were washed with Milli-Q water and dried in a stream of

high purity N_2 gas. Selected samples were further annealed in a standard horizontal furnace at a temperature of 300°C for 120 minutes in ambient air, with a heating and cooling ramp rate of 1 °C min^{-1}.

2.2.3 Characterization

The crystal phases were compared and characterized using X-ray diffraction (XRD) obtained with a Bruker AX 8: Discover with General Area Detector Diffraction System (GADDS). Raman spectra were recorded with a system incorporating an Ocean Optics QE 6500 spectrometer, and a 532 nm 40 mW laser as the excitation source. The surface morphologies were observed using scanning electron microscopy (SEM) and performed on a FEI Nova Nano instrument.

2.2.4 Gasochromic Measurements

Following characterization, selected annealed samples were covered with approximately 25 Å of palladium using DC sputtering. The in-situ gasochromic measurements were performed with the system attached to a computer controlled mass flow controller regulating the flow rate at 200 sccm into a customized gas testing chamber. The samples were mounted inside the chamber and initially flushed with synthetic air for 30 min to remove excess moisture and contaminants. N_2 diluted hydrogen gas (3% H_2 + 97% N_2) was introduced into the chamber for 5 mins to initiate the coloring process.

The expressions: “Air_1” and “H2_1” in this chapter corresponds to the samples exposed to “first time zero air exposure for 30 min” and “first time H_2 exposure for 5 min”.

2.3 Results and Discussion

In general, the pH of the electrolyte solution plays an important role in the electrodeposition of metal oxides.[95-96] This is demonstrated in Figure 2.1 which shows the

cyclic voltammetric behavior of a FTO electrode in an aqueous 0.01 M solution of Na_2MoO_4 at pH values of 6, 4, 2 and 1, respectively. This was achieved by adding H_2SO_4 to the unadjusted Na_2MoO_4 solution (pH = 6.9). It is clear from the CV data that very low currents are passed at pH 6, which increase in magnitude over the entire potential range as the pH is lowered to 1. Over a pH range of 2 to 6 a plateau region is observed from 0.0 to –0.4 V in all cases, which is followed by a well defined cathodic peak that is shifted to more positive potentials at a pH value of 2. At pH = 1 a well defined peak is not observed on the negative sweep. This is consistent with previous observations reported by Gómez[97] who also suggested that the anodic peaks that are observed on the reverse sweep are due to the oxidation of hydrogen formed during the reduction process, which is facilitated at the lower pH values. A recent study has demonstrated that MoO_3 is quite an active material for the hydrogen evolution reaction.[98]

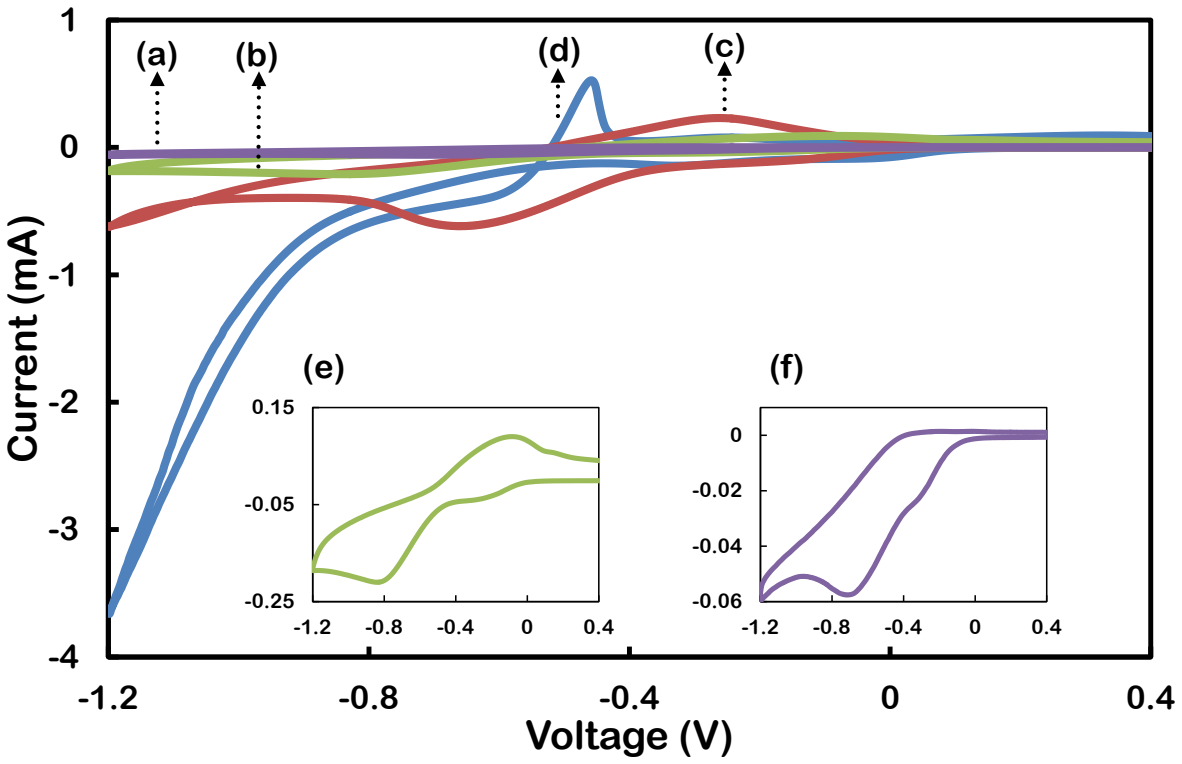

Figure 2.1 Cyclic voltammograms recorded at a FTO electrode in 0.01 M Na_2MoO_4 at a sweep rate of 0.2 V s^{-1} at a pH of (a) 6, (b) 4, (c) 2 and (d) 1. The inset figures represents a magnified view of the data at a pH of (e) 4 and (f) 6.

Under the above conditions no significant deposition of material was observed after one cycle. In order to obtain thicker films suitable for characterization, a repetitive potential cycling protocol over a potential range of 0.4 to -1.2 V at a sweep rate of 0.2 V s^{-1} was used. A blue film was formed on the FTO during the initial cycles (1 to 5) at all four pH levels; where a gradual increase in the color intensity of the film was observed when the pH was lowered from 6 to 1. With an increase in the number of cycles the films became thicker; however, dissolution occurred and the electrolyte solution gradually turned blue. The thickest films were formed at a pH of 4, as expected from the larger currents passed during the deposition process as seen in Figure 2.1 and this pH was employed for the rest of the chapter. However, it was noted that films suitable for micro-characterization required increasing the concentration of Na_2MoO_4 to 0.2 M while limiting the deposition process to one cycle to minimize dissolution of the film into solution.

The effect of sweep rate on the electrodeposition process was then investigated to study whether the rate of formation would significantly affect the film properties. Illustrated in Figure 2.2 shows CVs recorded at a FTO electrode in 0.2 M Na_2MoO_4 adjusted to a pH of 4 at a sweep rate of 3 mV s^{-1} (curve (a)), 5 mV s^{-1} (curve (b)), and 10 mV s^{-1} (curve (c)). It can be seen that the magnitude of the current does not increase from 3 to 5 mV s^{-1}, and that the increase observed at a sweep rate of 10 mV s^{-1}, is not consistent with a diffusion limited process which should show an increase consistent with the square root of the sweep rate.

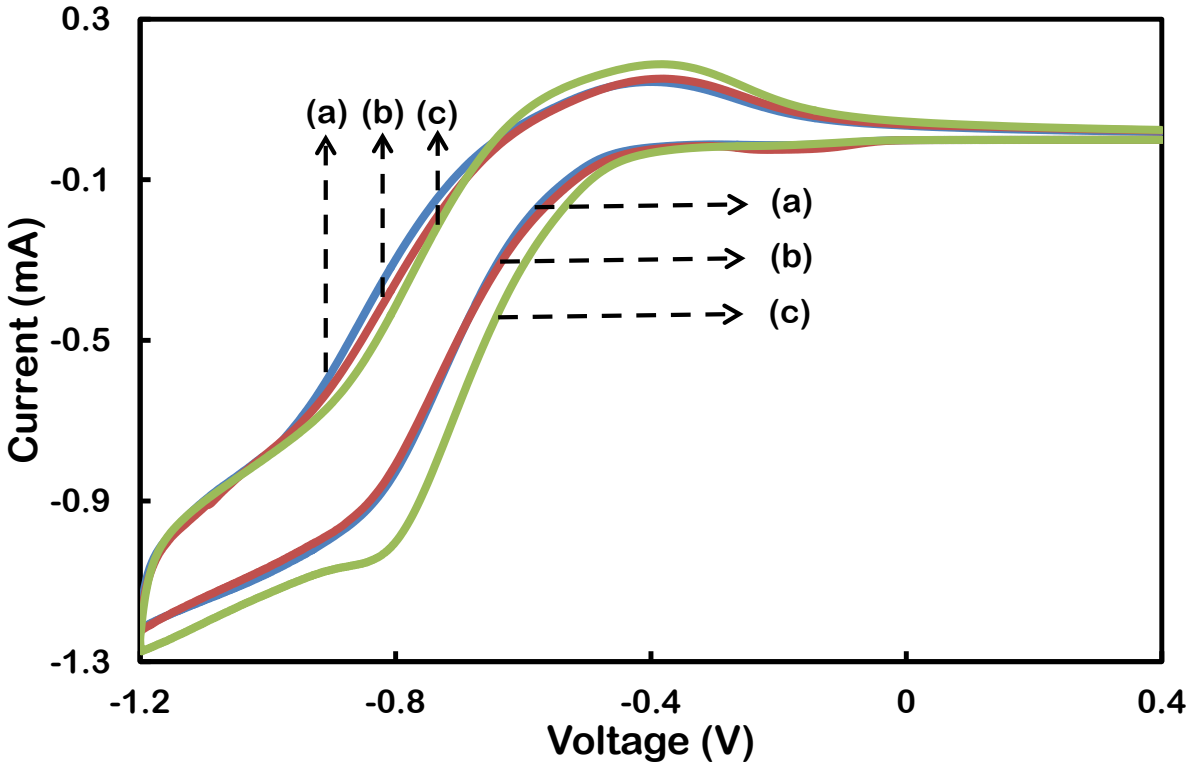

Figure 2.2 Cyclic voltammograms recorded at a FTO electrode in 0.2 M Na_2MoO_4, at a pH of 4, obtained at a sweep rate of (a) 3, (b) 5 and (c) 10 mV s^{-1}.

The author found that the sweep rate had a significant effect on the phase and crystallinity of the films, which was confirmed to be MoO_3 by Raman spectroscopy. Figure 2.3 (a) shows Raman scattering spectra showing the transition between α-MoO_3 and β-MoO_3 of the as deposited samples after one potential cycle. At a sweep rate of 5 mV s^{-1} (plot (ii)) films were produced that exhibited the properties of the thermodynamically stable, orthorhombic α-MoO_3 which is verified by observation of a peak at 821 cm^{-1} assigned to the double coordinated oxygen (Mo—O—Mo) stretching mode.[99] This mode results from corner-sharing oxygen between two MoO_6 octahedra. The peak at 666 cm^{-1} can be assigned to the edge sharing of triply coordinated oxygen (Mo—$O_{(3)}$) stretching mode, which results from edge-shared oxygen between three octahedral. The peak at 991 cm^{-1} is assigned to the terminal oxygen (Mo=O) stretching mode, which results from an unshared oxygen. When the sweep rate was decreased to 3 mV s^{-1} (plot (i)), additional peaks were observed in the Raman spectrum. The peaks at 894, 849, 774 and 343 cm^{-1} are assigned to the metastable, monoclinic β-MoO_3.[100] The amount of β-MoO_3 in the as

deposited film is significant, as the vibration intensity of the peaks dominate the peaks associated with α-MoO_3. In contrast, when the sweep rate was increased to 10 mV s^{-1} (plot (iii)), the vibration intensity of the peaks fell drastically and there was no longer any evidence of β-MoO_3 formation from the Raman spectrum.

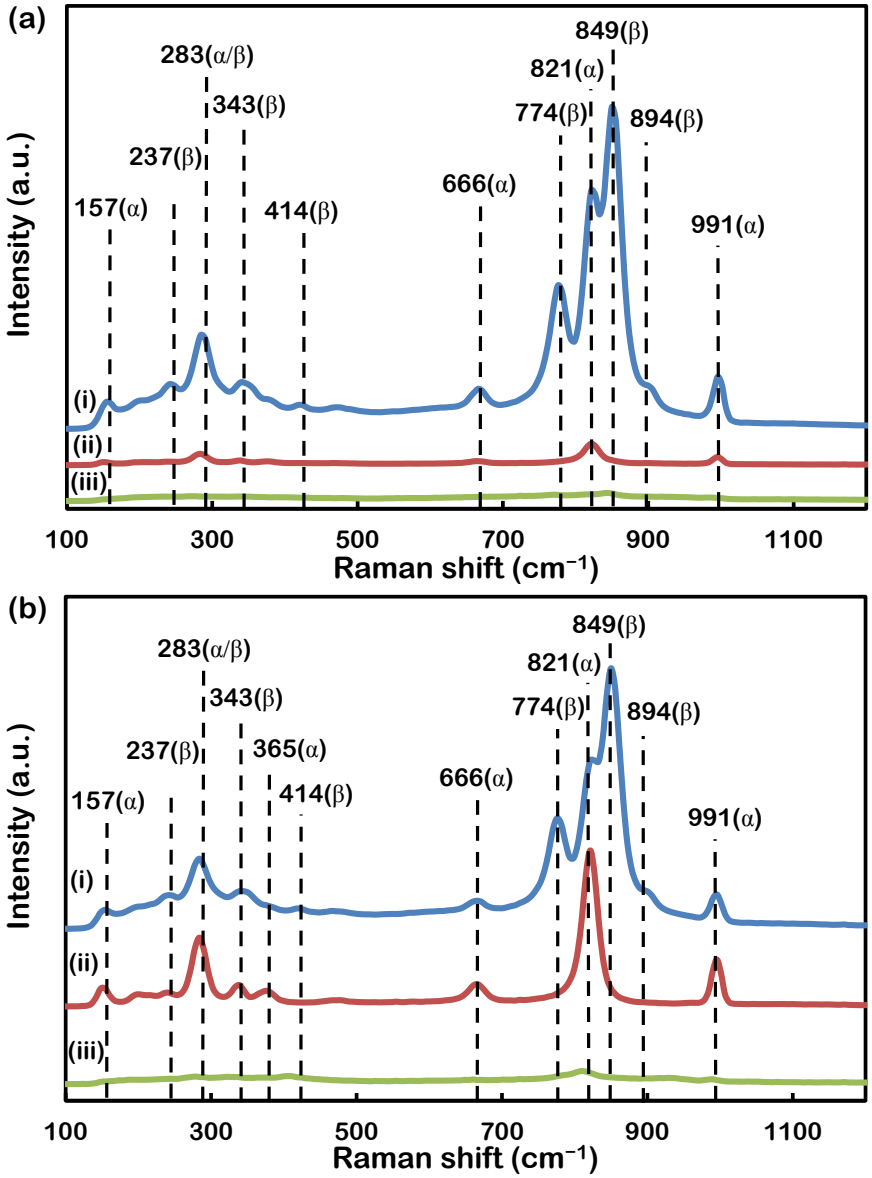

Figure 2.3 Raman spectra of (a) electrodeposited and (b) annealed MoO_3 films on FTO glass substrates obtained at a sweep rate of (i) 3 (ii) 5 and (iii) 10 mV s^{-1} in a 0.2 M Na_2MoO_4, at a pH of 4.

Given that the as deposited films were quasi-amorphous in nature as evidenced by a lack of any peaks in their XRD patterns (will be presented later) the samples were annealed to generate crystalline materials. Lack of peaks in the MoO_3 crystal XRD patterns of the as electrodeposited films, is generally assigned to the presence of the amorphous phase of

this metal oxide. However, Raman spectra of the electrodeposited films show the presence of β and α phases.[40, 101] It is the author's believe this is due to the existence of locally ordered crystal clusters.[102] These locally ordered clusters can generate Raman signals as they efficiently interact with phonons but randomly scatter the XRD beams to avoid the formation of any patterns or peaks.

The Raman spectra of the annealed samples are shown in Figure 2.3 (b). The existence of peaks at 894, 849, 774 and 343 cm^{-1}, in Figure 2.3 (b) plot (i), in the spectra after the sample was annealed at 300 °C for 2 hours verified the presence of β-MoO_3. In Figure 2.3 (b) plot (ii), the vibration intensity of the observed peaks is significantly sharper than the as deposited counterpart, showing that the crystal formation was evident during the annealing process for the sample deposited at the 5 mV s^{-1} rate. Interestingly, the same enhancement in the crystallinity of the material was not observed for the sample deposited at 10 mV s^{-1}. The dominance of the β-MoO_3 even after annealing is remarkable. β-MoO_3 is known to be metastable and a complete transition to α-MoO_3 has been reported for annealing temperatures above 350°C.[44, 103] However in this chapter, the author used an annealing temperature of 300°C, less than the reported optimum transition temperature of 350°C, which possibly allows the co-existence of both β-MoO_3 and α-MoO_3. Due to the author's observations, it seems that it is possible to obtain dominant ratios of β-MoO_3 to α-MoO_3 by manipulating the CV parameters during the electrodeposition process and still maintain these ratios even after annealing at moderate temperatures.

It has been shown previously in the case of gold nanocrystal electrodeposition under repetitive cycling conditions that the morphology of the deposit is affected by the choice of the upper and lower limits of the potential employed.[104] Therefore the upper limit of the voltage range was varied to observe the effect on the properties of the electrodeposited film. The electrolyte solution was kept at 0.2 M Na_2MoO_4 adjusted to a pH of 4 and run at a sweep rate of 5 mV s^{-1} for 1 cycle. Illustrated in Figure 2.4 are CVs recorded using a series of upper potential limits of –0.4, –0.1, 0.1, 0.4 and 1.0 V. It can be seen that the

CVs are essentially identical with no observation of additional processes at the more positive potential values which suggests that there are no lower oxidation state molybdenum oxide species generated during the electrosynthesis that can be detected in this potential range.

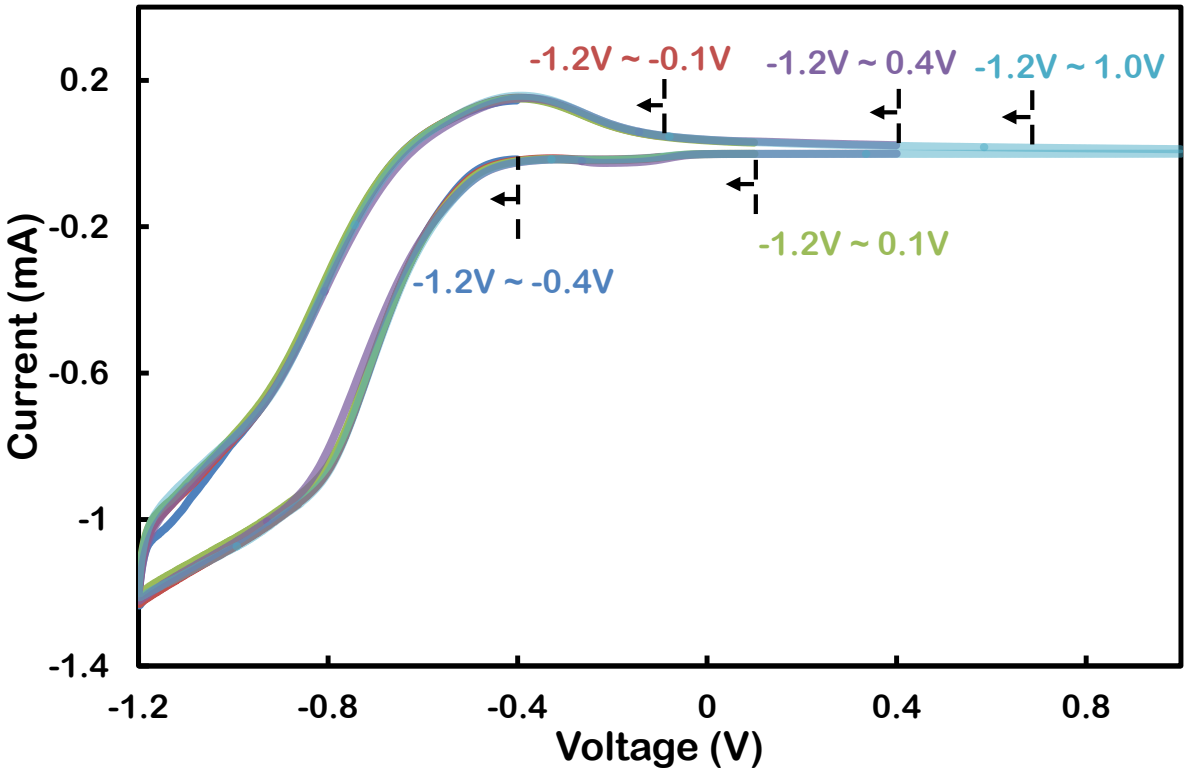

Figure 2.4 Cyclic voltammograms recorded at a FTO electrode in 0.2 M Na_2MoO_4, pH of 4, at a sweep rate of 5 mV s^{-1}, with varying upper potential limits.

However, even though changes were not observed in the cyclic voltammetric behavior, the Raman spectra of the resultant films indicate preferential β-MoO_3 growth as the upper limit is shifted towards more negative potentials (Figure 2.5). It can be seen from plots (iv) and (v), which correspond to an upper limit of +0.4 and +1 V, respectively, that the films were purely α-MoO_3. However as the upper limit was shifted towards more negative potential values, the presence of β-MoO_3 became more significant, in particular using an upper limit of -0.4 V (plot (i)) as can be seen via the emergence of strong β-MoO_3 vibration peaks.

As shown in Figure 2.5 (b), the Raman spectra of the annealed samples also verify the preferential growth of β-MoO_3 as the upper potential limit is shifted to more negative

potentials. It can also be seen that the ratio of β-MoO_3 to α-MoO_3 increases after annealing. Indeed, it was observed that the presence of α-MoO_3 almost completely disappeared (Figure 2.5 (b) plot (i)) when an upper limit of –0.4 V was used.

The dependence of the phase of MoO_3 on the upper potential limit is quite interesting. It seems that during the electrodeposition of MoO_3 on the negative sweep the kinetically favored β-phase is formed. The preferential formation of this phase is continued upon reversing the sweep until an upper potential limit of –0.40 V is reached. This is consistent with electrocrystallization of other semiconducting materials such as CuTCNQ in organic solvent, as reported by Neufeld *et. al.*,[105] who showed that the kinetically favored phase I is generated under electrodeposition conditions as opposed to the thermodynamically favored phase II.[106] The electrochemical conversion of phase I CuTCNQ into phase II CuTCNQ; however was achieved under aqueous conditions by cycling the potential at an upper limit of sufficiently positive potential.[105] It seems in the case of MoO_3 only one sweep is required into a more positive potential region to achieve conversion from the kinetically stable phase into the thermodynamically stable phase.

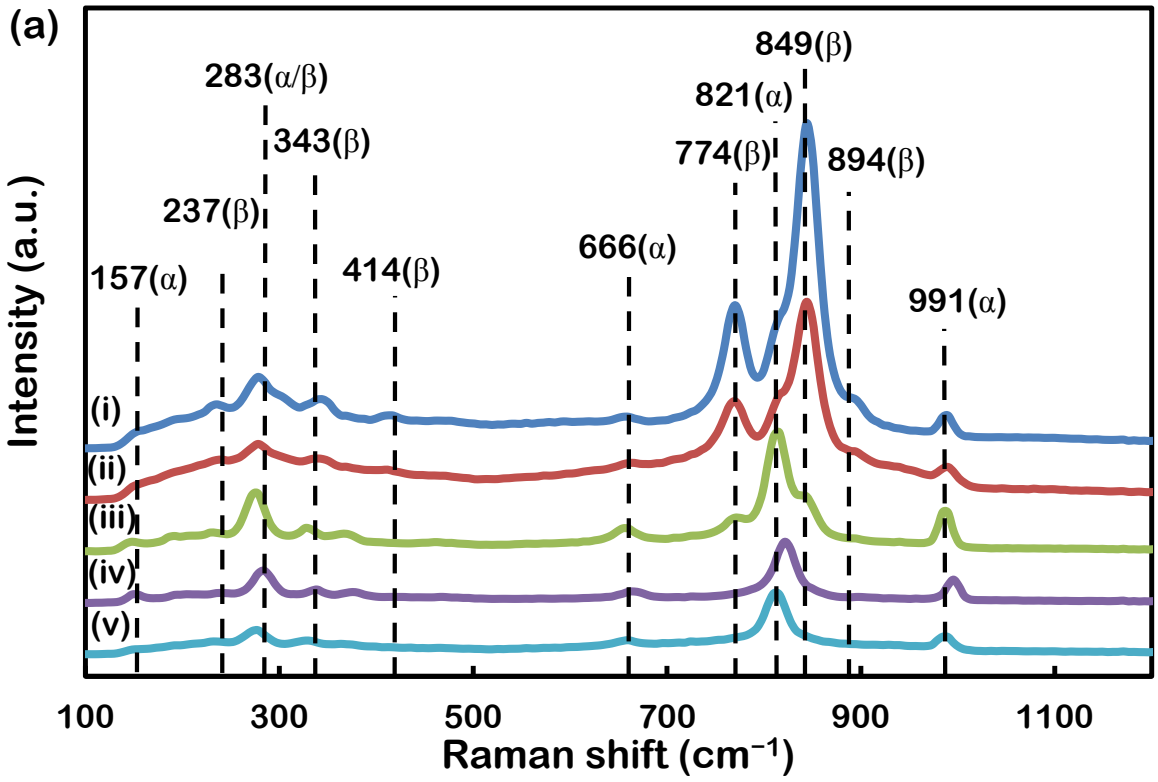

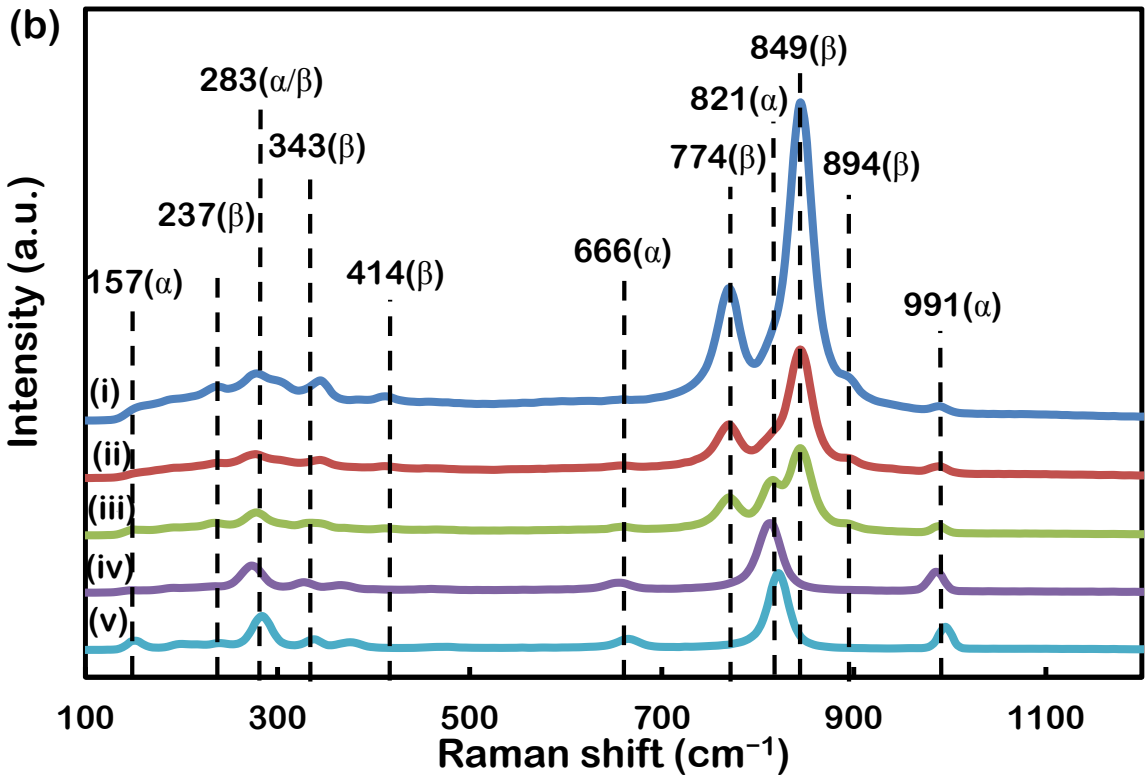

Figure 2.5 Raman spectra of (a) electrodeposited and (b) annealed films of MoO_3 electrodeposited at a sweep rate of 5 mV s^{-1} for one cycle over a potential range of (i) −1.2 to −0.4 V, (ii) −1.2 to −0.1 V, (iii) −1.2 to 0.1 V, (iv) −1.2 to 0.4 V and (v) −1.2 to 1.0 V.

Illustrated in Figure 2.6 are XRD patterns showing the evolution from quasi-amorphous to crystalline MoO_3 thin films. The as deposited films are quasi-amorphous and the sharp diffraction peaks seen in Figure 2.6 in plots (b) and (d) correspond to the reflections from the underlying FTO substrates. Upon annealing for 2 hours at 300 °C, many peaks emerge corresponding to the layered, orthorhombic α-MoO_3[43]. Only the peak at 23.7° can be assigned to reflections from either the (011) plane of the α-MoO_3 or the (110) plane of the β-MoO_3. It is observed that the annealed sample obtained at 5 mV s^{-1} (Figure 2.6 plot (a)) has preferential growth in the (111) plane, and the annealed sample prepared with a sweep rate of 3 mV s^{-1} (Figure 2.6 plot (c)) sample has preferential growth in the (021) plane.

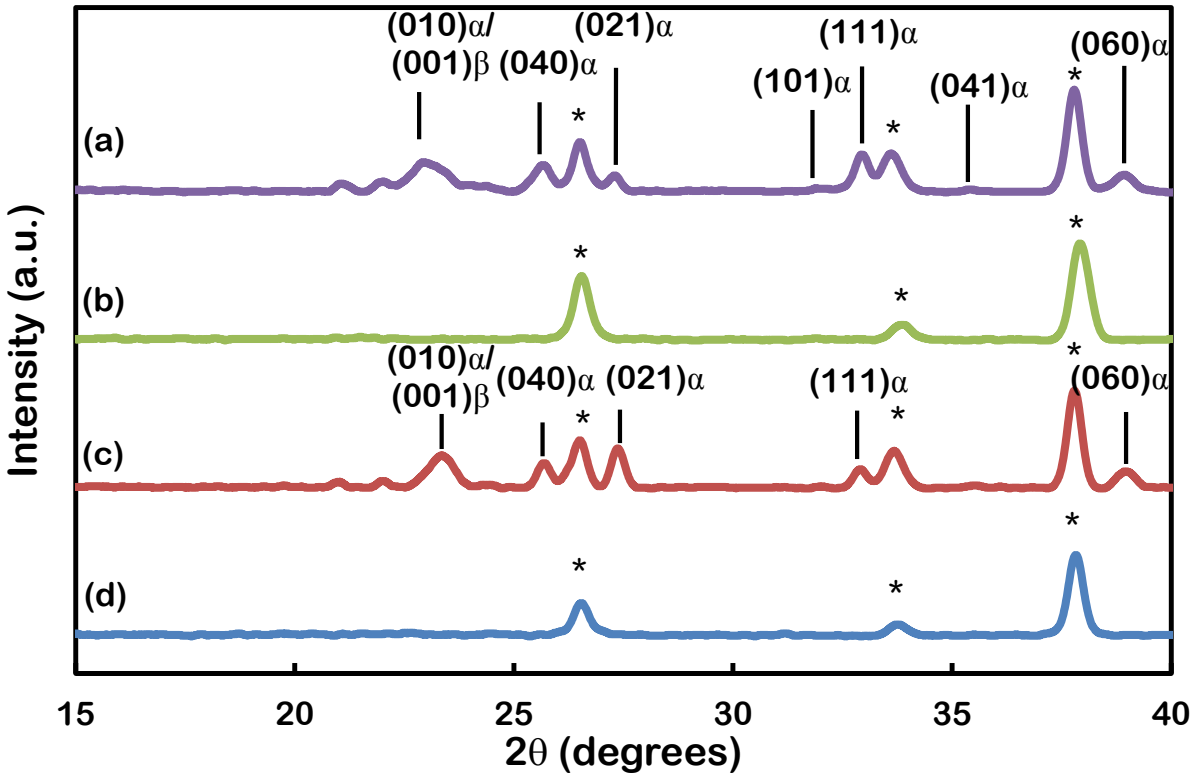

Figure 2.6 XRD patterns of MoO_3 electrodeposited on FTO at using a sweep rate of (a) 5 mV s^{-1} annealed at 300 °C for 2 hours (b) 5 mV s^{-1} as deposited, (c) 3 mV s^{-1} annealed at 300 °C for 2 hours and (d) 3 mV s^{-1} as deposited. Asterisk denotes FTO peaks.

Optical gas sensing measurements were conducted to assess the gasochromic property of the deposited films in response to H_2 and consequently H^+ intercalation of the films. A thin catalytic layer of Pd, in the order of 25 Å, was deposited onto the films to allow the dissociation of the H_2 gas on the samples. The films were exposed to synthetic air in between measurements for recovery and bleaching the samples.

The samples used for gasochromic measurements were obtained using a lower concentration of Na_2MoO_4 at 0.02 M. This was to decrease the deposition rate and film thickness which resulted in films with minimum cracks and shorter response time upon the gas exposure. Illustrated in Table 2.1 are the electrodeposition conditions utilized for each sample. The crystal phases of the films were confirmed using Raman spectroscopy and correlated with the data shown for the electrodeposited samples form a 0.2 M Na_2MoO_4 solution.

Table 2.1 Electrodeposition conditions used for synthesizing different phases and morphologies of MoO_3 from a solution containing 0.02 M Na_2MoO_4 at a pH of 4. All samples were annealed at 300°C after the deposition.

Sample no	Type	Electrodeposition conditions
1	Smooth α-MoO_3	−1.2 to 0.4 V at 10 mV s^{-1} for 1 cycle
2	Porous α-MoO_3	−1.2 to 0.4 V at 5 mV s^{-1} for 1 cycle
3	β-MoO_3	−1.2 to -0.4 V at 5 mV s^{-1} for 1 cycle

The SEM images of the samples and each sample's visible spectra, before and after exposure to H_2 gas, are presented in Figure 2.7. For sample 1 (Figure 2.7 (a)), a surface consisting of layered α-MoO_3 is observed. These layers are stacked on the top of one another, forming a continuous surface. Sample 2 (Figure 2.7 (b)) is mainly made of a transitioning porous surface with some visible remains of the layered α-MoO_3. Sample 3 (Figure 2.7 (c)) is the surface of the β type film. The film is made of corrugated grains of the order of 150 to 200 nm.

In these experiments, Samples 1 and 3 were compared to reveal the differences of the gasochromic responses between the materials crystal phases. Samples 1 and 2 were compared to shed light on the difference between the surface porosities in response to H_2 gas.

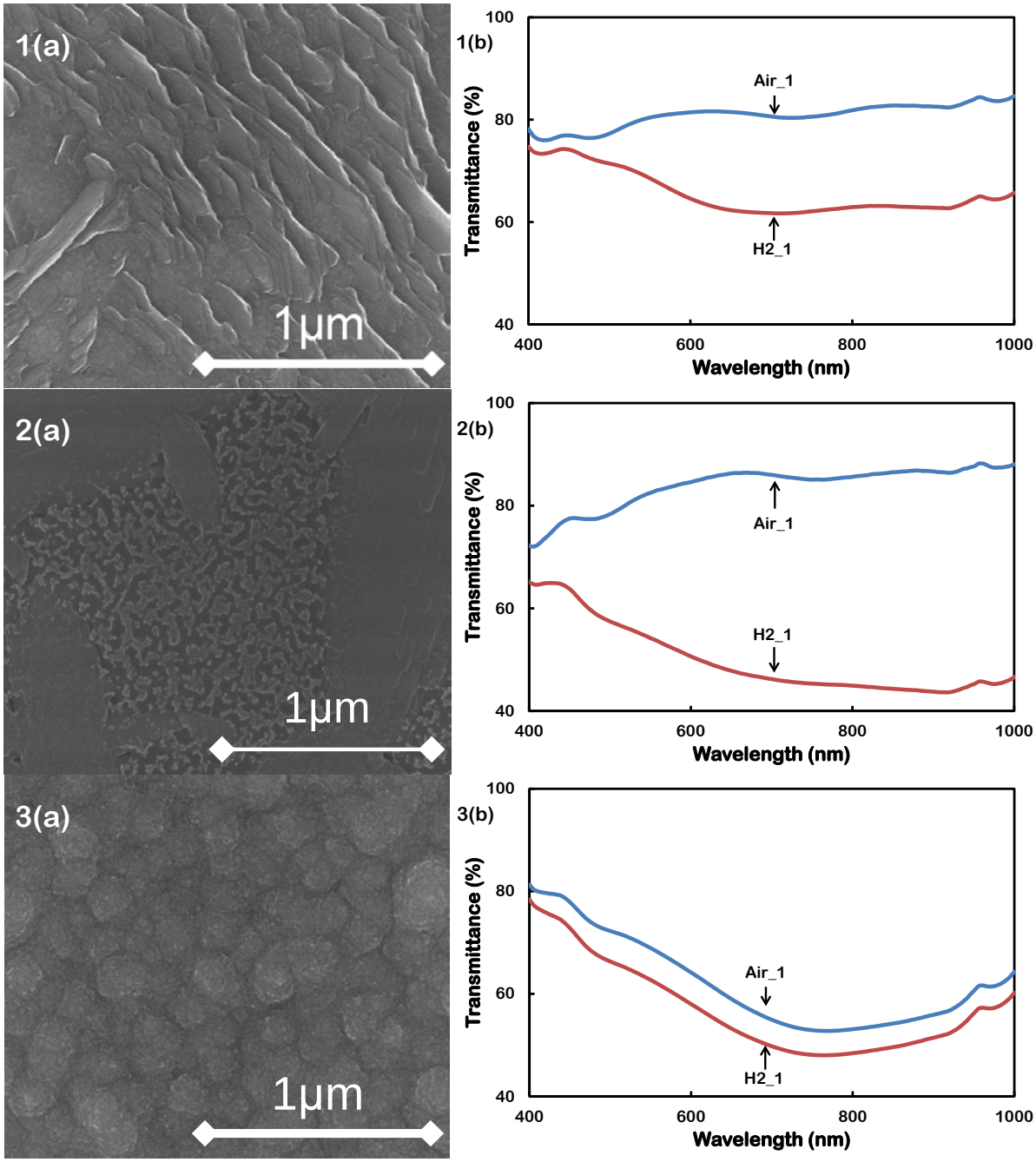

Figure 2.7 (1) SEM images and (2) Visible transmittance spectra after exposure to "Air_1" and "H2_1": (a) smooth α-MoO_3, (b) porous α-MoO_3 and (c) β-MoO_3 films.

In the H_2 gasochromic measurements, the visible spectra of the samples in both air and after exposure to H_2 are demonstrated. Figure 2.7 (1b) shows the spectra of the smooth α-MoO_3 after initial "Air_1" exposure and then consequently to "H2_1". In the presence of H_2, the film transmittance change was negligible at 400 nm. However, the difference increased with wavelength and reached a plateau after approximately 650 nm. In this range, the change was consistently above 20%. Figure 2.7 (3b) shows the spectra of the β-MoO_3,

which indicates that in the presence of H_2, the film transmittance changed consistently throughout the plotted spectrum. This change was only ~5% which was much smaller than the α-MoO_3 sample in Figure 2.7 (1b). Illustrated in Figure 2.7 (2a) is the transmittance modulation for the porous α-MoO_3 sample after exposure to H_2. The change was approximately 7% at 400 nm and increased with wavelength, and this difference reached a plateau with a magnitude of over 40% after 900 nm. In contrast to the smooth α-MoO_3 sample, the response is significantly larger. This suggests that the samples with higher surface-to-volume ratios offer greater Pd catalytic surface sites for H_2 interaction, hence dissociating more H^+ ions to interact with MoO_3.

In previous work by Ou *et al*[2] on *in situ* Raman spectroscopy of H_2 interactions with α-MoO_3 shows that after dissociation of H_2 into H^+ ions, they mainly interact with lattice oxygen and cause the crystal transformation from the original α-MoO_3 into the mixed structure of hydrogen molybdenum bronze and sub-stoichiometric MoO_3, to induce color modulation [64]. The measurement here showed that the β-MoO_3 sample response was significantly lower than the α-MoO_3 samples. This difference can be attributed to the intrinsic differences between the two phases. The most significant difference between these two phases is that α-MoO_3 is formed from both edge-sharing and corner sharing octahedra, which results in a layered structured. β-MoO_3, on the other hand, is only made from corner sharing octahedra and has a continuous crystal structure in three dimensions. Having a layered structure of the spacing in the order of 0.7 nm, α-MoO_3 can allow the penetration of the small H_2 molecules within the bulk of the material, providing a large surface to volume ratio for the gas interaction. Another reason, can be due to the presence of doubly bonded oxygen atoms at the edges rather than in between octahedra for α-MoO_3 providing a more favored surface energy for gasochromic interactions. Additionally, a final possible difference between these two phases is that the metastable β-MoO_3 being thermodynamically unstable, possesses more defects compared to α-MoO_3 phase and there are more oxygen vacancies for β-MoO_3, and therefore less H^+ ions are able interact

and form H_2O molecules. The author believes that a combination of the three abovementioned reasons reduces the sensitivity of β-MoO_3 across the entire spectrum towards H_2 exposure in comparison to α-MoO_3.

2.4 Summary

In this chapter, the author demonstrated a facile and well controlled electrochemical synthesis process for the fabrication of both α- and β-MoO_3 films. This cyclic voltametric electrodeposition process was carried out under ambient conditions which made this process versatile and compatible with electronic device industry standards. The experimental parameters offered fine control over both the phase of the material and its morphology. The author showed that preferential growth of both β-MoO_3 and α-MoO_3 could be achieved by simply varying the potential limits and sweep rate under which the deposition is carried out. Additionally, this chapter showed that the α-MoO_3 is substantially more active for H_2 gas interaction than β-MoO_3 that can be mainly ascribed to the layered nature of α-MoO_3.

In the next chapter, the author will present binary electrochromic EC devices based on anodized ordered TiO_2 nanotubes coated with electrodeposited MoO_3. The chapter will focus on the investigation of combining complimentary TMOs to overcome individual chromic performance limitations.

References

1. Ulrike, D., The Surface Science of Titanium Dioxide. *Surf. Sci. Rep.* 2003, *48*, 53-229.

2. Zheng, H. D.; Ou, J. Z.; Strano, M. S.; Kaner, R. B.; Mitchell, A.; Kalantar-Zadeh, K., Nanostructured Tungsten Oxide - Properties, Synthesis, and Applications. *Adv. Funct. Mater.* 2011, *21*, 2175-2196.

3. Chang, W. C.; Qi, X. D.; Kuo, J. C.; Lee, S. C.; Ng, S. K.; Chen, D., Post-Deposition Annealing Control of Phase and Texture for the Sputtered MoO_3 Films. *Crystengcomm* 2011, *13*, 5125-5132.

4. Wang, Z. L., Zinc Oxide Nanostructures: Growth, Properties and Applications. *J. Phys.: Condens. Matter* 2004, *16*, R829-R858.

5. Ohler, N.; Bell, A. T., Selective Oxidation of Methane over MoO_x/SiO_2: Isolation of the Kinetics of Reactions Occurring in the Gas Phase and on the Surfaces of Sio2 and Moox. *J. Catal.* 2005, *231*, 115-130.

6. Rahmani, M. B.; Keshmiri, S. H.; Yu, J.; Sadek, A. Z.; Al-Mashat, L.; Moafi, A.; Latham, K.; Li, Y. X.; Wlodarski, W.; Kalantar-zadeh, K., Gas Sensing Properties of Thermally Evaporated Lamellar MoO_3. *Sensor Actuat B-Chem* 2010, *145*, 13-19.

7. Riley, L. A.; Lee, S.-H.; Gedvilias, L.; Dillon, A. C., Optimization of MoO_3 Nanoparticles as Negative-Electrode Material in High-Energy Lithium Ion Batteries. *J. Power Sources* 2010, *195*, 588-592.

8. Ding, Q. P.; Huang, H. B.; Duan, J. H.; Gong, J. F.; Yang, S. G.; Zhao, X. N.; Du, Y. W., Molybdenum Trioxide Nanostructures Prepared by Thermal Oxidization of Molybdenum. *J. Cryst. Growth* 2006, *294*, 304-308.

9. Comini, E.; Yubao, L.; Brando, Y.; Sberveglieri, G., Gas Sensing Properties of MoO_3 Nanorods to CO and CH_3OH. *Chem. Phys. Lett.* 2005, *407*, 368-371.

10. Chandrappa, G. T.; Livage, J., Synthesis and Characterization of Mo-Oxide Nanoribbons. *Synthesis and Reactivity in Inorganic Metal-Organic and Nano-Metal Chemistry* 2006, *36*, 23-28.

11. Lou, X. W.; Zeng, H. C., Complex Alpha-MoO_3 Nanostructures with External Bonding Capacity for Self-Assembly. *J. Am. Chem. Soc.* 2003, *125*, 2697-2704.

12. Lou, X. W.; Zeng, H. C., Hydrothermal Synthesis of Alpha-MoO_3 Nanorods Via Acidification of Ammonium Heptamolybdate Tetrahydrate. *Chem. Mater.* 2002, *14*, 4781-4789.

13. Niederberger, M.; Krumeich, F.; Muhr, H.-J.; Muller, M.; Nesper, R., Synthesis and Characterization of Novel Nanoscopic Molybdenum Oxide Fibers. *J. Mater. Chem.* 2001, *11*, 1941-1945.

14. Patzke, G. R.; Michailovski, A.; Krumeich, F.; Nesper, R.; Grunwaldt, J.-D.; Baiker, A., One-Step Synthesis of Submicrometer Fibers of MoO_3. *Chem. Mater.* 2004, *16*, 1126-1134.

15. Chen, J. S.; Cheah, Y. L.; Madhavi, S.; Lou, X. W., Fast Synthesis of Alpha-MoO_3 Nanorods with Controlled Aspect Ratios and Their Enhanced Lithium Storage Capabilities. *J. Phys. Chem. C* 2010, *114*, 8675-8678.

16. Zhou, L.; Yang, L.; Yuan, P.; Zou, J.; Wu, Y.; Yu, C., α-MoO_3 Nanobelts: A High Performance Cathode Material for Lithium Ion Batteries. *J. Phys. Chem. C* 2010, *114*, 21868-21872.

17. McEvoy, T. M.; Stevenson, K. J.; Hupp, J. T.; Dang, X., Electrochemical Preparation of Molybdenum Trioxide Thin Films: Effect of Sintering on Electrochromic and Electroinsertion Properties. *Langmuir* 2003, *19*, 4316-4326.

18. Carcia, P. F.; McCarron Iii, E. M., Synthesis and Properties of Thin Film Polymorphs of Molybdenum Trioxide. *Thin Solid Films* 1987, *155*, 53-63.

19. Kalantar-zadeh, K.; Tang, J. S.; Wang, M. S.; Wang, K. L.; Shailos, A.; Galatsis, K.; Kojima, R.; Strong, V.; Lech, A.; Wlodarski, W.; Kaner, R. B., Synthesis of Nanometre-Thick MoO_3 Sheets. *Nanoscale* 2010, *2*, 429-433.

20. Tanisaki, S., Crystal Structure of Monoclinic Tungsten Trioxide at Room Temperature. *J. Phys. Soc. Jpn.* 1960, *15*, 573-581.

21. Machiels, C. J.; Cheng, W. H.; Chowdhry, U.; Farneth, W. E.; Hong, F.; McCarron, E. M.; Sleight, A. W., The Effect of the Structure of Molybdenum Oxides on the Selective Oxidation of Methanol. *Appl. Catal.* 1986, *25*, 249-256.

22. Bhosle, V.; Tiwari, A.; Narayan, J., Epitaxial Growth and Properties of MoO_x ($2 < x < 2.75$) Films. *J. Appl. Phys.* 2005, *97*, 083539.

23. Prasad, A. K.; Kubinski, D. J.; Gouma, P. I., Comparison of Sol-Gel and Ion Beam Deposited MoO_3 Thin Film Gas Sensors for Selective Ammonia Detection. *Sensor Actuat B-Chem* 2003, *93*, 25-30.

24. Navas, I.; Vinodkumar, R.; Lethy, K. J.; Detty, A. P.; Ganesan, V.; Sathe, V.; Pillai, V. P. M., Growth and Characterization of Molybdenum Oxide Nanorods by Rf Magnetron Sputtering and Subsequent Annealing. *J. Phys. D: Appl. Phys.* 2009, *42*, 175305.

25. Bouzidi, A.; Benramdane, N.; Tabet-Derraz, H.; Mathieu, C.; Khelifa, B.; Desfeux, R., Effect of Substrate Temperature on the Structural and Optical Properties of MoO_3 Thin Films Prepared by Spray Pyrolysis Technique. *Mater. Sci. Eng., B* 2003, *97*, 5-8.

26. Young Jung, L.; William, T. N.; Dae-Gun, K.; Young Do, K., Chemical Vapour Transport Synthesis and Optical Characterization of MoO_3 Thin Films. *J. Phys. D: Appl. Phys.* 2009, *42*, 115419.

27. Siciliano, T.; Tepore, A.; Filippo, E.; Micocci, G.; Tepore, M., Characteristics of Molybdenum Trioxide Nanobelts Prepared by Thermal Evaporation Technique. *Mater. Chem. Phys.* 2009, *114*, 687-691.

28. Xie, Y. L.; Cheong, F. C.; Zhu, Y. W.; Varghese, B.; Tamang, R.; Bettiol, A. A.; Sow, C. H., Rainbow-Like MoO_3 Nanobelts Fashioned Via Afm Micromachining. *J. Phys. Chem. C* 2009, *114*, 120-124.

29. Wang, S.; Zhang, Y.; Ma, X.; Wang, W.; Li, X.; Zhang, Z.; Qian, Y., Hydrothermal Route to Single Crystalline α-MoO_3 Nanobelts and Hierarchical Structures. *Solid State Commun.* 2005, *136*, 283-287.

30. Padmanab.Kr, Preparation of MoO_3 Films by Anodization. *Rev. Sci. Instrum.* 1974, *45*, 593-593.

31. Gacitua, M.; Boutaleb, Y.; Cattin, L.; Abe, S. Y.; Lare, Y.; Soto, G.; Louarn, G.; Morsli, M.; Rehamnia, R.; del Valle, M. A.; Drici, A.; Bernède, J. C., Electrochemical Preparation of MoO_3 Buffer Layer Deposited onto the Anode in Organic Solar Cells. *physica status solidi (a)* 2010, *207*, 1905-1911.

32. Guerfi, A.; Paynter, R. W.; Dao, L. H., Characterization and Stability of Electrochromic MoO_3 Thin Films Prepared by Electrodeposition. *J. Electrochem. Soc.* 1995, *142*, 3457-3464.

33. McEvoy, T. M.; Stevenson, K. J., Electrochemical Quartz Crystal Microbalance Study of the Electrodeposition Mechanism of Molybdenum Oxide Thin Films from Peroxo-Polymolybdate Solution. *Anal. Chim. Acta* 2003, *496*, 39-51.

34. Plowman, B. J.; Bhargava, S. K.; O'Mullane, A. P., Electrochemical Fabrication of Metallic Nanostructured Electrodes for Electroanalytical Applications. *Analyst* 2011, *136*, 5107-5119.

35. Yang, Y. A.; Cao, Y. W.; Loo, B. H.; Yao, J. N., Microstructures of Electrochromic MoO_3 Thin Films Colored by Injection of Different Cations. *J. Phys. Chem. B* 1998, *102*, 9392-9396.

36. Hirata, T.; Ishioka, K.; Kitajima, M., Raman Spectra of MoO_3 Implanted with Protons. *Appl. Phys. Lett.* 1996, *68*, 458-460.

37. Yao, D. D.; Ou, J. Z.; Latham, K.; Zhuiykov, S.; O'Mullane, A. P.; Kalantar-zadeh, K., Electrodeposited α- and β-Phase MoO_3 Films and Investigation of Their Gasochromic Properties. *Cryst. Growth Des.* 2012, *12*, 1865-1870.

38. Gomez, E.; Pellicer, E.; Valles, E., Influence of the Bath Composition and the Ph on the Induced Cobalt-Molybdenum Electrodeposition. *J. Electroanal. Chem.* 2003, *556*, 137-145.

39. Skoog, D. A.; Holler, F. J.; Crouch, S. R., *Principles of Instrumental Analysis*. Thomson Brooks/Cole: 2007.

40. Gómez, E.; Pellicer, E.; Vallés, E., Intermediate Molybdenum Oxides Involved in Binary and Ternary Induced Electrodeposition. *J. Electroanal. Chem.* 2005, *580*, 238-244.

41. Phuruangrat, A.; Ham, D. J.; Thongtem, S.; Lee, J. S., Electrochemical Hydrogen Evolution over MoO_3 Nanowires Produced by Microwave-Assisted Hydrothermal Reaction. *Electrochem. Commun.* 2009, *11*, 1740-1743.

42. Nazri, G. A.; Julien, C., Far-Infrared and Raman Studies of Orthorhombic MoO_3 Single-Crystal. *Solid State Ionics* 1992, *53*, 376-382.

43. Haro-Poniatowski, E.; Jouanne, M.; Morhange, J. F.; Julien, C.; Diamant, R.; Fernandez-Guasti, M.; Fuentes, G. A.; Alonso, J. C., Micro-Raman Characterization of WO_3 and MoO_3 Thin Films Obtained by Pulsed Laser Irradiation. *Appl. Surf. Sci.* 1998, *127*, 674-678.

44. Julien, C.; Khelfa, A.; Hussain, O. M.; Nazri, G. A., Synthesis and Characterization of Flash-Evaporated MoO_3 Thin Films. *J. Cryst. Growth* 1995, *156*, 235-244.

45. Gesheva, K.; Szekeres, A.; Ivanova, T., Optical Properties of Chemical Vapor Deposited Thin Films of Molybdenum and Tungsten Based Metal Oxides. *Sol. Energy Mater. Sol. Cells* 2003, *76*, 563-576.

46. Kalantar-zadeh, K.; Vijayaraghavan, A.; Ham, M.-H.; Zheng, H.; Breedon, M.; Strano, M. S., Synthesis of Atomically Thin WO_3 Sheets from Hydrated Tungsten Trioxide. *Chem. Mater.* 2010, *22*, 5660-5666.

47. Juárez Ramírez, I.; Martínez-de la Cruz, A., Synthesis of [Beta]-MoO_3 by Vacuum Drying and Its Structural and Electrochemical Characterisation. *Mater. Lett.* 2003, *57*, 1034-1039.

48. Wang, L.; Guo, S.; Hu, X.; Dong, S., Facile Electrochemical Approach to Fabricate Hierarchical Flowerlike Gold Microstructures: Electrodeposited Superhydrophobic Surface. *Electrochem. Commun.* 2008, *10*, 95-99.

49. Neufeld, A. K.; Madsen, I.; Bond, A. M.; Hogan, C. F., Phase, Morphology, and Particle Size Changes Associated with the Solid−Solid Electrochemical Interconversion of TCNQ and Semiconducting CuTCNQ (TCNQ = Tetracyanoquinodimethane). *Chem. Mater.* 2003, *15*, 3573-3585.

50. O'Mullane, A. P.; Neufeld, A. K.; Harris, A. R.; Bond, A. M., Electrocrystallization of Phase I, CuTCNQ (TTCNQ = 7,7,8,8-Tetracyanoquinodimethane), on Indium Tin Oxide and Boron-Doped Diamond Electrodes†. *Langmuir* 2006, *22*, 10499-10505.

51. Ou, J. Z.; Campbell, J. L.; Yao, D.; Wlodarski, W.; Kalantar-zadeh, K., In Situ Raman Spectroscopy of H_2 Gas Interaction with Layered MoO_3. *J. Phys. Chem. C* 2011, *115*, 10757-10763.

Chapter 3

Electrochromic Properties of TiO_2 Nanotubes Coated with Electrodeposited MoO_3

3.1 Introduction

In the previous chapter, the author showed a facile and well controlled electrochemical synthesis process for selective fabrication of both α- and β-phase molybdenum trioxide (MoO_3) films. Gasochromic devices based on α- and β-MoO_3 films were demonstrated, and the results revealed that α-MoO_3 displayed better optical modulation than β-MoO_3 while a porous structure performed better than stratified layered structure. However, the electrochromic (EC) performance of the developed devices could not be assessed due to the poor adhesion exhibited by the synthesized films. Overcoming this issue can be achieved by combining the α-MoO_3, which is a chromic transition metal oxide (TMO) with a durable TMO template. Many issues should be considered. The binary chromic system should be made of compatible TMOs, which offer merits that compliment each other. Subsequently, based on the analysis presented in chapter 1, the author chose to develop EC devices based on a combination of anodized titanium dioxide (TiO_2) and electrodeposited α-MoO_3, which are both in line with the core concept of electric field driven techniques for this thesis. The ordered TiO_2 nanotube (TNT) array was chosen for its well-known stability with a large surface area in addition to being a chromic material itself. The author planned to incorporate electrodeposited α-MoO_3, which served as the chromic coating to enhance the overall EC efficiency.

In this chapter, the author will present his work on the developtment of binary EC devices based on anodized ordered TNT templates with electrodposited MoO_3 coatings. A comprehensive characterization of the bare TNT films and MoO_3 coated films will be presented. As the performance of the EC devices depend on the MoO_3 coating, the author will investigate and provide theoretical and experimental correlation between the electrodeposited α-MoO_3 thickness and its impact on the overall EC system. Eventually, the devices based on the bare TNT template and the MoO_3 coated films will be evaluated for their EC performances. The work in this chapter was published as a full article in the jounral Nanoscale.[107]

3.2 Experimental

3.2.1 TNT formation

TNT layers were grown by anodic oxidation following the method of Zheng *et al.*[25] Ti films of ~0.3 μm were deposited by radio frequency (RF) sputtering system fitted with a Ti target (99.995% purity, Williams Advanced Materials). Ti was sputtered on fluorine-doped tin oxide (FTO, 15 Ω square^{-1}, Dyesol) glass substrates at 20×10^{-3} Torr and 100 W applied RF power and the substrate temperature of 300 °C for 60 min. The samples were then placed in a two-electrode cell configuration using the sample (~ 0.7 cm^{-2}) as an anode and a platinum (Pt) foil as the cathode. The anodization was carried out using a high-voltage potentiostat (CHI-413A electrochemical station) in an electrolyte mix of ethylene glycol (EG, 98% anhydrous, Sigma Aldrich), water (4 vol%) and ammonium fluoride (NH_4F 5 wt%) at 60 V for 270 s. This process formed nanotube layers with a tube length of ~ 1 μm. The samples were then annealed in a standard laboratory horizontal furnace at 450 °C for 120 min in ambient air, with ramp up and ramp down rates of 2 °C min^{-1}.

3.2.2 MoO_3 coating on TiO_2 nanotubular films

For the molybdenum oxide deposition, a molybdate solution was prepared by adding 5 mM sodium molybdate (Na_2MoO_4, 99% purity, Sigma Aldrich) into distilled water. Sulphuric acid (H_2SO_4) was added to adjust the pH to 4. The electrodeposition of MoO_3 was carried out at room temperature using a CHI-413A electrochemical station employing a standard three electrode cell configuration. The TNT samples with 0.7 cm^2 exposed area were used as the working electrode, a Pt wire (0.5 mm diameter, BASi Platinum Wire) as the counter electrode, together with an Ag/AgCl (3 M KCl) (BASi) reference electrode in a custom made electrochemical cell with rectangular sides. The chronoamperometry (CA) technique was utilized to manipulate and achieve the molybdenum oxide deposition onto the TNT samples. CA was carried out at an upper limit of 0 V and lower limit of −0.6 V for a duration of 60 s at initially −0.6 V and then at 0 V for 2, 4, 8 and 10 cycles. Upon the completion of the electrodeposition, samples were washed using Milli-Q water and dried in N_2. The coated samples were further annealed to remove water from the electrodeposited films and obtain the desired crystal phase in a standard laboratory horizontal furnace at 350 °C for 120 min in ambient air, with ramp up and ramp down rates of 1 °C min^{-1}.

3.2.3 Surface and crystal structure characterization

The TNT and molybdenum oxide films were characterized using X-ray diffraction (XRD) patterns were obtained with a Bruker AX 8: discover with general area detector diffraction system (GADDS), X-ray photoelectron spectroscopy (XPS) was performed using a Thermo Scientific K-alpha instrument with an Al Kα source. The High-Angle Annular Dark Field (HAADF) Scanning transmission electron microscopy (STEM) images were taken using JEOL2100F HRTEM operating at 200 kV and Raman measurements were performed using a 532 nm laser at 0.9 mW power with a Jobin Yvon Horiba TRIAX320 spectrometer system incorporating an Olympus BX41 microscope with a 50X objective. The surface morphologies were observed using scanning electron microscopy (SEM) and performed on a FEI Nova Nano instrument.

3.2.4 Electronic and optical characterization

The bandgap energies of the films were obtained using their UV-Vis spectra. Transmittance measurements were carried out using a Fiber Ocean Optics Spectrometer using a UV-Vis-NIR light source (DH-2000, Mikropack, Ocean Optics). *In situ* transmittance characterizations were conducted at room temperature also using the CHI-413A electrochemical station *via* a three electrode configuration, employing the coated samples as working electrode (exposed area of 0.5 cm^2), and the counter and reference electrodes described in the previous chapter. The electrolyte used was 0.1 M $LiClO_4$ in polypropylene carbonate (PC, 98% anhydrous, Sigma Aldrich).

3.3 Results and Discussions

A pictorial representation of the TNT anodization and subsequent MoO_3 coating are shown in Figure 3.1. In order to verify the presence of MoO_3 on the coated TNT films, SEM images of TNT films with different thicknesses of MoO_3 coating were obtained. The degree of MoO_3 coating was controlled by changing the number of chronoamperometry cycles during the electrodeposition. Represented in Figure 3.2a is the surface morphology of the bare TNT film. It was observed that the TNT film comprised of compact vertically aligned nanotubes of ~ 1 μm length, with inner and outer diameters of approximately 70 and 95 nm, respectively (Figure 3.2b). The coated TNT films (Figure 3.2c – 2f) revealed MoO_3 layers encased the entirety of TNT surface, thereby reducing the interior diameter of the nanotubes. It was apparent, that the pore diameter of TNT changed with MoO_3 growth. The inner diameters of the coated TNTs measured from the SEM images (Figure 3.3 and Table 3.1) showed a reduction to ~60, 50, 40 and 41 nm after 2, 4, 8 and 10 deposition cycles, respectively. Interestingly, visible perpendicular growth of MoO_3 was evident on the surface of the tubes (Figure 3.4) which was in agreement with the XRD data discussed below that demonstrated the growth of MoO_3 layers to be parallel to the surface of the tubes.

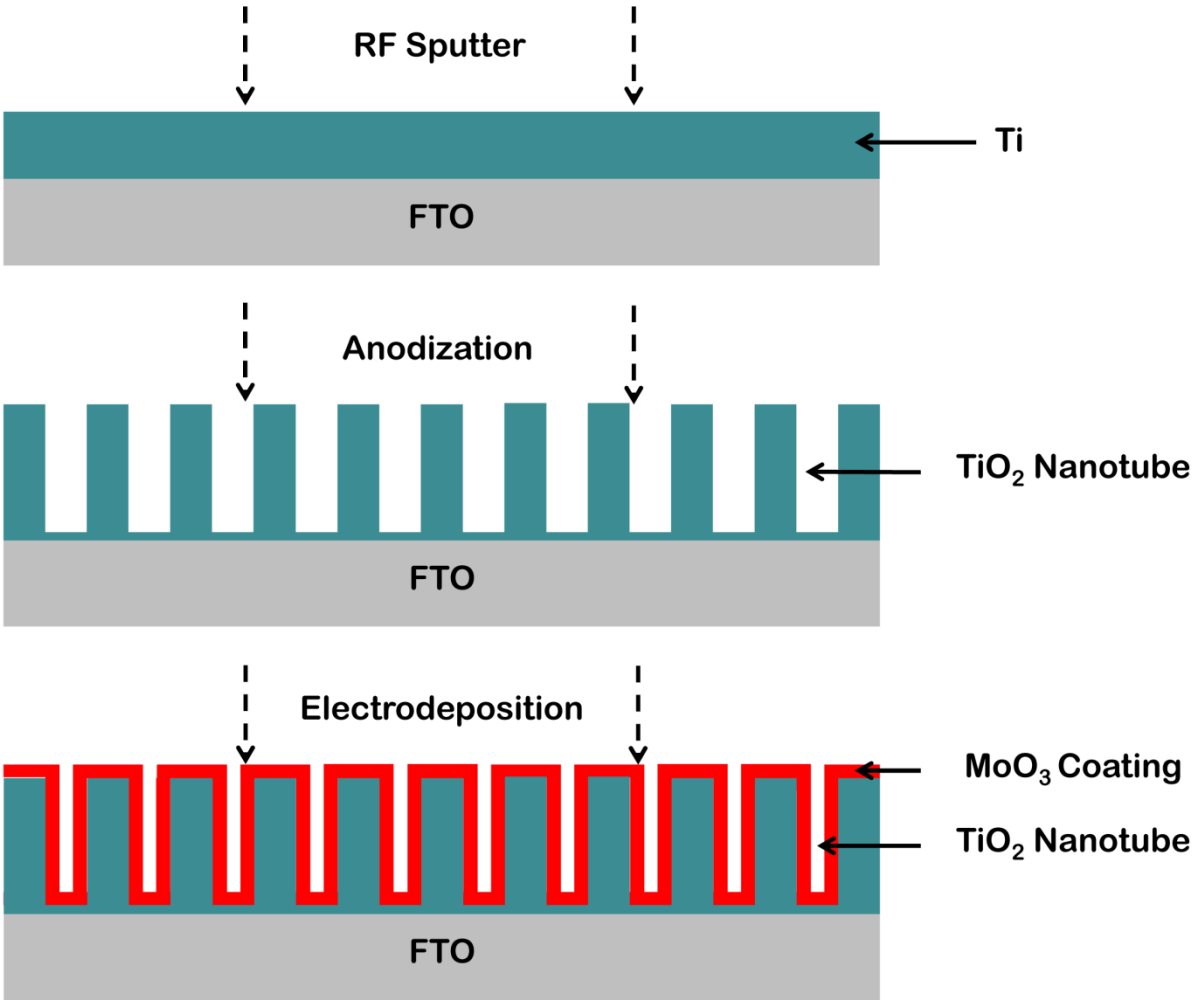

Figure 3.1 Pictorial representations of the TNT anodization and subsequent MoO_3 coating

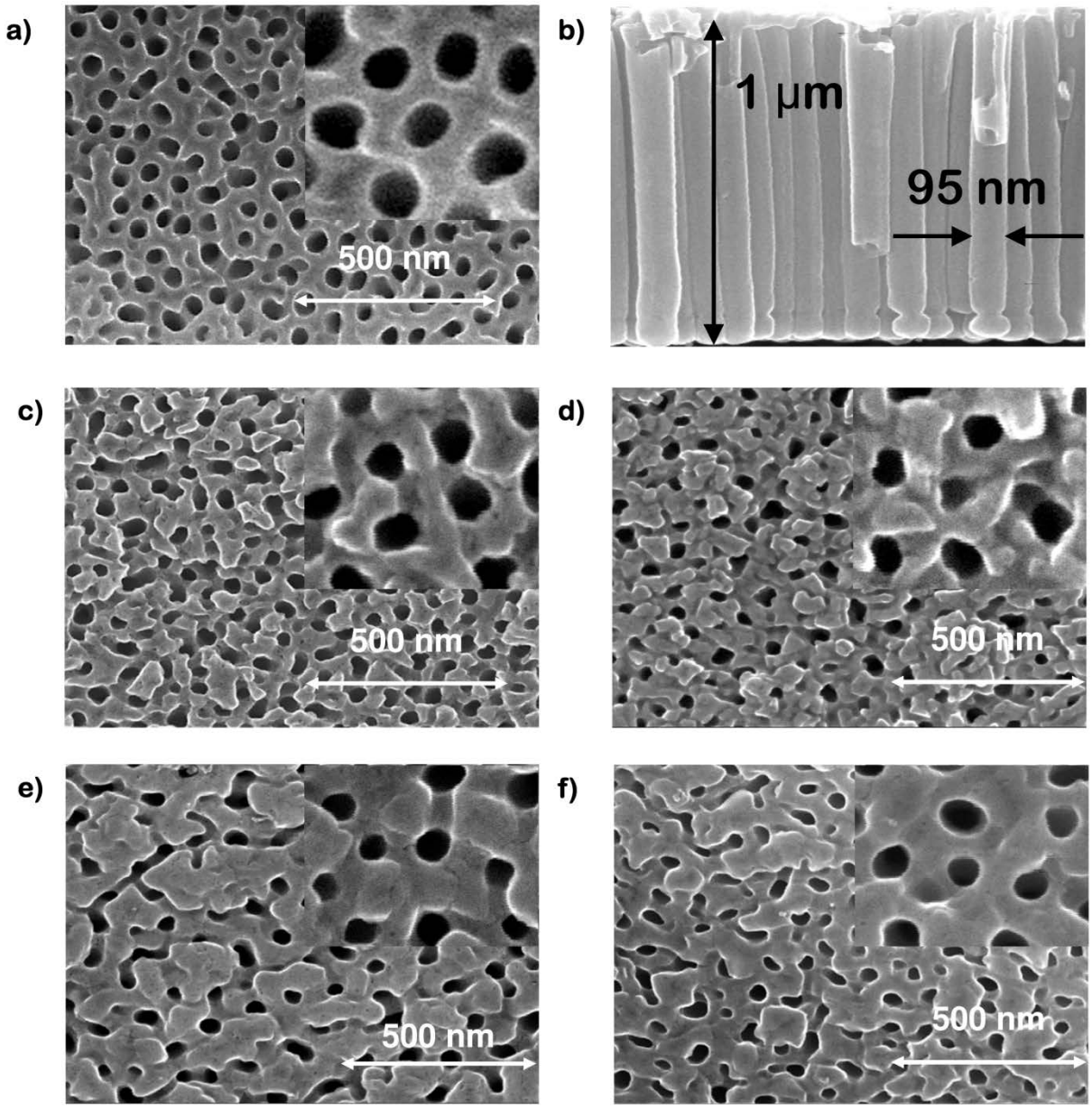

Figure 3.2 a) SEM images of bare TNT film with b) the TNT cross section, c - f) SEM images of 2, 4, 8 and 10 deposition cycles of MoO_3 coated TNT films

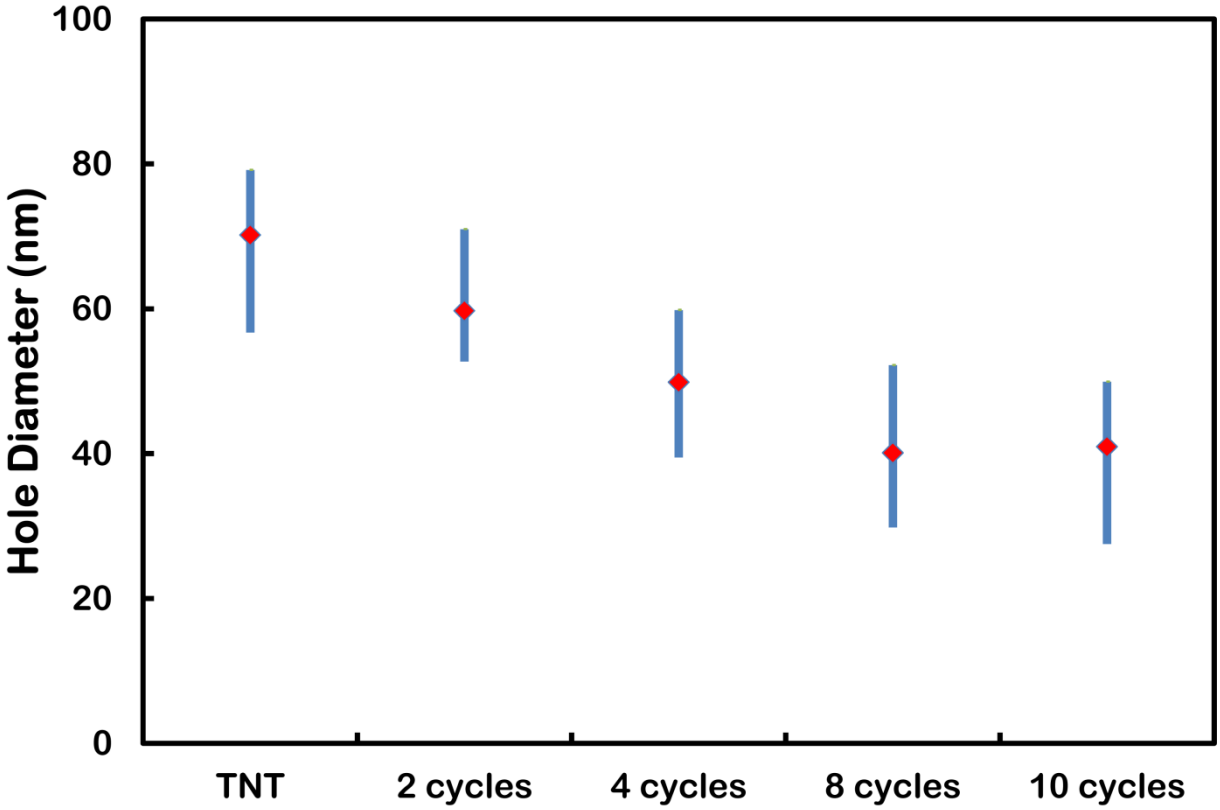

Figure 3.3 The measured average pore diameter of the bare TNT and MoO_3 coated samples from SEM

Table 3.1 Measurements for pore diameters for the samples are carried out and an average for each sample was calculated

	TNT	2 cycles	4 cycles	8 cycles	10 cycles
Average	70.18	59.69	49.84	40.08	40.93
Minimum	56.71	52.71	39.47	29.81	27.53
Maximum	79.14	70.98	59.81	52.2	49.93

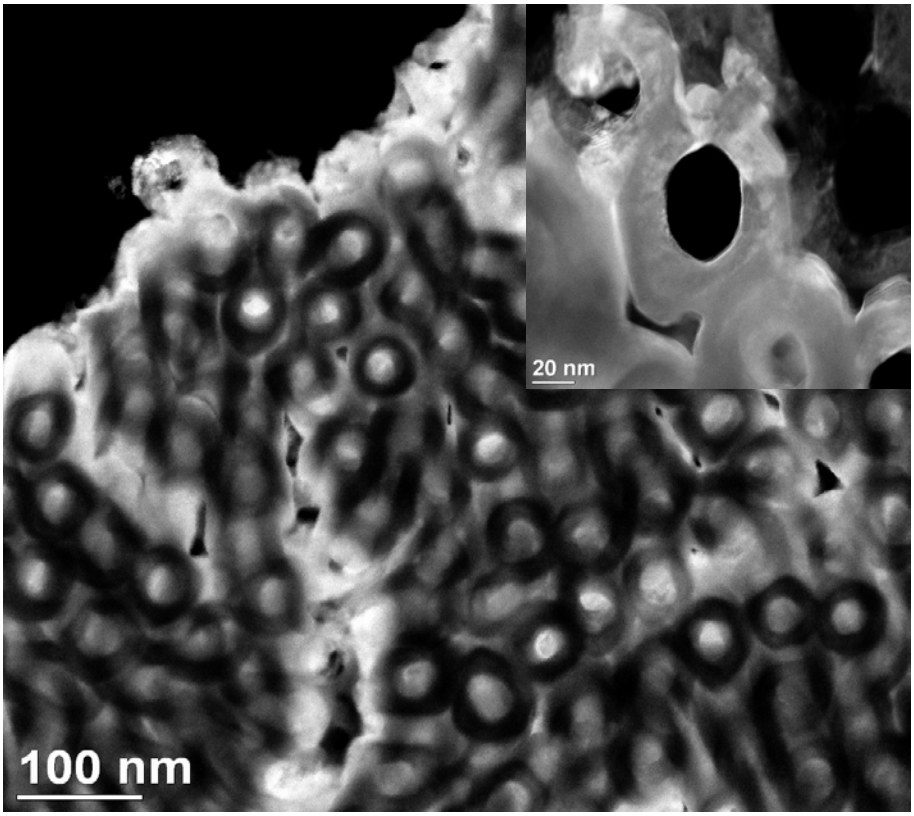

Figure 3.4 High-angle annular dark field (HAADF) scanning transmission electron microscopy (STEM) image of the MoO_3 coated TNT surface and (inset) zoomed in image

Illustrated in Figure 3.5 are the XRD patterns of the MoO_3 coated TNT, bare TNT and the FTO substrate. For brevity only the thickest MoO_3 coating (10 cycles) is shown. The major sharp peaks observed (Figure 3.5a) in both TNT and coated sample matches the reported anatase TiO_2 diffraction pattern.[25, 108] Given that the thickness of coated MoO_3 layer was approximately ~15 nm (for 10 cycles) as deduced from the SEM image (Figure 3.2); it was difficult to obtain high intensity peaks, with reference to the TNT peaks. However, as observed in Figure 3.5b, the enlarged section of the XRD pattern reveals a diffraction peak at 24.3° matching the (110) plane of the α-phase MoO_3. This provides strong evidence that the MoO_3 coating is made of layered planar crystals parallel to the surface of TNT. The number of double layers (1.4 nm for each double layer) of MoO_3 is 10 according to Kalantar-zadeh *et al*..[10, 109]

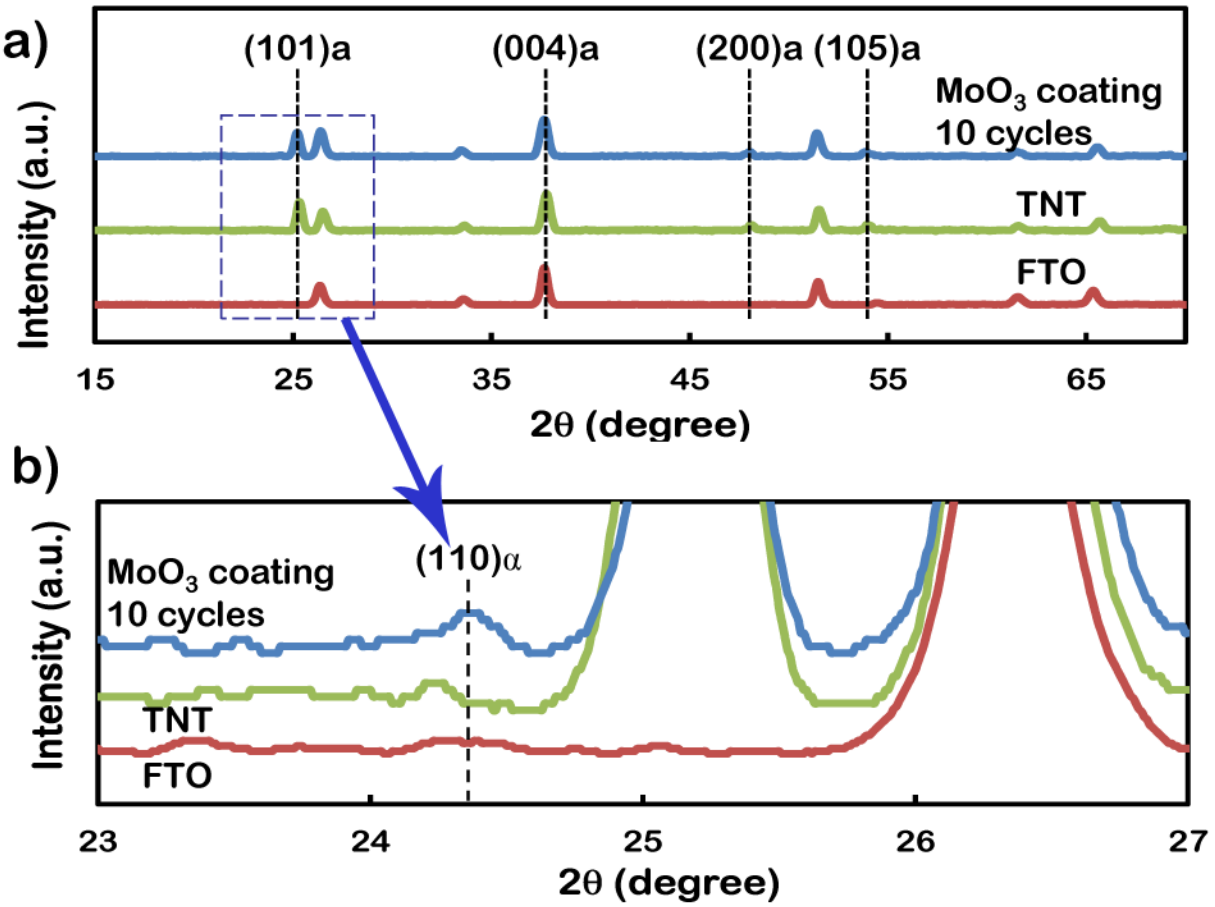

Figure 3.5 a) XRD patterns of the MoO_3 coated TNT film, bare TNT film and FTO substrate, b) zoomed in XRD patterns of a)

In order to ascertain the presence, stoichiometry and crystal phase of the coated MoO_3, XPS and Raman spectra measurements were also carried out. The resulted XPS spectra and data in Figure 3.6 and Table 3.2 illustrate the characteristic binding energies of the Mo 3d photoelectron peaks. XPS spectra of the MoO_3 coated TNT film surface (Figure 3.6) revealed two main peaks located at 235.4 and 232.6 eV, corresponding to Mo $3d_{3/2}$ and Mo $5d_{5/2}$ peaks for Mo^{6+}. Incremental depth profiles were conducted to assess the coverage of the TNT with MoO_3 coating (Table 3.3). The values for the coated sample using 2 cycles are presented in Table 3.2. The atomic content of MoO_3 was higher at the surface, almost dropped to half just under the surface level (depth of 70 nm), and remained constant to a penetration depth of ~1 μm. This is a good indication that the coating was homogenously distributed on the walls of TNT.

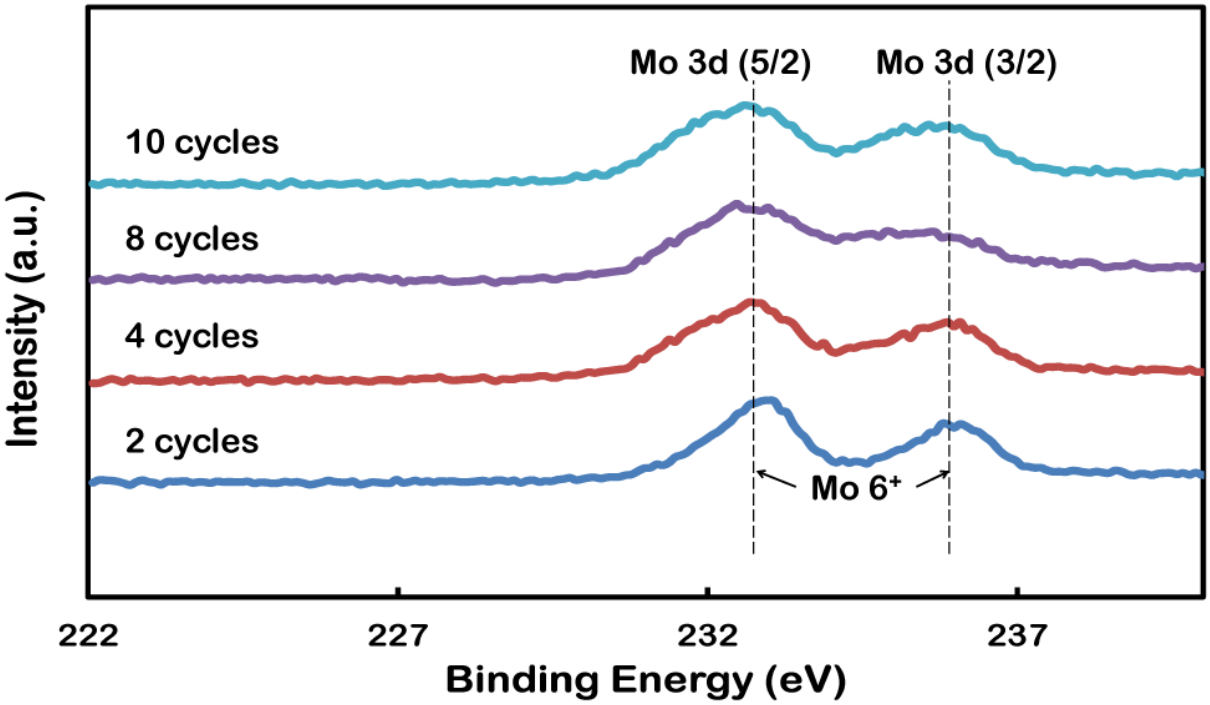

Figure 3.6 XPS spectra of MoO_3 coated TNT films

Table 3.2 XPS depth profile of MoO_3 coated TNT films (for 2 cycles)

Depth (nm)	Atomic percentage (%)
0	3.66
70	1.91
140	1.53
210	1.55
280	1.62
350	1.72
420	1.91
490	1.80
560	1.80
630	1.79
700	1.86
770	1.78
840	1.84
910	1.90
980	1.85

Table 3.3 XPS depth profile of MoO_3 coated TNT films showing the atomic percentage of MoO_3 at the surface and depth of 490 nm for samples formed using 2, 4, 8 and 10 cycles.

Depth	2c	4c	8c	10c
Surface	3.66	4.00	3.74	3.74
490nm	1.80	1.63	2.61	2.12

The deposited MoO_3 crystal phase was further investigated using Raman spectroscopy (Figure 3.7). Two low intensity broad peak regions centred at ca. ~800 and ~980 cm^{-1} are visible in each of the MoO_3 coated samples, corresponding to α-MoO_3. Additionally a peak at ~667 cm^{-1} should also be present for α-MoO_3, however, this peak is overwhelmed by the stronger anatase TiO_2 peak at 663 cm^{-1}. Annealing at 350 °C transformed the as-deposited hydrated MoO_3 coating into crystalline layered α-MoO_3. The presence of α phase MoO_3 is beneficial as it has been reported that this phase (in comparison to the β phase which is obtained at lower annealing temperatures)[77] exhibit more efficient positive ion accommodation and better charge transfer due to its layered nature, which consequently promotes electrochromic responses.

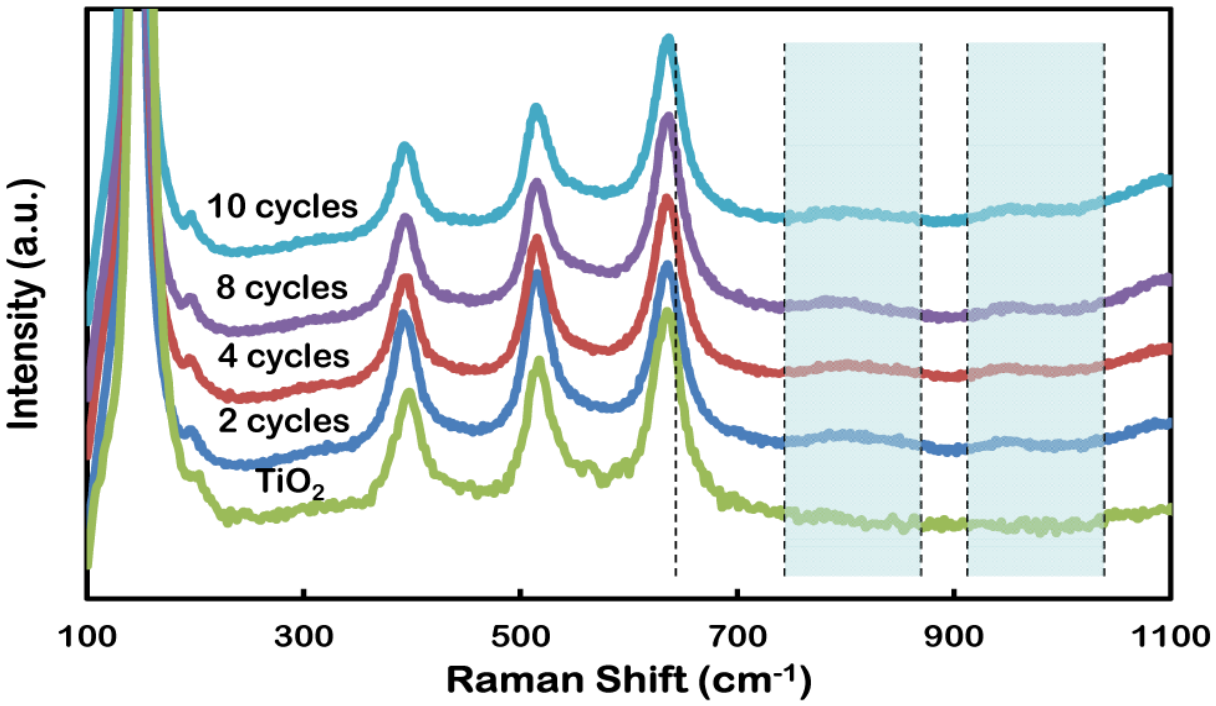

Figure 3.7 Raman shift of bare TNT and MoO_3 coated TNT films

In order to investigate the band-structure properties of the TNT and the coated TNT with MoO_3 (the 10 cycle sample was chosen to obtain the maximum optical effect by MoO_3), Tauc plots of both samples were obtained by extracting their UV-Vis absorbance spectra to estimate their bandgap energies. From Figure 3.8a, it is observed that the bare TNT film bandgap energy (E_g) was measured at 3.34 eV, which is shifted in comparison to bulk anatase TiO_2. This shift in bandgap might be due to the quantization effect, where lattice distortion in nanotube-array films is likely higher, and potentially forcing vacancies along the nanotube walls to become trap states that lead to lower band-to-band transition energy.[110] The coated film had a smaller E_g of 3.29 eV (Figure 3.8a). This alteration of the bandgap structure was induced by the inherently narrower bandgap of pure MoO_3 (~3 eV).[111]

The modification of bandgap-structure between the bare TNT and MoO_3 coated films was also evident from CV measurements (Figure 3.8b) which were carried out at a sweep rate of 0.1 Vs^{-1} between −1 and 1 V in 0.1 M $LiClO_4$. During the negative potential cycle, it was revealed that the MoO_3 coated sample showed the larger amount Li^+ intercalation as presented by the larger cathodic current peak and area. Furthermore, the onset potential

of the cathodic current peak was observed to shift towards more positive potentials which indicate reduced interfacial charge transfer resistance and most likely an altered ionization affinity of the TNT platform underneath. A higher positive maxima (defined as the anodic peak) was seen for the MoO_3 coated sample, which indicated higher electron de-intercalation during the reverse potential sweep. The anodic peak for the coated sample also shifted towards more positive potential, which also indirectly reflected a change in the film's band edge. This suggests that the MoO_3 coating of the TNT film increases the film's capability to accommodate more intercalated charges, and alters the band structure of the TiO_2 platform. Additionally, it is expected that implementing electron scavenging materials with the proper electronic structures, with reference to the electronic structure of MoO_3, can improve the charge transfer and subsequently augment the electrochromic performance.

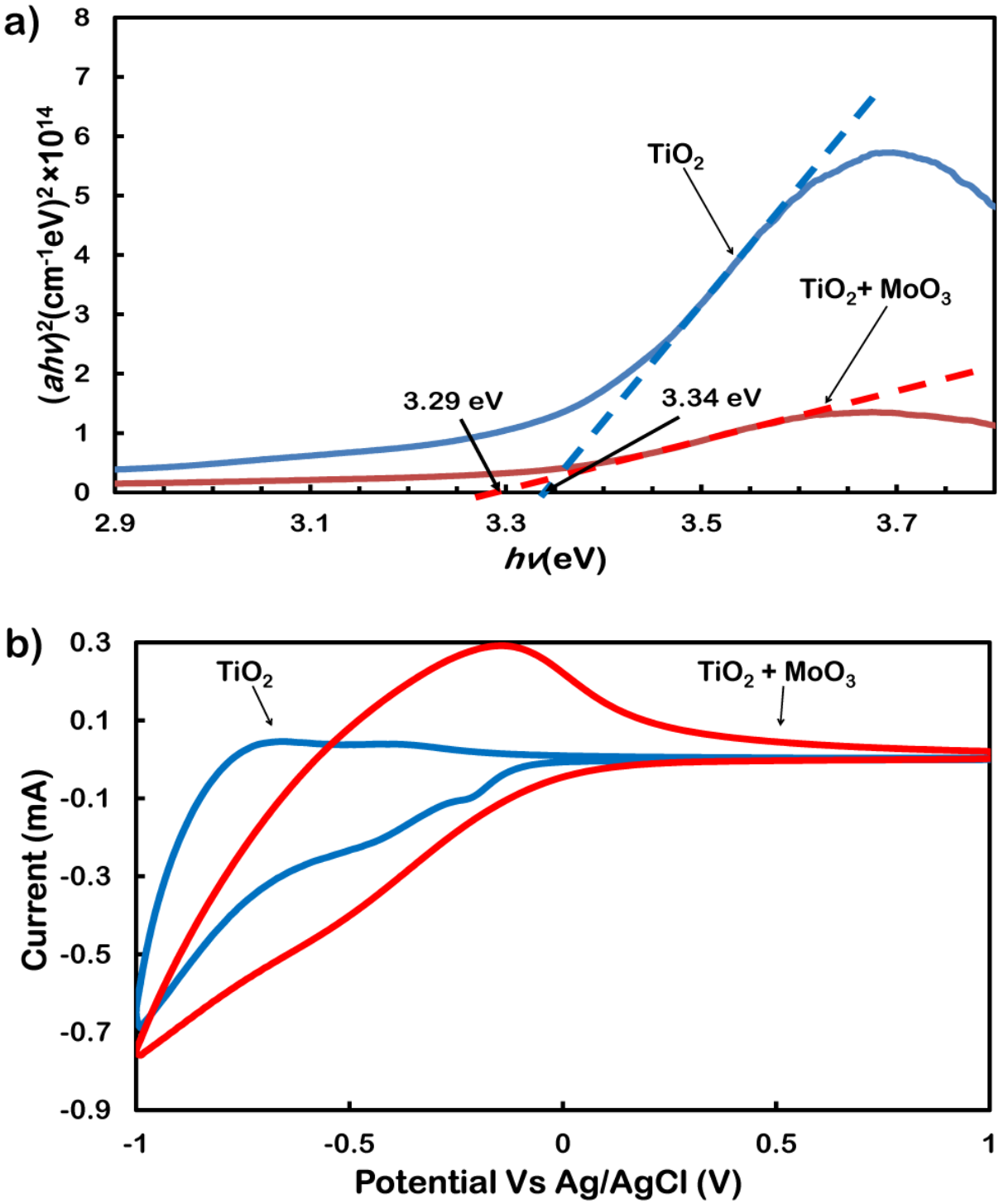

Figure 3.8 a) Tauc plot illustrating the bandgap of the bare TNT and MoO_3 coated film, b) Cyclic voltammogram of bare TiO_2 and MoO_3 coated films.

In situ transmittance measurements were carried out in conjunction with CVs during the band structure investigation after an initial measurement of the transparency (Figure 3.9) for all samples.

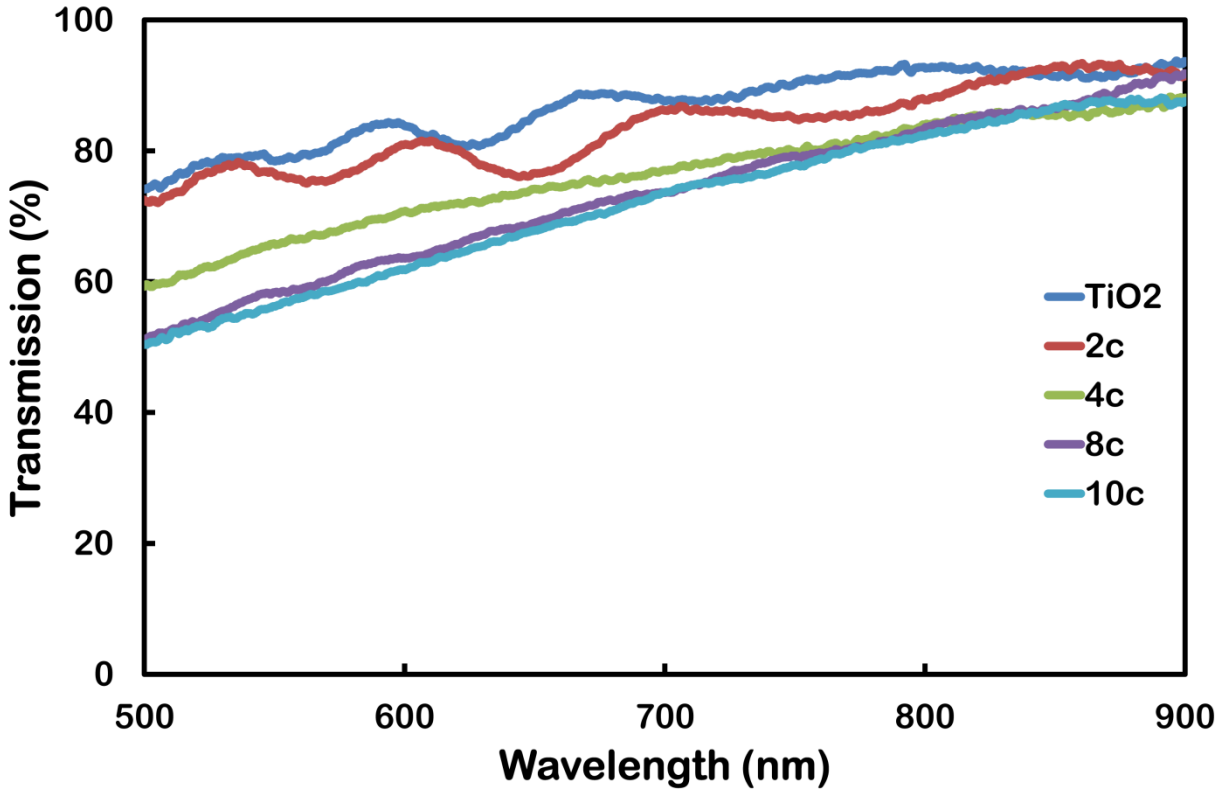

Figure 3.9 The pre-coloration transmission of every sample is presented to compare the initial transparency.

The resulting *in situ* transmittance responses at 550 nm were obtained for the bare TNT and MoO_3 coated films (Figure 3.10a). The optical modulation is presented by the optical density change (ΔOD) of the electrochromic (EC) layer. The ΔOD is a crucial factor in determining the performance of EC materials and it can be calculated from the following equation:[3]

$$\Delta OD = \log(\frac{T_b}{T_c}) \qquad (1)$$

where T_b and T_c refer to the transmittance of the EC layer in its bleached and coloured states, respectively. The bare TNT film achieved ~ 0.02 ΔOD and all MoO_3 coated films achieved higher ΔOD. These results indicated coated films exhibited superior electron injection efficiency between the MoO_3 and TiO_2 layers, which drastically increased the EC capabilities of the bare TNT films. Interestingly, the ΔOD values for the samples prepared with 8 and 10 deposition cycles decreased in comparison to the lower deposition cycles.

The MoO_3 coating using 4 cycles is seen to achieve the optimal response having obtained the best ΔOD of 0.08, which is 4-fold higher than that of the bare TNT film (Figure 3.11). The repeatability of this sample was also investigated (Figure 3.10b and Figure 3.12). Significantly, no noticeable degradation in the optical modulation, response and recovery kinetics up to 1000 continuous coloration/bleaching cycles was observed. The discussion regarding the better performance of the coating obtained at 4 cycles is presented later in this section.

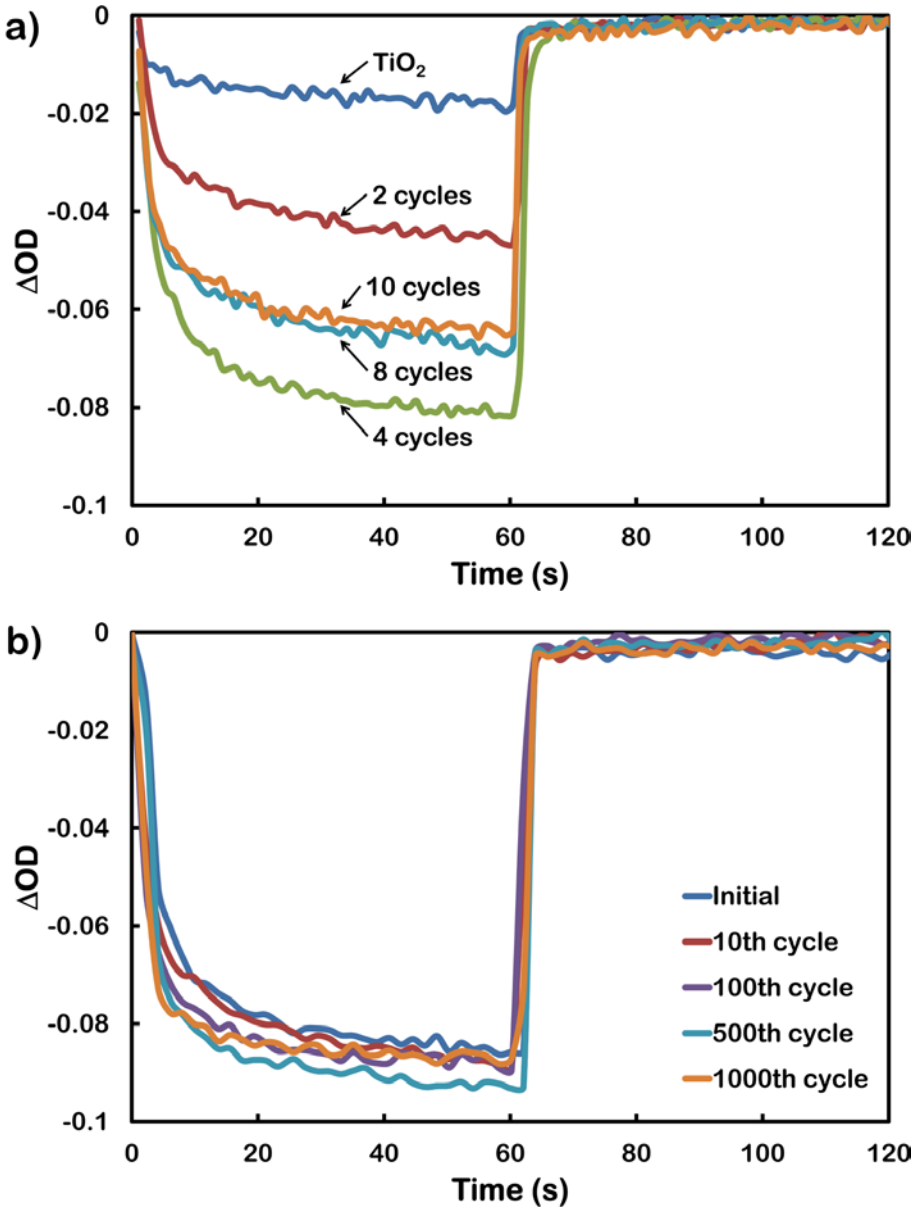

Figure 3.10 a) *In situ* transmittance of bare TNT and coated samples and b) Electrochromic stability of the 4 cycled MoO_3 coated TNT

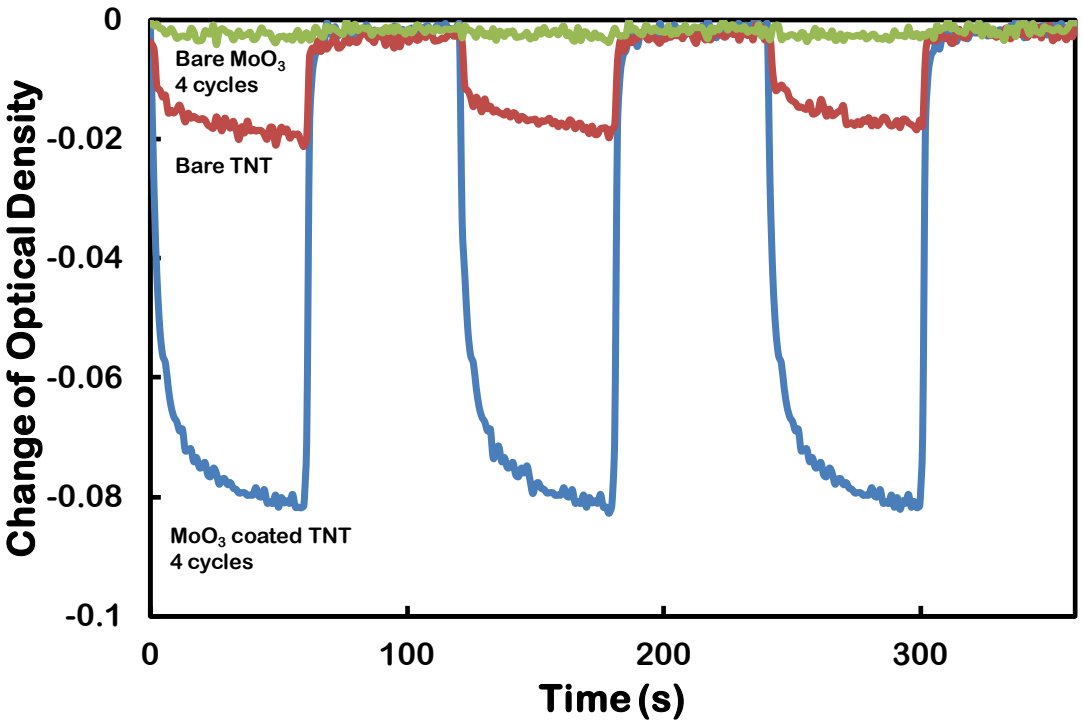

Figure 3.11 In situ transmittance of bare TNT, 4 cycled MoO_3 coated TNT

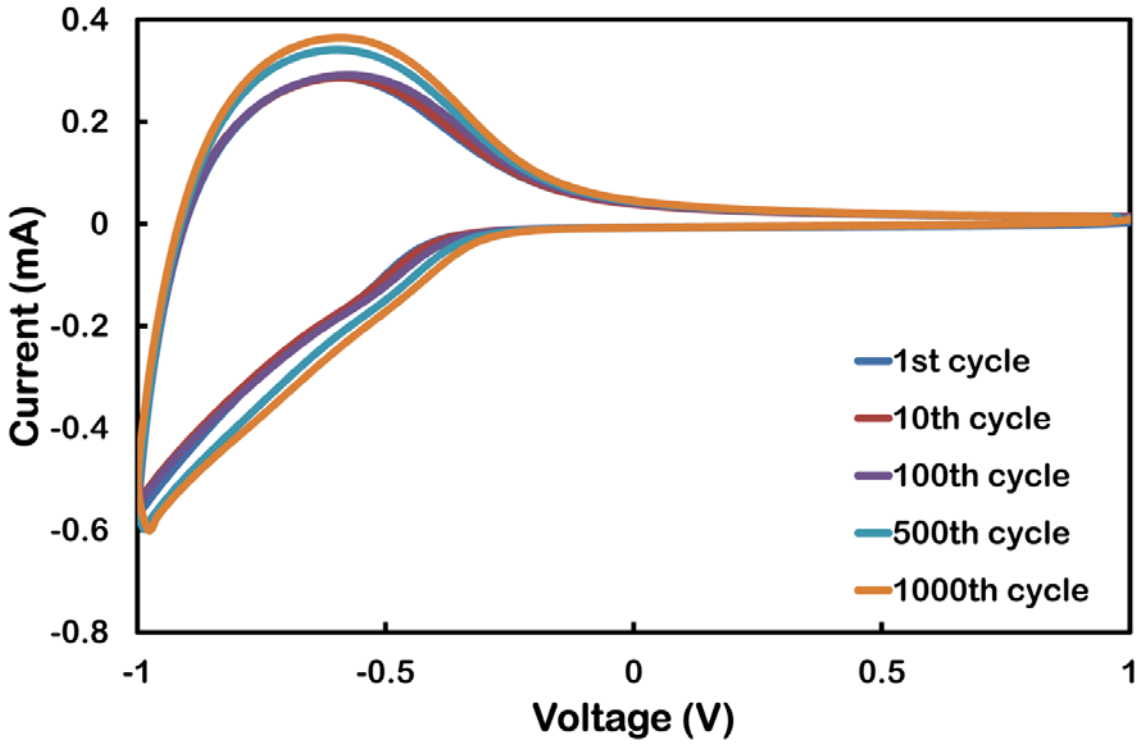

Figure 3.12 Cyclic voltammograms of the stability test for the 4 cycled coated sample

During the EC process, equal quantities of positive ions (*i.e.* Li^+ in this work) and electrons are injected upon the application of a sufficiently negative potential. A transition in the valence states of the metal ions in the EC material induces the coloration phenomenon.[6]

Such an electro-optical process can be further divided into two states. The ‘shallow’ state refers to the initial ions and electron intercalation state in an EC material, where Li^+ ions are free to diffuse throughout the host structure of the metal oxides.[6] The local polarisation induces a transition from the ‘shallow’ state to a ‘trapped’ state, in which a polarisation of the intercalated Li^+ ions to nearby electrons alters the valence state of the adjacent metal atoms. This changes the bandgap of TMOs and results in coloration. The reverse occurs during the bleaching process. We therefore ascribe the superior EC performance of MoO_3 coated TNT in comparison to bare TNT to the following reasons:

MoO_3 coating of the TNT platform forcibly alters the conduction bands towards more negative values (Figure 3.8 and Figure 3.13). Therefore the coated material more readily accommodates Li^+ ions and electrons at relatively lower applied potentials.

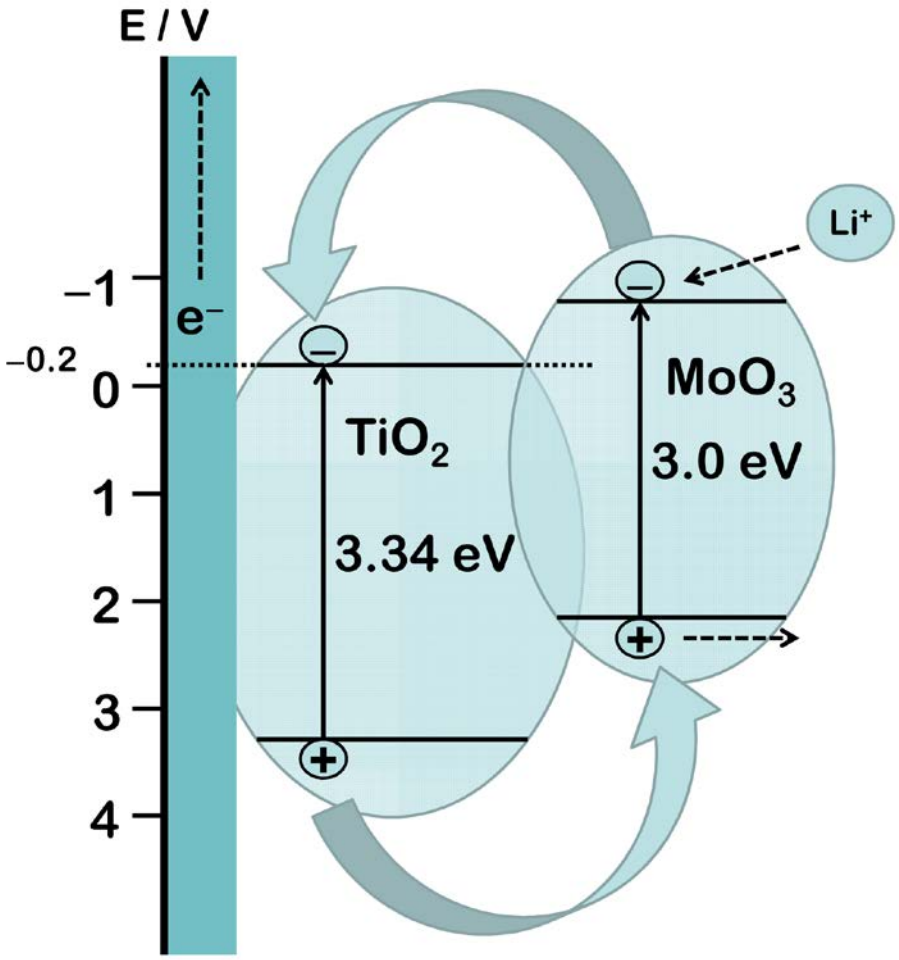

Figure 3.13 Band structure coupling of TNT and coated MoO_3

The deposited MoO_3 has been annealed at 350 °C to produce α-MoO_3. This coated α-

MoO_3 offers excellent intercalation sites due to its intrinsically layered structure and exhibits better charge carrier transportation and provides low scattering conduction paths in comparison to TNT (Figure 3.14).[109]

With the coatings achieved using 2 and 4 deposition cycles, the deposited MoO_3 layers are quite thin (less than 5 nm) and in the few nanometre range (schematically shown in Figure 3.14b), intercalated Li^+ ions and electrons experience only the 'shallow' states, and therefore can efficiently diffuse into the underlying TNT platform.[6] However using 8 and 10 deposition cycles, the deposited MoO_3 layer is much thicker (~10 nm), and therefore some of the intercalated Li^+ ions and electrons are trapped in the MoO_3 layers (Figure 3.14c), which are unable to diffuse as effectively into the TNT as seen for the thinner samples.

Another possibility in the reduction of the EC effect for the 8 and 10 cycle samples is the small size of the pores. Smaller pores hinder the effective diffusion of the electrolyte into the pores and therefore reduce the chance of Li^+ interaction with the surface of MoO_3 (Figure 3.14c)

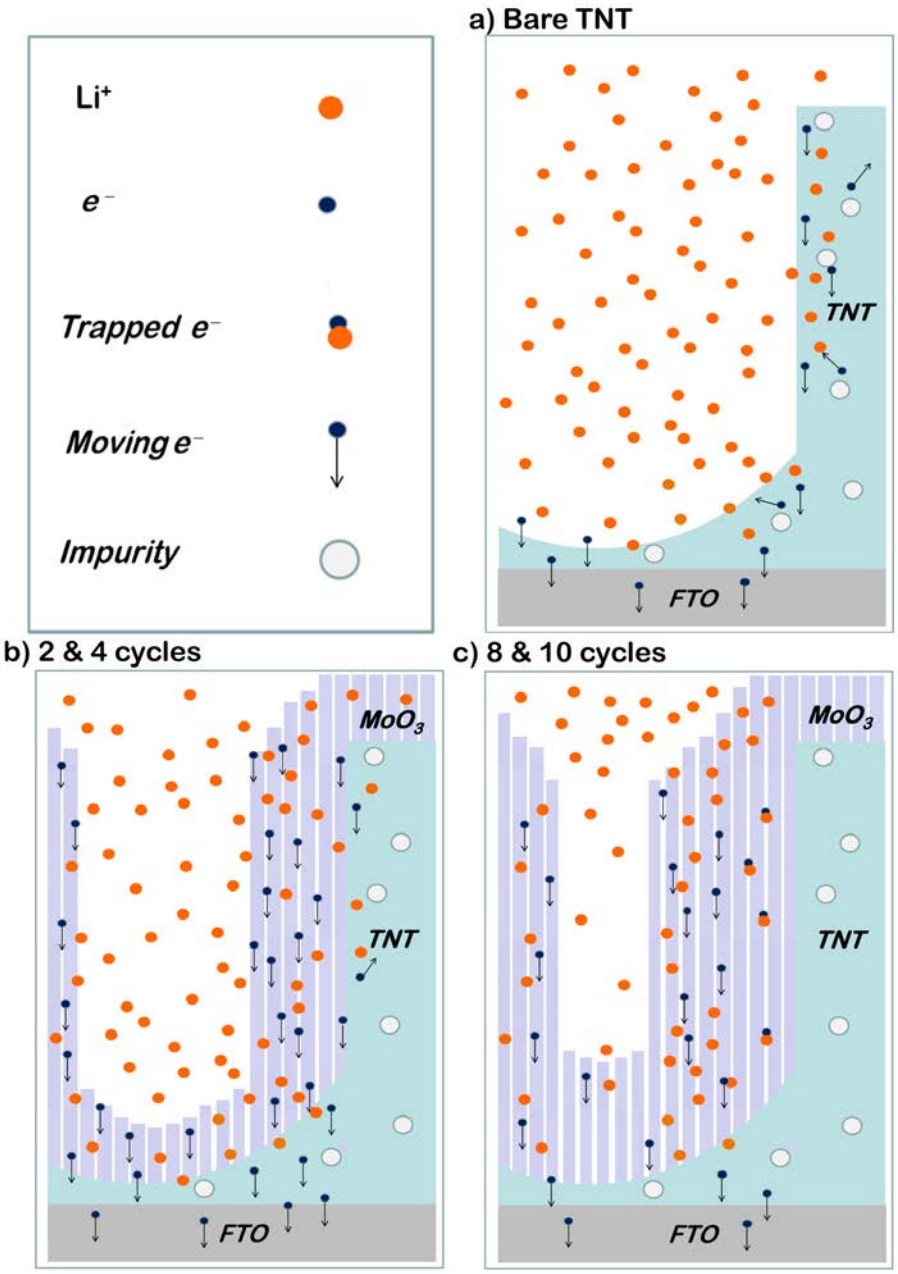

Figure 3.14 Schematic of Li^+ intercalation in bare TNT and MoO_3 coated TNT obtained at different cycles

3.4 Summary

In this chapter, the author demonstrated the synthesis of highly ordered TiO_2 nanotube arrays of 1 μm thickness with 70 and 95 nm inner and outer diameters, respectively, on FTO substrates using an anodization method. He achieved uniform MoO_3 coatings from 5 to 15 nm on the TNT platform by employing a facile electrodeposition technique. The results here revealed that the coating was the α-phase of MoO_3 which deposited parallel to the surface of the TNT platform in a highly homogenous manner. UV-Vis and EC

measurements of these coated films demonstrated a reduction in the bandgap and shifting of the band edges of the overall system which resulted in superior charge transfer performance. These augmentations gave rise to significant improvements in the electrochromic properties of the MoO_3 coated TNT in comparison to bare TNT in terms of both optical density and repeatability. These results indicate that coating TNT with thin layers of MoO_3 offers a viable method for the fabrication of efficient electrochromic devices. For future investigations, the author believes other molybdenum oxide compounds such as MoO_2 also exhibit potential as complimentary material for nanoscale coatings and should be investigated.[13, 112]

In the next chapter, the author will present EC devices based on well ordered anodized Nb_2O_5 as an additional TMO candidate for chromic systems.

References

1. Yao, D. D.; Field, M. R.; O'Mullane, A. P.; Kalantar-zadeh, K.; Ou, J. Z., Electrochromic Properties of TiO_2 Nanotubes Coated with Electrodeposited MoO_3. *Nanoscale* 2013, *5,* 10353-10359.

2. Zheng, H. D.; Sadek, A. Z.; Breedon, M.; Yao, D.; Latham, K.; du Plessis, J.; Kalantar-Zadeh, K., Fast Formation of Thick and Transparent Titania Nanotubular Films from Sputtered Ti. *Electrochem. Commun.* 2009, *11*, 1308-1311.

3. Zhang, W. F.; He, Y. L.; Zhang, M. S.; Yin, Z.; Chen, Q., Raman Scattering Study on Anatase TiO_2 Nanocrystals. *J. Phys. D-Appl. Phys.* 2000, *33*, 912-916.

4. Balendhran, S.; Walia, S.; Nili, H.; Ou, J. Z.; Zhuiykov, S.; Kaner, R. B.; Sriram, S.; Bhaskaran, M.; Kalantar-zadeh, K., Two-Dimensional Molybdenum Trioxide and Dichalcogenides. *Adv. Funct. Mater.* 2013, *32*, 3952-3970.

5. Kalantar-zadeh, K.; Tang, J. S.; Wang, M. S.; Wang, K. L.; Shailos, A.; Galatsis, K.; Kojima, R.; Strong, V.; Lech, A.; Wlodarski, W.; Kaner, R. B., Synthesis of Nanometre-Thick MoO_3 Sheets. *Nanoscale* 2010, *2*, 429-433.

6. Yao, D. D.; Ou, J. Z.; Latham, K.; Zhuiykov, S.; O'Mullane, A. P.; Kalantar-zadeh, K., Electrodeposited A- and B-Phase MoO_3 Films and Investigation of Their Gasochromic Properties. *Cryst. Growth Des.* 2012, *12*, 1865-1870.

7. Mor, G. K.; Varghese, O. K.; Paulose, M.; Grimes, C. A., Transparent Highly Ordered TiO_2 Nanotube Arrays Via Anodization of Titanium Thin Films. *Adv. Funct. Mater.* 2005, *15*, 1291-1296.

8. Chu, C.-W.; Li, S.-H.; Chen, C.-W.; Shrotriya, V.; Yang, Y., High-Performance Organic Thin-Film Transistors with Metal Oxide/Metal Bilayer Electrode. *Appl. Phys. Lett.* 2005, *87*, 193508.

9. Ou, J. Z.; Balendhran, S.; Field, M. R.; McCulloch, D. G.; Zoolfakar, A. S.; Rani, R. A.; Zhuiykov, S.; O'Mullane, A. P.; Kalantar-zadeh, K., The Anodized Crystalline WO_3 Nanoporous Network with Enhanced Electrochromic Properties. *Nanoscale* 2012, *4*, 5980-5988.

10. Bueno, P. R.; Gabrielli, C.; Perrot, H., Coloring Ionic Trapping States in WO_3 and Nb_2O_5 Electrochromic Materials. *Electrochim. Acta* 2008, *53*, 5533-5539.

11. Zhou, L.; Wu, H. B.; Wang, Z.; Lou, X. W., Interconnected MoO_2 Nanocrystals with Carbon Nanocoating as High-Capacity Anode Materials for Lithium-Ion Batteries. *ACS Appl. Mater. Interfaces* 2011, *3*, 4853-4857.

12. Wang, Z.; Chen, J. S.; Zhu, T.; Madhavi, S.; Lou, X. W., One-Pot Synthesis of Uniform Carbon-Coated MoO_2 Nanospheres for High-Rate Reversible Lithium Storage. *Chem. Commun.* 2010, *46*, 6906-6908.

Chapter 4

High Performance Electrochromic Devices based on Anodized Nanoporous Nb_2O_5

4.1 Introduction

In the previous chapter, the author showed binary electrochromic (EC) devices based on anodized ordered titanium dioxide (TiO_2) nanotube templates and coated them with electrodeposited α-MoO_3. He demonstrated uniform MoO_3 coatings from 5 to 15 nm on the TiO_2 nanotubular templates by employing a facile electrodeposition technique. The results revealed that the stratified α-MoO_3 coating was made of layers parallel to the template surface in a highly homogenous manner. Comprehensive characterization revealed these coated films demonstrated a reduction in the bandgap and shifting of the band edges over the overall system which resulted in a superior charge transfer performance. These augmentations gave rise to significant improvements in the electrochromic (EC) properties of the binary system in comparison to the bare TiO_2 platform in terms of both optical density and repeatability, thus overcoming the performance limitations of each individual transition metal oxides (TMOs) used.

Having demonstrated valid experimental results for overcoming performance limitations of binary TMOs based on anodized TiO_2 template, the author chose to investigate anodized niobium oxide (Nb_2O_5). Based on analysis presented in chapter 1, Nb_2O_5 is potentially a great candidate for chromic systems. Nb_2O_5 is a TMO with excellent durability and specific chromic performance. However, due to its relatively high bandgap, it has been frequently discredited as a viable EC material. In this PhD research, the author developed EC devices based on anodized ordered nanoporous Nb_2O_5, which is in line with the core focus

of the electric field driven techniques for this thesis. The author will show some specific advantages in using anodized Nb_2O_5 for EC systems for the first time.

In this chapter, the author will present the outcomes of the study on the development of EC devices based on anodized ordered nanoporous Nb_2O_5. A comprehensive characterization of the anodized Nb_2O_5 will be presented. The influence of the anodized ordered nanostructure on the performance of the EC devices will be described. Eventually, the fabricated EC devices performance will be compared with devices based on different Nb_2O_5 nanostructures and synthesis methods reported by other groups. The work in this chapter was published as a full article in the Journal of Physical Chemistry C.[113]

4.2 Experimental

4.2.1 Fabrication of nanoporous Nb_2O_5

Nb films of 0.25, 0.37 and 0.5 μm were deposited using a radio frequency (RF) sputtering system fitted with a Nb target (99.95% purity). These Nb films were sputtered onto fluorine-doped tin oxide (FTO, 15 Ω square^{-1}, Dyesol) glass substrates after 15, 22.5 and 30 min at 20×10^{-3} Torr vacuum, 100 W applied RF power and an elevated substrate temperature of 300 °C to enhance film adhesion during anodization. The samples were then placed in a two-electrode cell configuration using the sample (0.8 cm^2) as an anode and a platinum (Pt) foil as the cathode. The anodization was carried out using a potentiostat (CHI-413A electrochemical station) in an electrolyte mix of 50 mL of ethylene glycol (98% anhydrous, Sigma Aldrich) with 0.15 g of NH_4F (98% purity, Sigma Aldrich) and 4% deionized (DI) water. An optimized potential of 10 V was applied between the anode and cathode during anodization. These values for the electrolyte and optimized applied potential were investigated and obtained by Ou *et al*.[24]

The electrolyte was kept at a constant temperature of 50 °C during the anodization process. The anodization duration of 8, 20 and 30 minh for Nb films of 0.25, 0.37 and 0.5

μm thicknesses resulted in obtaining Nb_2O_5 films of 500 nm, 750 nm and 1 μm thicknesses. Similar to the anodization of Ti films, the anodization of Nb layers produced Nb_2O_5 films of almost double the initial metal layer thickness.[25] After the anodization, the samples were carefully washed with DI water and dried in a nitrogen stream. Post anodization annealing was carried out in ambient air at a temperature of 450 °C for 60 min with a slow ramp up and down rate of 2 °C min^{-1}. The thicknesses of the Nb_2O_5 films did not change after the annealing process.

4.2.2 Structural characterization

The Nb_2O_5 films were characterized to assess their structural and morphological properties. X-ray photoelectron spectroscopy (XPS) was conducted using a Thermo Scientific K-alpha instrument with Al Kα source (1486.7 eV). A flood gun was employed during the XPS analysis in order to remove sample charging. X-ray diffraction (XRD) patterns were obtained with a Bruker AX 8: Discover using general area detector diffraction system (GADDS). The Raman spectroscopies were performed using a 532 nm laser at 0.9 mW power with a Jobin Yvon Horiba TRIAX320 spectrometer system incorporating an Olympus BX41 microscope with a 50× objective with ±2 cm^{-1} error margin. Surface morphologies were observed using scanning electron microscopy (SEM) and performed on a FEI Nova Nano instrument.

4.2.3 Electrochromic characterization

Transmittance measurements were carried out using a Fiber Ocean Optics Spectrometer using a UV-Vis-NIR light source (DH-2000, Mikropack, Ocean Optics). *In situ* transmittance characterization was conducted at room temperature also using the CHI-413A electrochemical station *via* a three electrode configuration, employing the coated samples as working electrode (exposed area of 0.8 cm^2), and a Pt wire (0.5 mm diameter,

BASi Platinum Wire) as the counter electrode, together with an Ag/AgCl (3 M KCl) (BASi) reference electrode. The electrolyte used was 0.1 M $LiClO_4$ in propylene carbonate (98% anhydrous, Sigma Aldrich).

4.3 Results and discussions

The Nb anodization process, which is used in this work, has been previously developed and investigated by Ou *et al* and Rani *et al* to fabricate Nb_2O_5 nanoporous films for DSSC applications.[24, 28] They demonstrated that the anodized Nb_2O_5 exhibit low embedded impurities *via* carefully chosen parameters that are also used in work by Ou *et al* (as described in the Experimental section).[24] Their films were stable and rigid up to the thickness of 5 µm. Additionally, the surface area has been impressively large: effectively double that of the area of the anodized TiO_2 counterpart with the same thickness. In this paper, the same method has been adopted to produce films with thicknesses of less than 1 µm that are appropriate for electrochromic applications.

The XPS spectra of the annealed Nb_2O_5 samples were taken in order to investigate the binding energy of the anodized Nb species and verify their stoichiometry after annealing. As shown in Figure 4.1 only two peaks were observed at 207.5 and 210.3 eV, which corresponds to the $3d_{5/2}$ and $3d_{3/2}$ peaks of the Nb^{5+} species, respectively.[114-115] The measured peaks were identical for the 500 nm, 750 nm and 1 µm thick samples, signifying the synthesis technique produces Nb_2O_5 films with consistent stoichiometry over a wide range of thicknesses at the given fabrication parameters.

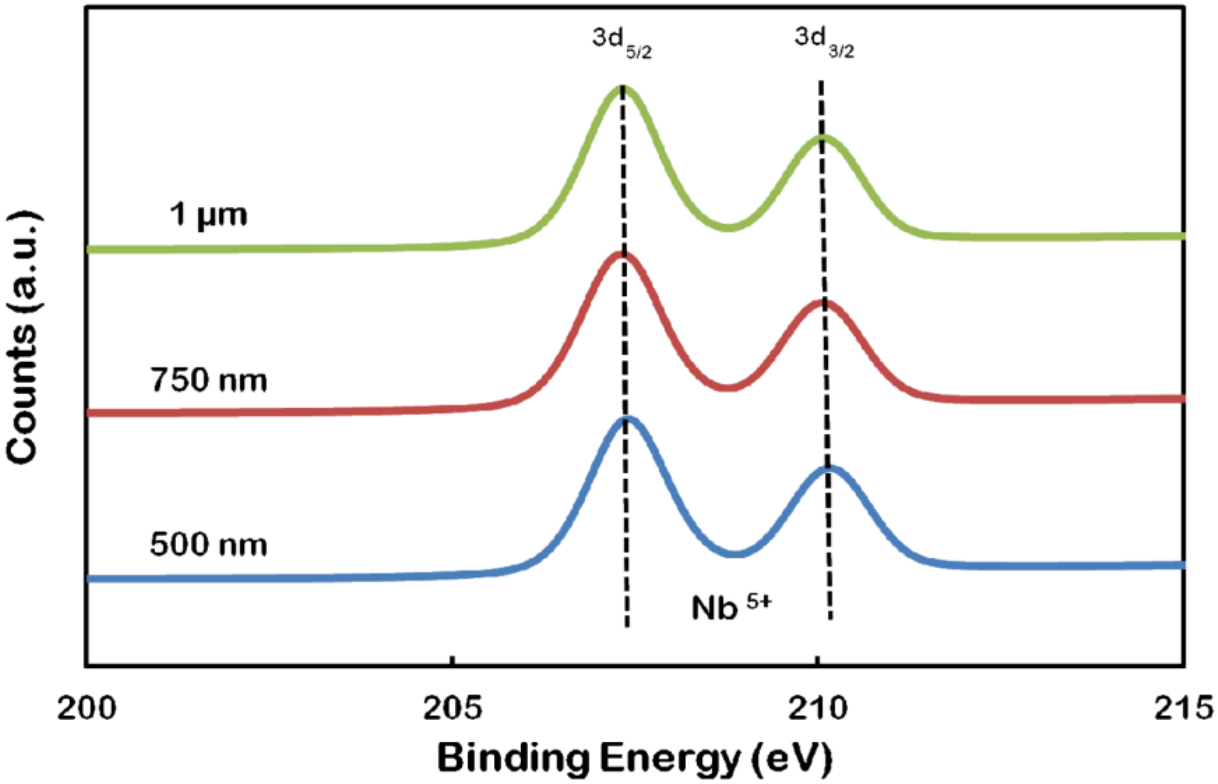

Figure 4.1 XPS spectra of Nb_2O_5 films with 500 nm, 750 nm and 1 µm thicknesses.

XRD measurements were carried out to examine the crystalline structures, and the resulting XRD patterns are shown in Figure 4.2. As can be observed, the as-anodized film revealed some Nb diffraction peaks in addition to the obvious FTO peaks. However a lack of Nb_2O_5 diffraction peaks indicates the film was amorphous. The as-anodized films underwent a significant crystallization as a result of annealing. The annealing temperature of 450 °C transformed the as-anodized amorphous Nb_2O_5 to orthorhombic phase of Nb_2O_5. The 60 min annealing duration caused a complete phase transition with minimal morphology structure breakdown. As a result, visible sharp peaks at 22.6°, 28.4°, 36.6°, 46.2° and 55.1° corresponding to orthorhombic structure Nb_2O_5 (a = 6.175 Å, b = 29.175 Å, and c = 3.93 Å) are seen.[24, 82, 116] There are noticeably more FTO peaks post-annealing, however these are merely the byproducts of different diffraction angle during XRD analysis, and it does not affect the Nb_2O_5 film characteristics in any way.

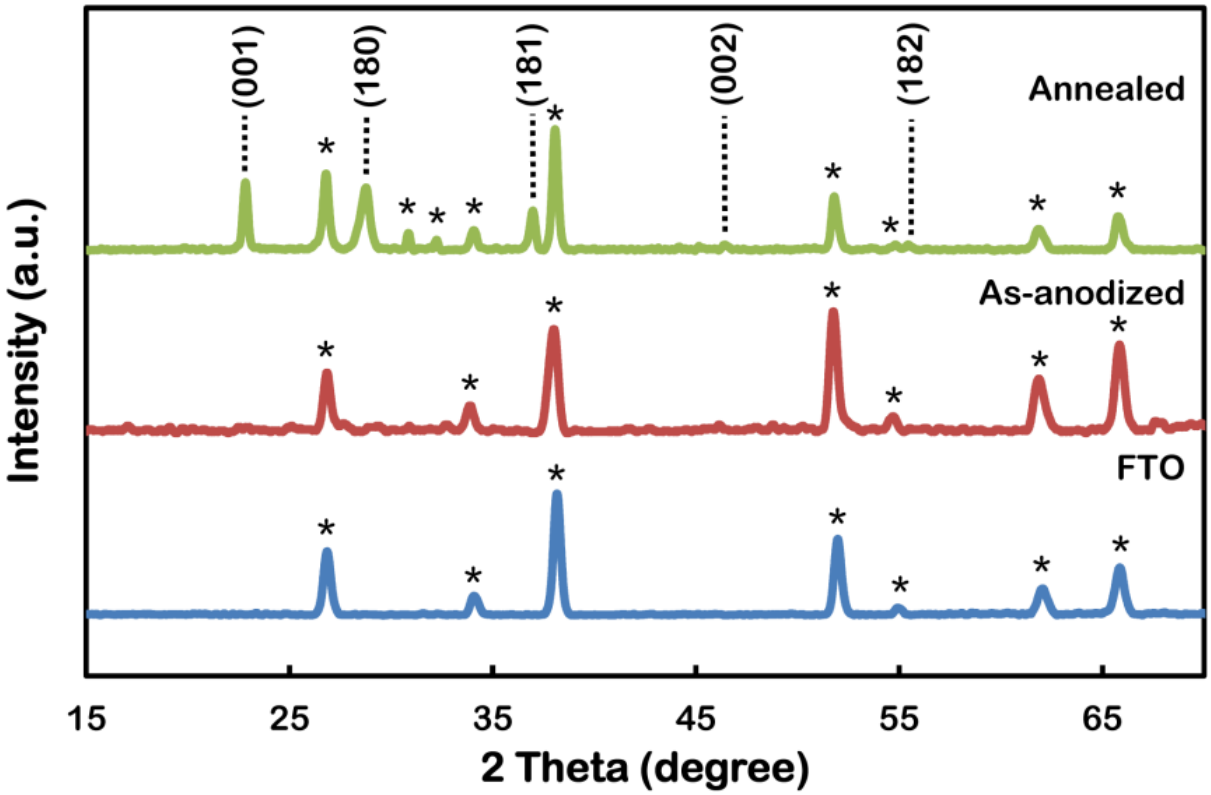

Figure 4.2 XRD diffraction patterns of the FTO substrate, as-anodized and annealed samples. * denotes FTO peaks.

This result was further verified by the Raman spectra presented in Figure 4.3. The broad peaks centered over 250 cm^{-1} (stretching mode *v* O−Nb−O) and 650 cm^{-1} (bending mode Nb−O−Nb) are indicative of the amorphous niobium oxide. After annealing, sharp peaks at 248, 305 and 694 cm^{-1} rose dominantly over the rest of the spectra which correspond to the orthorhombic phase of crystalline Nb_2O_5.

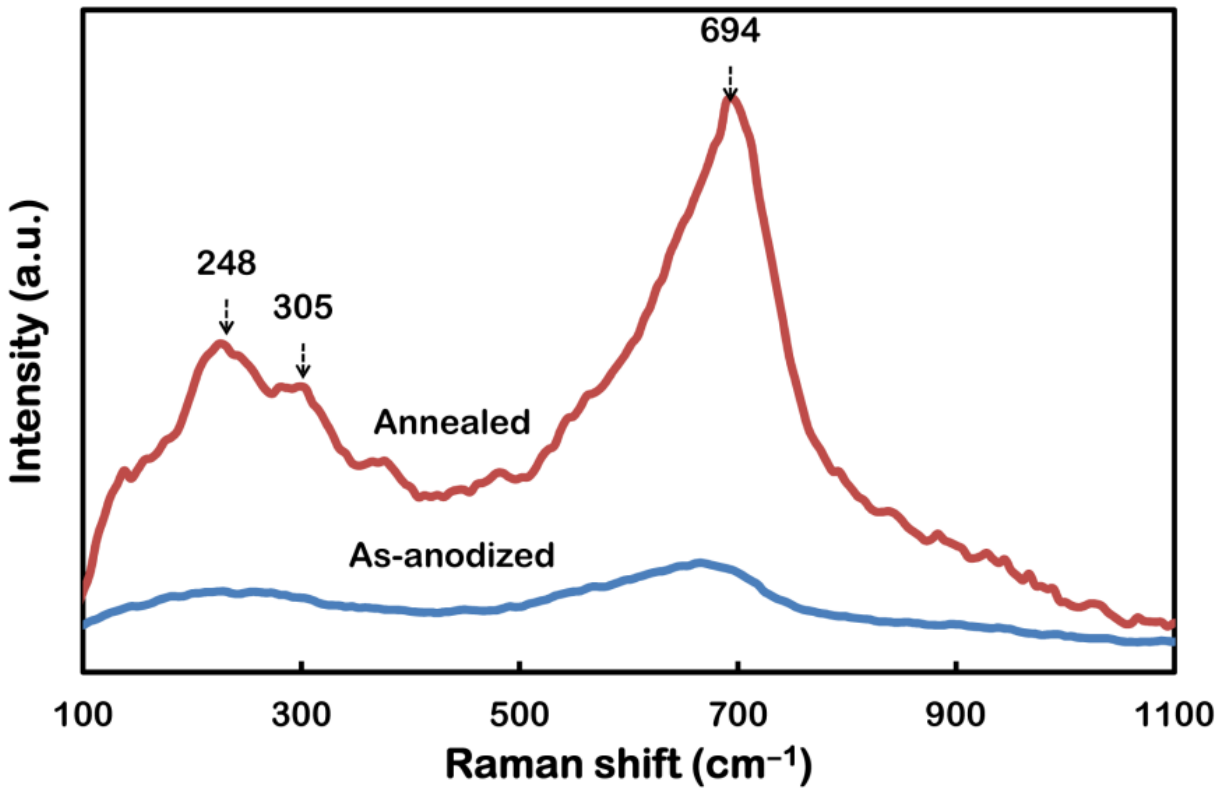

Figure 4.3 Raman spectra of the as-anodized and annealed Nb_2O_5 films.

The surface and cross sectional SEM images of the as-anodized and annealed Nb_2O_5 films are presented in Figure 4.4. The anodized films appeared indistinguishable before and after annealing (Figure 4.5), suggesting the as-anodized films are thermally stable up to 450 °C. Nanoporous morphologies are visible on the surface of Nb_2O_5 films in agreement with previous report.[24] Upon closer examination from the cross-sectional SEM images (Figure 4.4 c and d), it is revealed that the morphology resembles that of a three dimensional (3D) nanoporous network with a good vertical order. This nanoporous network holds great prospect for Li^+ intercalation, as the significantly increased surface area allows substantial amount of Nb_2O_5 exposure to Li^+ ions in the electrolyte.

The initial optical properties of the Nb_2O_5 films are investigated by comparing visible transmittance spectra in bleached and colored states. It is observed (Figure 4.6) that for all samples the bleached state has an exceptionally high transparency with the thickest sample of 1 µm being over 80% transparency, while both the 750 and 500 nm thick samples are over 90% transparency. Higher transparency during the bleached state enables larger optical modulation, which provides an excellent basis for high performance

EC devices. In order to assess the optical modulation of the Nb_2O_5 films, chronoamperometric (CA) measurements were performed by applying alternating potentials at ± 1, ±1.5 and ±2 V (*vs.* Ag/AgCl in 3M KCl) in 60 s steps. Each negative potential step (−1, −1.5 and −2 V) induces a coloration state (intercalation of Li^+ ions) and the respective positive potential steps induce the corresponding bleached states (deintercalation).

$$\mathrm{Nb_2O_5} + x\mathrm{Li^+} + xe^- \Leftrightarrow \mathrm{Li}_x\mathrm{Nb_2O_5} \qquad (1)$$

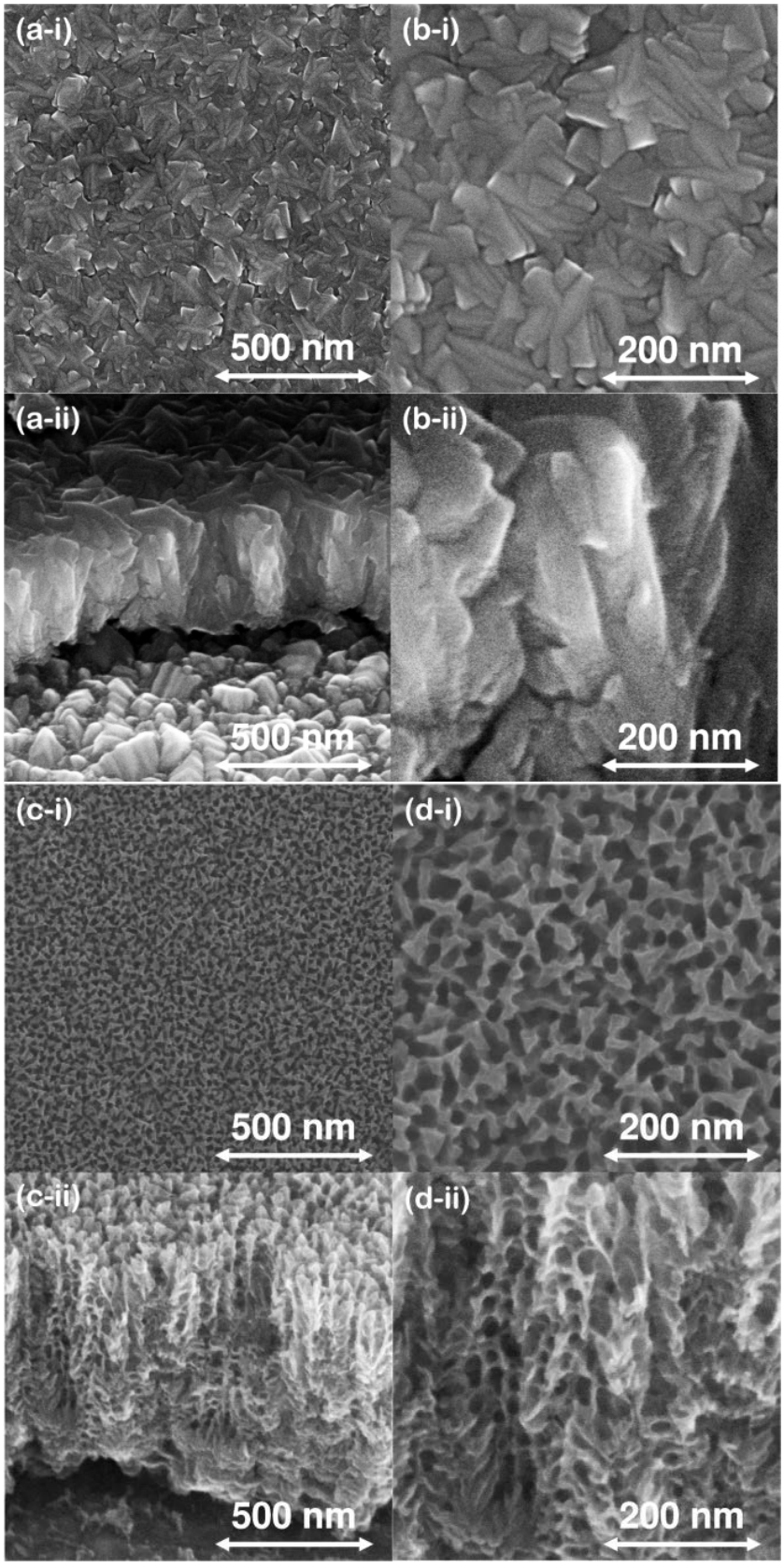

Figure 4.4 SEM images of the (a) and (b) as-sputtered Nb films and (c) and (d) as-anodized Nb_2O_5 films (i) surface and (ii) cross-section views.

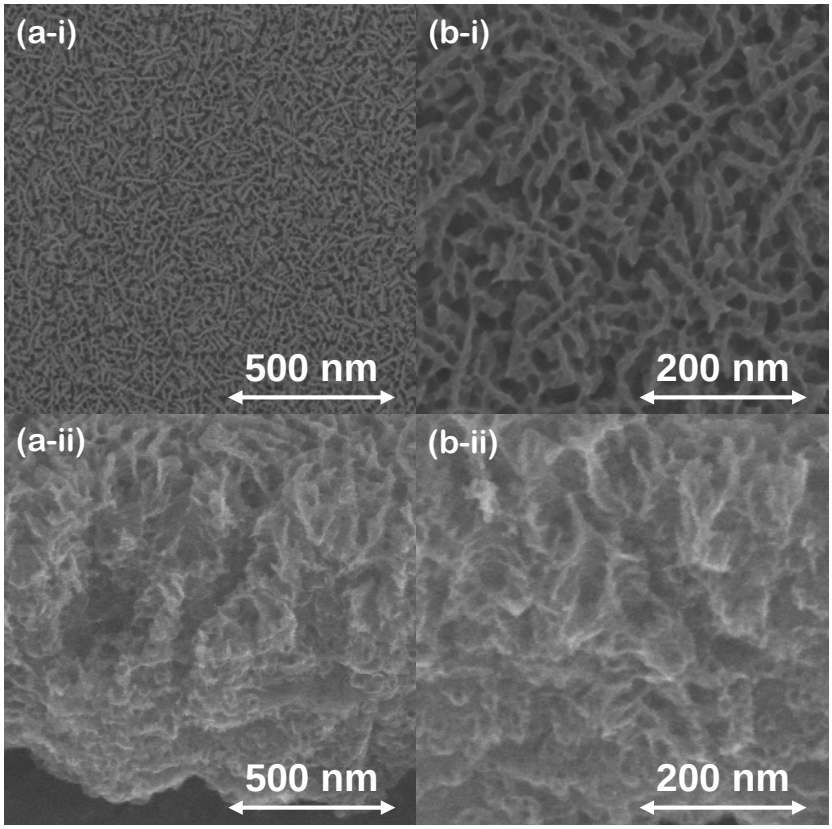

Figure 4.5 Scanning electron microscopy (SEM) images of the (a) and (b) annealed Nb_2O_5 films (i) surface and (ii) cross-section views.

It is observed that while the initial transparencies of the films are quite high, a low potential of −1 V can only achieve optical modulations in the range of 10% to 20% for the 1 μm to 500 nm thick samples. Over 50% optical modulations was achieved from −1.5 V potential across all samples and over 70% optical modulations for −2 V applied potential.

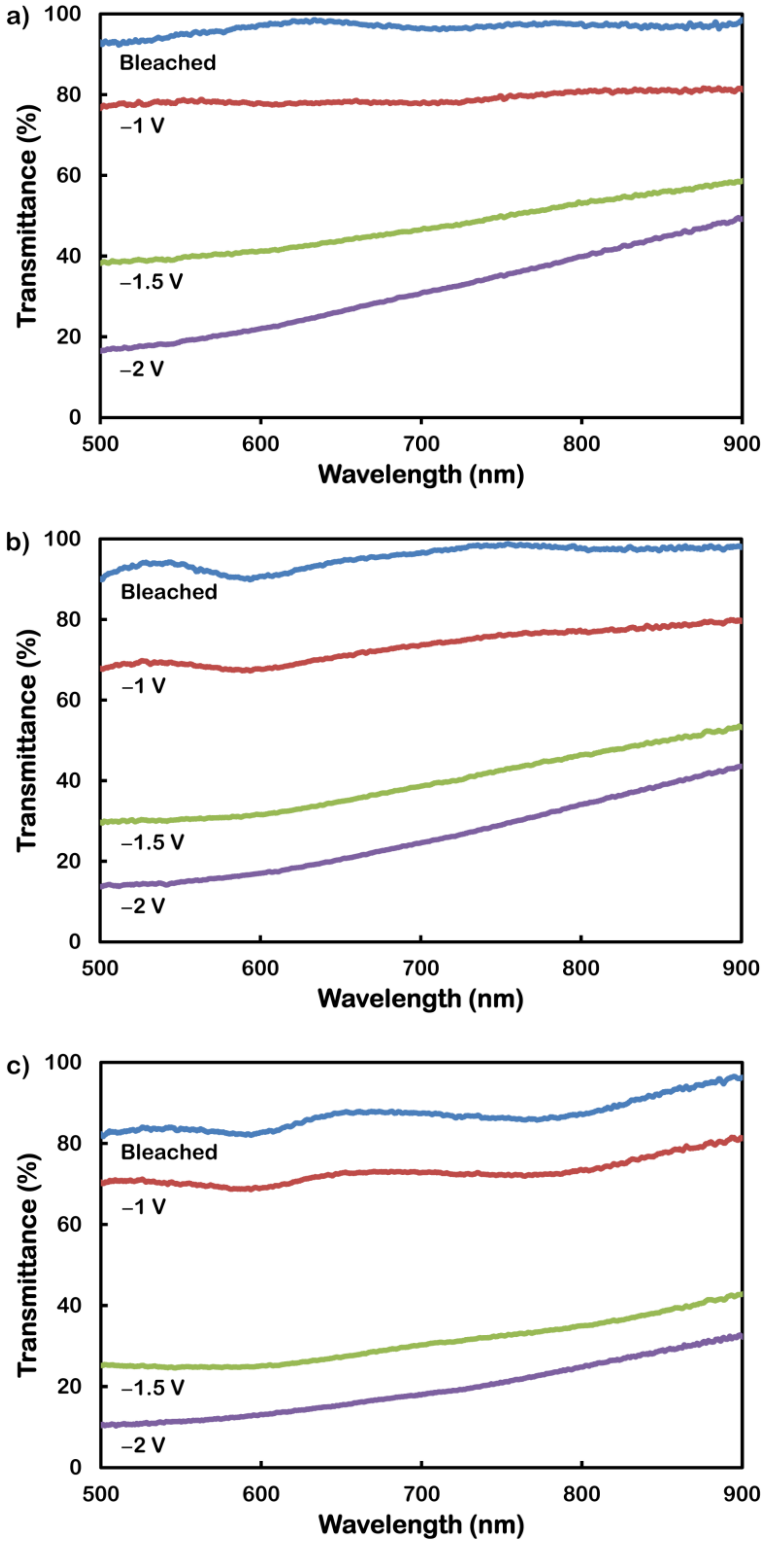

Figure 4.6 The visible transmittance spectra of the Nb_2O_5 films with thicknesses (a) 500 nm, (b) 750 nm and (c) 1 μm at different applied potentials.

The assessment of the coloration-bleaching kinetics and optical modulation are vital for the evaluation of optical and electronic properties of the films. Therefore, *in situ* transmittance changes measured at 550, 650 and 750 nm were carried out in during the CA measurements (Figure 4.7). It is observed that the 500 nm thick sample performed better

in terms of optical modulation and coloration/bleaching time (time estimate for 80% change in full transmittance modulation), also the reversibility appeared to be noticeably superior to the 750 nm and 1 µm thick samples. From Table 4.1, it is evident that the 500 nm thick sample has the overall fastest coloration and bleaching responses. A noticeable feature is that the thicker the samples became, the slower the coloration and bleaching responses became at reaching the corresponding optical modulations. The corresponding chronoamperograms of the *in situ* electrochromic measurements are illustrated in Figure 4.8.

Table 4.1 Coloration and bleaching time for Nb_2O_5 films of different thicknesses.

	±1v		±1.5v		±2v	
Thickness	Color (s)	Bleach (s)	Color (s)	Bleach (s)	Color (s)	Bleach (s)
500 nm	27.4	2.2	17.6	5.1	13.3	7.5
750 nm	30.9	1.9	27.8	6.4	22.6	12.9
1 µm	31.5	2.8	30.7	8.6	24.8	13.1

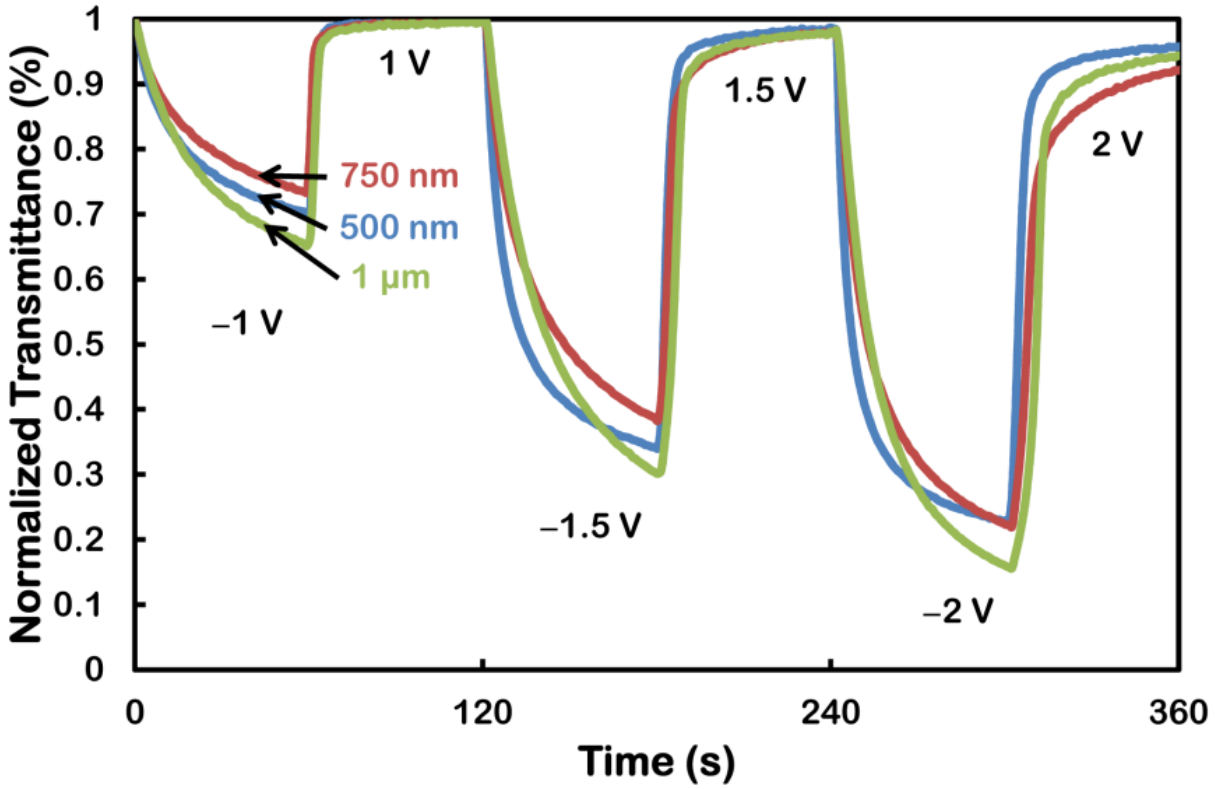

Figure 4.7 *In situ* normalized transmittance for Nb_2O_5 films with thicknesses of 500 nm, 750 nm and 1 µm at ±1, ±1.5 and ±2 V applied potentials for the optical wavelength of 550 nm.

The CE of the Nb_2O_5 films, which is defined as the change in optical density (ΔOD) per unit of charge (ΔQ) intercalated into the EC layers, is a crucial characteristic parameter for comparing the EC performance of the materials. CE and ΔOD can be obtained from the following equations:

$$\mathrm{CE} = \frac{\Delta OD}{\Delta Q} \qquad (2)$$

$$\Delta OD = \log\left(\frac{T_b}{T_c}\right) \qquad (3)$$

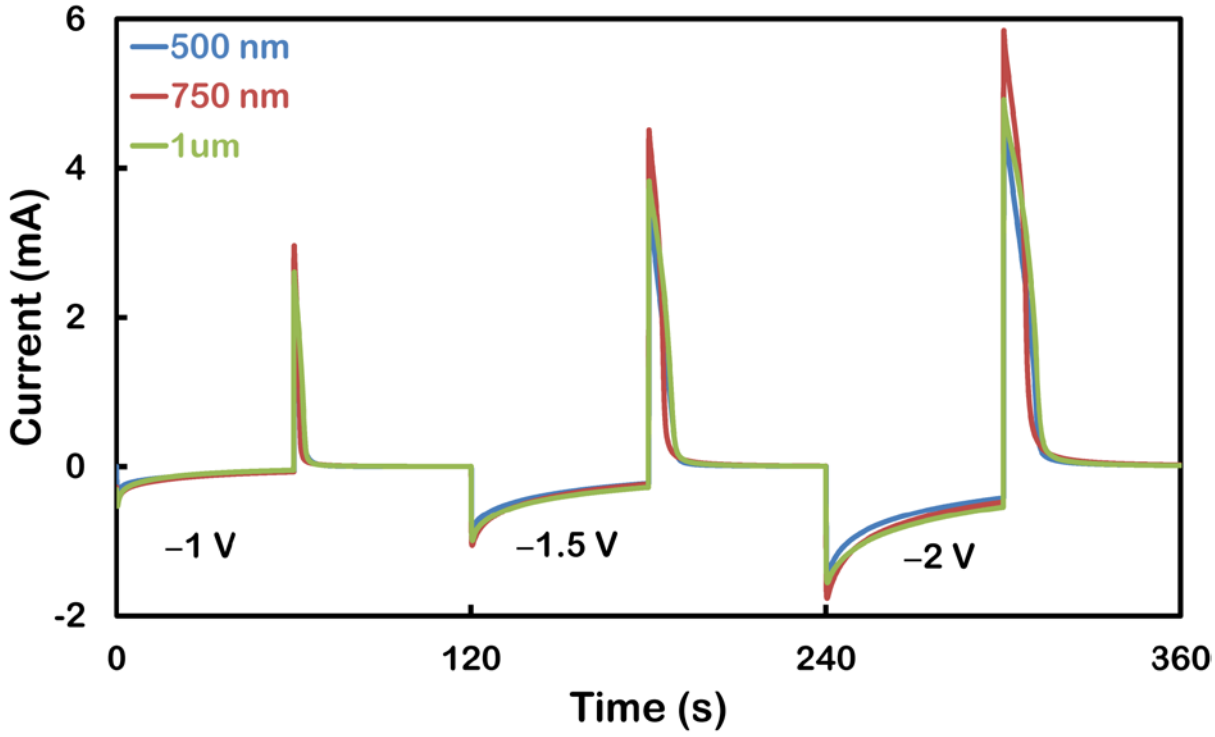

Figure 4.8 Chronoamperometric measurements in correspondence to the *in situ* electrochromic measurements.

where T_b and T_c refer to the transmittance of the layer in its bleached and colored states, respectively. The CE values for each of the three samples (with the thicknesses of 500 nm, 750 nm and 1 μm) at the three different applied potentials (−1, −1.5 and −2 V) are illustrated in Figure 4.9. For the 500 nm thick sample, the calculated CEs are 37.9, 47.0 and 40.3 $cm^2\ C^{-1}$ at −1, −1.5 and −2 V, respectively. As the sample thickness increased to 750 nm, the calculated CEs became 25.7, 27.1 and 25.5 $cm^2\ C^{-1}$ and then 24.2, 25.5 and 22.0 $cm^2\ C^{-1}$ for the thickest sample (1 μm), respectively.

It was evident the Nb_2O_5 films exhibited higher coloration efficiency at an applied potential of –1.5 V even though the optical modulation approached saturation. This is due to the fact that nanostructured Nb_2O_5 innately possess a wider bandgap (~3.8 eV)[87] with respect to other known EC materials such as MoO_3 (~3.1 eV)[111, 117] and WO_3 (~2.8 eV).[118] Therefore, additional energy is required to initiate the intercalation phenomenon for inducing the EC effect. This impedes the efficiency at which Nb_2O_5 may respond to very low potential EC applications.

The stability of the films was assessed by carrying out repeated CVs (Figure 4.10) to investigate the EC performance over 500 continuous coloration-bleaching cycles. It is noted that no major degradation was visible up to 100 cycles, with minor degradation as the continuous CVs approached 500 cycles (Figure 4.11).

In this work, the best CE of 47.0 $cm^2\ C^{-1}$ was calculated at an applied potential of −1.5 V for the 500 nm thick sample. To the authors' knowledge, this CE value, for this set of anodized Nb_2O_5 films, is higher than any previously reported Nb_2O_5 films of other synthesis techniques including sol-gel (42.4 $cm^2\ C^{-1}$ at 633 nm),[119] pulse-laser deposition (40.0 $cm^2\ C^{-1}$ at 550 nm),[86] spray pyrolysis (25.5 $cm^2\ C^{-1}$ at 660 nm)[7] and RF sputtering (16.68 $cm^2\ C^{-1}$ at 550 nm).[85] In comparison to other EC materials fabricated using anodization methods (25 $cm^2\ C^{-1}$ at 550 nm for TiO_2[120] and 141.5 $cm^2\ C^{-1}$ at 750 nm for WO_3[3]), Nb_2O_5 places itself as a competitive EC material with merits such as high bleached state transparencies, multi-color EC performance[78] and versatile options in fabrication.[7, 85-86, 119]

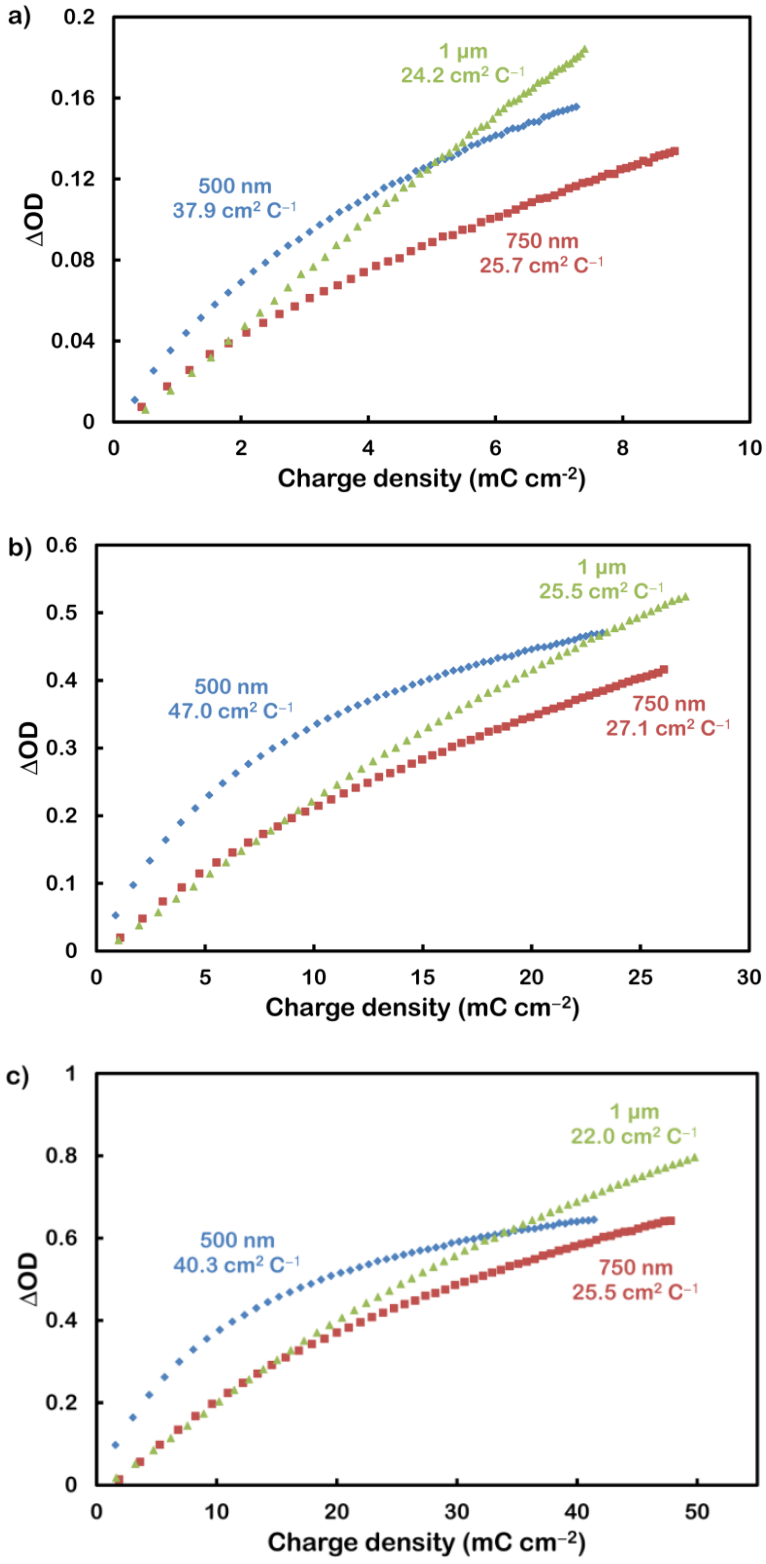

Figure 4.9 Coloration efficiency of the 500 nm, 750 nm and 1 µm thick Nb_2O_5 films under CA at (a) ±1, (b) ±1.5 and (c) ±2 V applied potential for the optical wavelength of 550 nm.

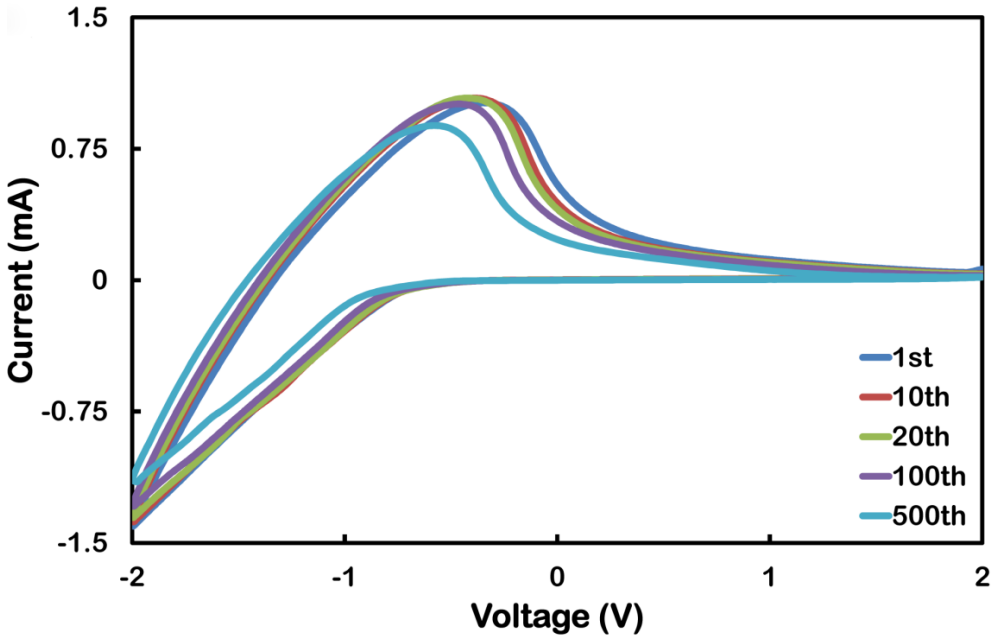

Figure 4.10 Cyclic voltammograms for investigating the stability measurements of the 500 nm thick Nb_2O_5 electrochromic device - up to 500 continuous cycles.

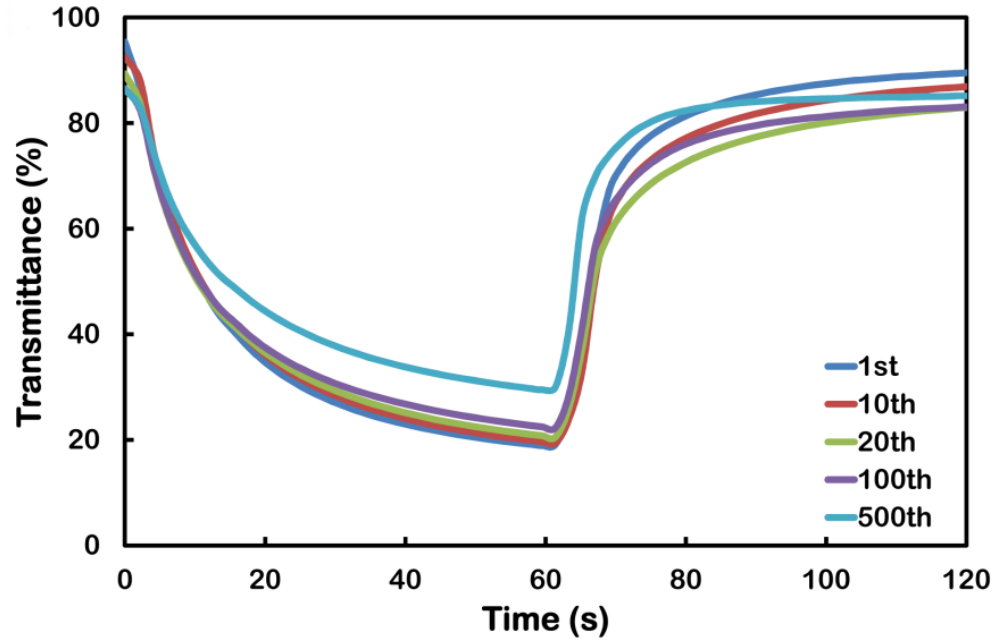

Figure 4.11 *In situ* transmittance of the 500 nm thick Nb_2O_5 sample over 500 continuous cycles for the optical wavelength of 550 nm.

4.4 Summary

In this chapter, the author synthesized compact 3D Nb_2O_5 nanoporous networks with thicknesses of 500 nm, 750 nm and 1 µm by employing a combination of RF sputtering and electrochemical anodization methods. The results here were revealed that the as-synthesized Nb_2O_5 films exhibited extraordinary EC performances in 0.1 M $LiClO_4$ electrolyte at low applied potentials. The compact 3D nanoporous networks with high active surface areas demonstrated excellent coloration efficiency (500 nm thick sample achieved 47.0 cm^2 C^{-1} at 550 nm) that exceeded any previously reported Nb_2O_5 EC system. Coupling these merits with high bleached state transparency, large optical modulation, and consistent cyclic stability make Nb_2O_5 a suitable choice for EC devices. The author believes for future outlook, combining Nb_2O_5 with low bandgap EC materials such as MoO_3 or WO_3 will potentially improve its EC performance and efficiency.[92, 107, 121] Additionally, multi-color EC performance of the 3D Nb_2O_5 should be explored.

In the next chapter, the author will present binary electrochromic EC devices based on the anodized ordered Nb_2O_5 nanochannelled templates coated with electrodeposited MoO_3. The chapter will focus on the investigation of combining these complimentary TMOs in order to overcome their individual chromic performance limitations.

Reference

1. Yao, D. D.; Rani, R. A.; O'Mullane, A. P.; Kalantar-zadeh, K.; Ou, J. Z., High Performance Electrochromic Devices Based on Anodized Nanoporous Nb_2O_5. *J. Phys. Chem. C* 2013.

2. Ou, J. Z.; Rani, R. A.; Ham, M. H.; Field, M. R.; Zhang, Y.; Zheng, H.; Reece, P.; Zhuiykov, S.; Sriram, S.; Bhaskaran, M.; Kanee, R. B.; Kalantar-Zadeh, K., Elevated Temperature Anodized Nb_2O_5: A Photoanode Material with Exceptionally Large Photoconversion Efficiencies. *ACS Nano* 2012, *6*, 4045-4053.

3. Zheng, H. D.; Sadek, A. Z.; Breedon, M.; Yao, D.; Latham, K.; du Plessis, J.; Kalantar-Zadeh, K., Fast Formation of Thick and Transparent Titania Nanotubular Films from Sputtered Ti. *Electrochem. Commun.* 2009, *11*, 1308-1311.

4. Rani, R. A.; Zoolfakar, A. S.; Ou, J. Z.; Ab. Kadir, R.; Nili, H.; Latham, K.; Sriram, S.; Bhaskaran, M.; Zhuiykov, S.; Kaner, R. B.; Kalantar-zadeh, K., Reduced Impurity-Driven Defect States in Anodized Nanoporous Nb_2O_5: The Possibility of Improving Performance of Photoanodes. *Chem. Commun.* 2013, *49*, 6349-6351.

5. Özer, N.; Chen, D.-G.; Lampert, C. M., Preparation and Properties of Spin-Coated Nb_2O_5 Films by the Sol-Gel Process for Electrochromic Applications. *Thin Solid Films* 1996, *277*, 162-168.

6. O'Neill, S. A.; Parkin, I. P.; Clark, R. J. H.; Mills, A.; Elliott, N., Atmospheric Pressure Chemical Vapour Deposition of Thin Films of Nb_2O_5 on Glass. *J. Mater. Chem.* 2003, *13*, 2952-2956.

7. Le Viet, A.; Jose, R.; Reddy, M. V.; Chowdari, B. V. R.; Ramakrishna, S., Nb_2O_5 Photoelectrodes for Dye-Sensitized Solar Cells: Choice of the Polymorph. *J. Phys. Chem. C* 2010, *114*, 21795-21800.

8. Kodama, R.; Terada, Y.; Nakai, I.; Komaba, S.; Kumagai, N., Electrochemical and in Situ Xafs-Xrd Investigation of Nb_2O_5 for Rechargeable Lithium Batteries. *J. Electrochem. Soc.* 2006, *153*, A583-A588.

9. Liu, J.; Xue, D. F.; Li, K. Y., Single-Crystalline Nanoporous Nb_2O_5 Nanotubes. *Nanoscale Research Letters* 2011, *6,* DOI:10.1186/1556-276X-6-138.

10. Chu, C.-W.; Li, S.-H.; Chen, C.-W.; Shrotriya, V.; Yang, Y., High-Performance Organic Thin-Film Transistors with Metal Oxide/Metal Bilayer Electrode. *Appl. Phys. Lett.* 2005, *87*, 193508.

11. Ramana, C. V.; Atuchin, V. V.; Groult, H.; Julien, C. M., Electrochemical Properties of Sputter-Deposited MoO_3 Films in Lithium Microbatteries. *J. Vac. Sci. Technol. A* 2012, *30*, 04D105.

12. Vemuri, R. S.; Engelhard, M. H.; Ramana, C. V., Correlation between Surface Chemistry, Density, and Band Gap in Nanocrystalline WO_3 Thin Films. *ACS Appl. Mater. Interfaces* 2012, *4*, 1371-1377.

13. Orel, B.; Opara Krašovec, U.; Maček, M.; Švegl, F.; Lavrenčič Štangar, U., Comparative Studies of “All Sol–Gel” Electrochromic Devices with Optically Passive Counter-Electrode Films, Ormolyte Li^+ Ion-Conductor and WO_3 or Nb_2O_5 Electrochromic Films. *Sol. Energy Mater. Sol. Cells* 1999, *56*, 343-373.

14. Fu, Z. W.; Kong, J. J.; Qin, Q. Z., Electrochemical and Electrochromic Properties of Niobium Oxide Thin Films Fabricated by Pulsed Laser Deposition. *J. Electrochem. Soc.* 1999, *146*, 3914-3918.

15. Romero, R.; Dalchiele, E. A.; Martín, F.; Leinen, D.; Ramos-Barrado, J. R., Electrochromic Behaviour of Nb_2o_5 Thin Films with Different Morphologies Obtained by Spray Pyrolysis. *Sol. Energy Mater. Sol. Cells* 2009, *93*, 222-229.

16. Huang Yin-Song, Z. Y.-Z., Hu Xing-Fang, Electrochromic Properties of Niobium Oxide Thin Films Fabricated by Rf Sputtering. *J. Inorg. Mater.* 2002, *17*, 632-636.

17. Sorar, I.; Pehlivan, E.; Niklasson, G. A.; Granqvist, C. G., Electrochromism of Dc Magnetron Sputtered TiO_2 Thin Films: Role of Deposition Parameters. *Sol. Energy Mater. Sol. Cells* 2013, *115*, 172-180.

18. Ou, J. Z.; Balendhran, S.; Field, M. R.; McCulloch, D. G.; Zoolfakar, A. S.; Rani, R. A.; Zhuiykov, S.; O'Mullane, A. P.; Kalantar-zadeh, K., The Anodized Crystalline WO_3 Nanoporous Network with Enhanced Electrochromic Properties. *Nanoscale* 2012, *4*, 5980-5988.

19. Heusing, S.; Sun, D. L.; Otero-Anaya, J.; Aegerter, M. A., Grey, Brown and Blue Coloring Sol–Gel Electrochromic Devices. *Thin Solid Films* 2006, *502*, 240-245.

20. Yao, D. D.; Field, M. R.; O'Mullane, A. P.; Kalantar-zadeh, K.; Ou, J. Z., Electrochromic Properties of TiO_2 Nanotubes Coated with Electrodeposited MoO_3. *Nanoscale* 2013, *21,* 10353-10359.

21. Wang, Z. Y.; Madhavi, S.; Lou, X. W., Ultralong Alpha-MoO_3 Nanobelts: Synthesis and Effect of Binder Choice on Their Lithium Storage Properties. *J. Phys. Chem. C* 2012, *116*, 12508-12513.

22. Chen, J. S.; Cheah, Y. L.; Madhavi, S.; Lou, X. W., Fast Synthesis of Alpha-MoO_3 Nanorods with Controlled Aspect Ratios and Their Enhanced Lithium Storage Capabilities. *J. Phys. Chem. C* 2010, *114*, 8675-8678.

Chapter 5

Enhanced Coloration Efficiency for Electrochromic Devices based on Anodized Nb_2O_5 / Electrodeposited MoO_3 Binary Systems

5.1 Introduction

In the previous chapter, the author demonstrated electrochromic (EC) devices based on anodized ordered niobium pentoxide (Nb_2O_5) nanoporous films. He demonstrated synthesis of compact three dimensional (3D) Nb_2O_5 nanoporous networks with varied thicknesses by employing a combination of RF sputtering and electrochemical anodization methods. The results revealed the as-synthesised films exhibited extraordinary EC performance. As a transition metal oxide (TMO), Nb_2O_5 possesses a relatively large bandgap, which causes difficulty for the EC devices base on Nb_2O_5 to perform at low operating voltages. Additionally, the coloration efficiency (CE) was also limited. However having shown the extraordinary results from TMO binary EC systems in chapter 3, the author chose to investigate a similar path for anodized Nb_2O_5. He developed binary EC devices based on a combination of anodized Nb_2O_5 and electrodeposited α-MoO_3, which the synthesis methods for both are in line with the core concept of the electric field driven techniques for this thesis. The ordered Nb_2O_5 nanostructure was chosen to be the device template with stratified α-MoO_3 as the chromic coating. A discussion regarding the advantages of creating such a binary EC device has been presented in Chapter 1.

In this chapter, the author will present his work on the development of binary EC devices based on anodised ordered Nb_2O_5 nanochanneled templates with MoO_3 coatings. A comprehensive characterization of the bare Nb_2O_5 films and MoO_3 coated films will be presented. As the performance of the EC devices vary with the thickness of the MoO_3

coating, the author will investigate and provide experimental correlation between the deposited MoO_3 and the impact on the overall EC system. Eventually, the performance of the bare Nb_2O_5 template and the binary system will be evaluated for EC performance against other known EC TMOs. The work in this chapter has been submitted for publication.

5.2 Experimental

5.2.1 Fabrication of nanochanneled Nb_2O_5

Nb films of 0.25, 0.37 and 0.5 μm were deposited using a radio frequency (RF) sputtering system fitted with a Nb target (99.95% purity). These Nb films were sputtered onto fluorine-doped tin oxide (FTO, 15 Ω square^{-1}, Dyesol) glass substrates after 30 min at 20×10^{-3} Torr vacuum, 100 W applied RF power with a substrate temperature of 300 °C. These conditions were used for promoting the strongest adhesion of the films onto the substrates,[24] and they resulted in Nb films of 0.25 μm thicknesses. The samples were then placed in a two-electrode cell configuration using the sample (of 0.8 cm^2 surface area) as an anode and a platinum (Pt) foil as the cathode. The anodization was carried out using a potentiostat (CHI-413A electrochemical station) in an electrolyte mix of 50 mL of ethylene glycol (98% anhydrous, Sigma Aldrich) with 0.15 g of NH_4F (98% purity, Sigma Aldrich) and 4% deionized (DI) water. An optimized potential of 10 V was applied between the anode and cathode during the anodization process. These values for the electrolyte composition and optimized applied potential were previously investigated and obtained by Ou *et al*.[24] The films contain very low amounts of impurities, as it has been previously demonstrated,[28] that provide defect free pathways for enhanced charge transfer.

The electrolyte was kept at a constant temperature of 50 °C during the anodization process. The anodization duration of 8, 20 and 30 min for Nb films of 0.25 μm thicknesses resulted in Nb_2O_5 films of 500 nm thicknesses. A thickness of 500 nm was chosen as it

provides the best EC performance for bare Nb_2O_5 according to our previous report.[113] Similar to the anodization of Ti films, the anodization of Nb layers produced Nb_2O_5 films of almost double the initial metal layer thickness.[25] After the anodization, the samples were carefully washed with DI water and dried in a nitrogen stream. Post anodization annealing was carried out in ambient air at a temperature of 450 °C for 60 min with a slow ramp up and down rate of 2 °C min^{-1}. The thicknesses of the Nb_2O_5 films did not change after annealing.

5.2.2 MoO_3 coating on Nb_2O_5 nanochanneled films

For the MoO_3 deposition, the procedure that has been previously adopted by the authors was used.[77] A molybdate solution was prepared by adding 5 mM sodium molybdate (Na_2MoO_4, 99% purity, Sigma Aldrich) into distilled water. Sulphuric acid (H_2SO_4) was added to adjust the pH to 4. The electrodeposition of MoO_3 was carried out at room temperature using a CHI-413A electrochemical station employing a standard three electrode cell configuration. The Nb_2O_5 samples of 0.7 cm^2 exposed area were used as the working electrode, a Pt wire (0.5 mm diameter, BASi) as the counter electrode, together with an Ag/AgCl (3 M KCl) (BASi) reference electrode in a custom made electrochemical cell with rectangular sides. The chronoamperometry (CA) technique was utilized in order to control the deposition of MoO_3 onto the Nb_2O_5 samples. CA was carried out at an upper limit of 0 V and lower limit of –0.7 V for a duration of 60 s at initially –0.7 V and then at 0 V for 20, 40, 80 and 120 cycles. Upon the completion of the electrodeposition, samples were washed using Milli-Q water and dried in N_2. The coated samples were further annealed to dehydrate the films and obtain the desired crystal phase in a standard laboratory horizontal furnace at 350 °C for 120 min in ambient air, with ramp up and ramp down rates of 1 °C min^{-1}.

5.2.3 Structural characterization

The bare Nb_2O_5 and MoO_3 coated Nb_2O_5 films were characterized to assess their structural and morphological properties. X-ray photoelectron spectroscopy (XPS) was conducted using a Thermo Scientific K-alpha instrument with Al Kα source. X-ray diffraction (XRD) was obtained with a Bruker AX 8: Discover using general area detector diffraction system (GADDS). Raman spectroscopy was performed using a 532 nm laser at 0.9 mW power with a Jobin Yvon Horiba TRIAX320 spectrometer system incorporating an Olympus BX41 microscope with a 50× objective. Surface morphologies were observed using scanning electron microscopy (SEM) and performed on a FEI Nova Nano instrument.

5.2.4 EC characterization

Transmittance measurements were carried out using a Fiber Ocean Optics Spectrometer using a UV-Vis-NIR light source (DH-2000, Mikropack, Ocean Optics). *In situ* transmittance characterizations were conducted at room temperature also using the CHI-413A electrochemical station *via* a three-electrode configuration, employing the coated samples as the working electrode (exposed area of 0.7 cm^2), and a Pt wire (0.5 mm diameter, BASi) as the counter electrode, together with an Ag/AgCl (3 M KCl) (BASi) reference electrode. The electrolyte used was 0.1 M $LiClO_4$ in propylene carbonate (98% anhydrous, Sigma Aldrich).

5.3 Results and discussions

5.3.1 Characterizations of the samples

In order to assess the conditions of the samples with and without the MoO_3 coatings, XPS spectra of the bare Nb_2O_5 and MoO_3 coated Nb_2O_5 films were acquired (Figure 5.1). XPS spectra of the annealed Nb_2O_5 templates demonstrate the binding energy of the anodized

Nb species and verify their stoichiometry after annealing. As shown in Figure 5.1(a) only two peaks were observed at 207.5 and 210.3 eV, which corresponds to the Nb $3d_{5/2}$ and $3d_{3/2}$ of the Nb^{5+} species, respectively.[115] Figure 5.1(b) illustrates the binding energies of the Mo 3d photoelectron peaks. XPS spectra of the MoO_3 coated Nb_2O_5 film surfaces revealed two main peaks located at 235.4 and 232.6 eV, corresponding to Mo $3d_{3/2}$ and Mo $5d_{5/2}$ peaks for Mo^{6+}.[107] XPS depth profiling was carried out at incremental steps with a combination of ion etching and film characterization from the surface of the MoO_3 coating, through the Nb_2O_5 template until the underlying FTO substrate was reached. The resulting XPS spectra illustrate the coverage of MoO_3 coating on the Nb_2O_5 nanochannel as shown in Figure 5.1(c). It is obvious that additional MoO_3 deposition cycles increases the MoO_3 atomic percentage. The atomic percentage of MoO_3 within the analysis area is relatively constant between a depth of 100 and 400 nm, indicating that the coverage of MoO_3 was uniform. The discrepancy in the first 100 nm is due to the morphology of the sample surface, where different areas of analysis contained different MoO_3 growth morphologies. A diminishing MoO_3 content approaching a depth of 500 nm is visible due to the etching procedure of the XPS depth profiling,

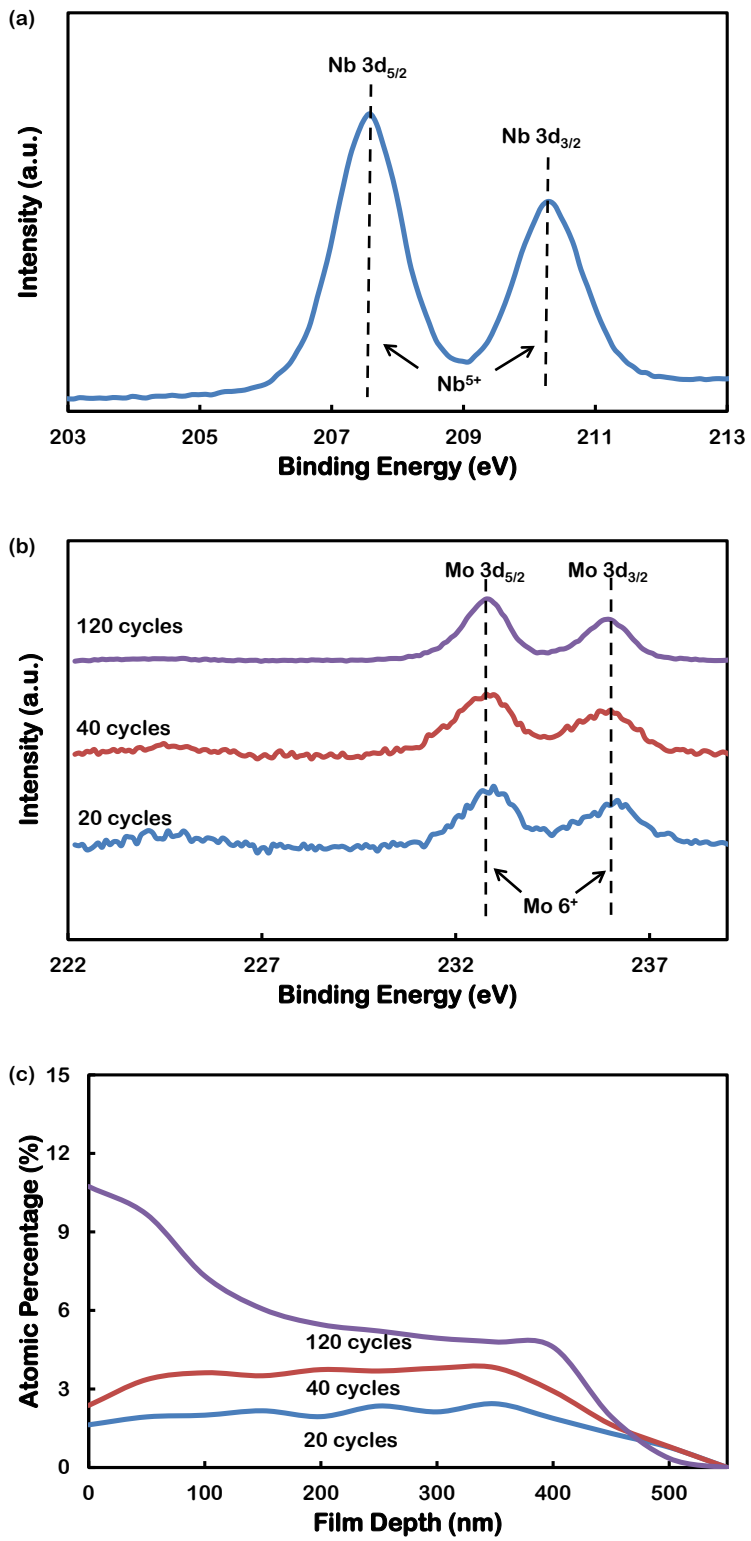

Figure 5.1 XPS spectra of (a) annealed Nb_2O_5, (b) annealed MoO_3 coating (normalized values) and (c) the depth profile of the MoO_3 coating (non-normalized values)

XRD measurements were carried out to examine the crystallinity and structure of the samples, and the resulting XRD patterns are shown in Figure 5.2. As can be observed, the as-anodized film revealed some Nb diffraction peaks in addition to the obvious FTO peaks. The as-anodized films underwent a significant crystallization as a result of the annealing

process, and visible sharp peaks at 22.6°, 28.4° and 36.6° corresponding to the orthorhombic structure of Nb_2O_5 (a = 6.175 Å, b = 29.175 Å, and c = 3.93 Å) are seen.[82, 114] As observed in Figure 2, the XRD pattern reveals diffraction peaks at 13.0° and 24.3°, matching the (020) and (110) planes of α-phase MoO_3, respectively, for the thickest MoO_3 coated film.[77, 107] These peaks were less visible for films that were formed using a lower number of cycles and as such only the sample formed after 120 cycles is shown.

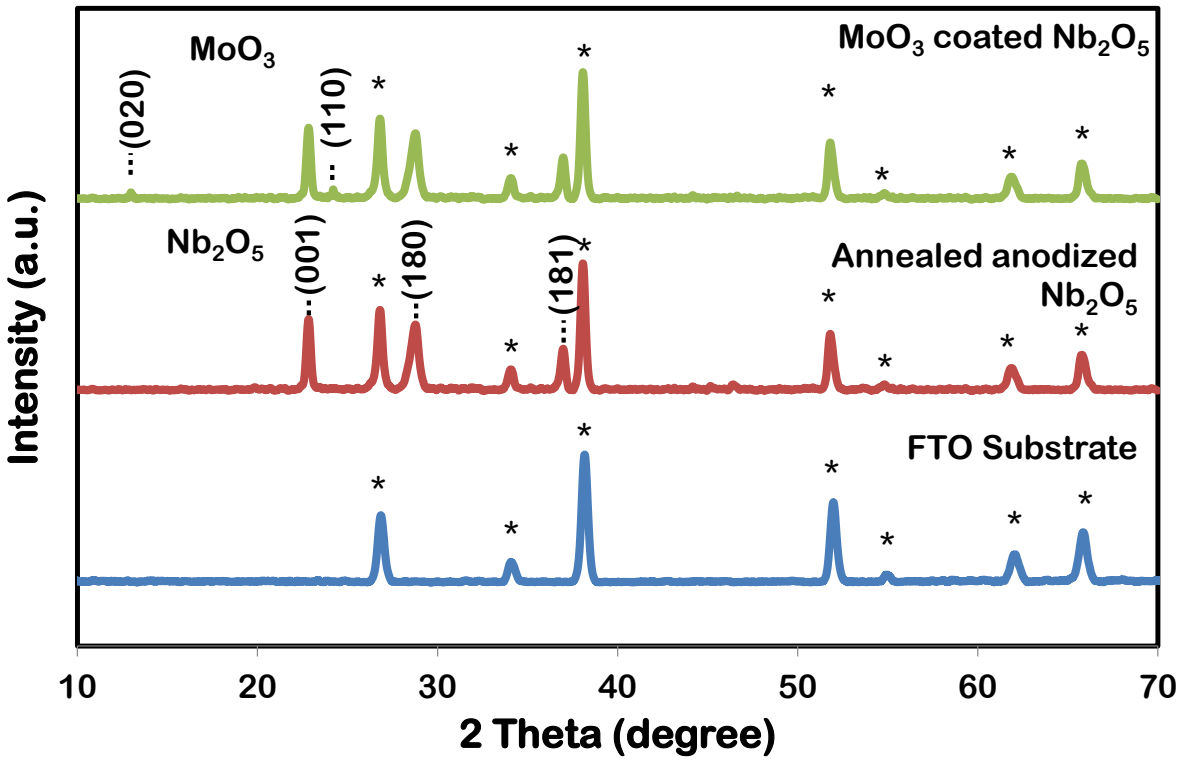

Figure 5.2. XRD diffraction patterns of the FTO substrate, bare Nb_2O_5 film and MoO_3 coated Nb_2O_5, * denotes FTO diffraction peaks.

The XPS and XRD data interpretation was further verified by the Raman spectra presented in Figure 5.3. The broad peaks at 248, 305 and 694 cm^{-1} represent the orthorhombic phase of crystalline Nb_2O_5.[24] The deposited MoO_3 crystal phase was also investigated using Raman spectroscopy (Figure 3). Sharp peaks at 667 cm^{-1} (stretching mode Mo—$O_{(3)}$), 821 (stretching mode Mo—O—Mo) and 998 cm^{-1} (stretching mode Mo=O) with additional peaks at 157 and 283 cm^{-1} are visible in each of the MoO_3 coated samples, which confirms that the deposited MoO_3 is crystalline α-MoO_3.[77]

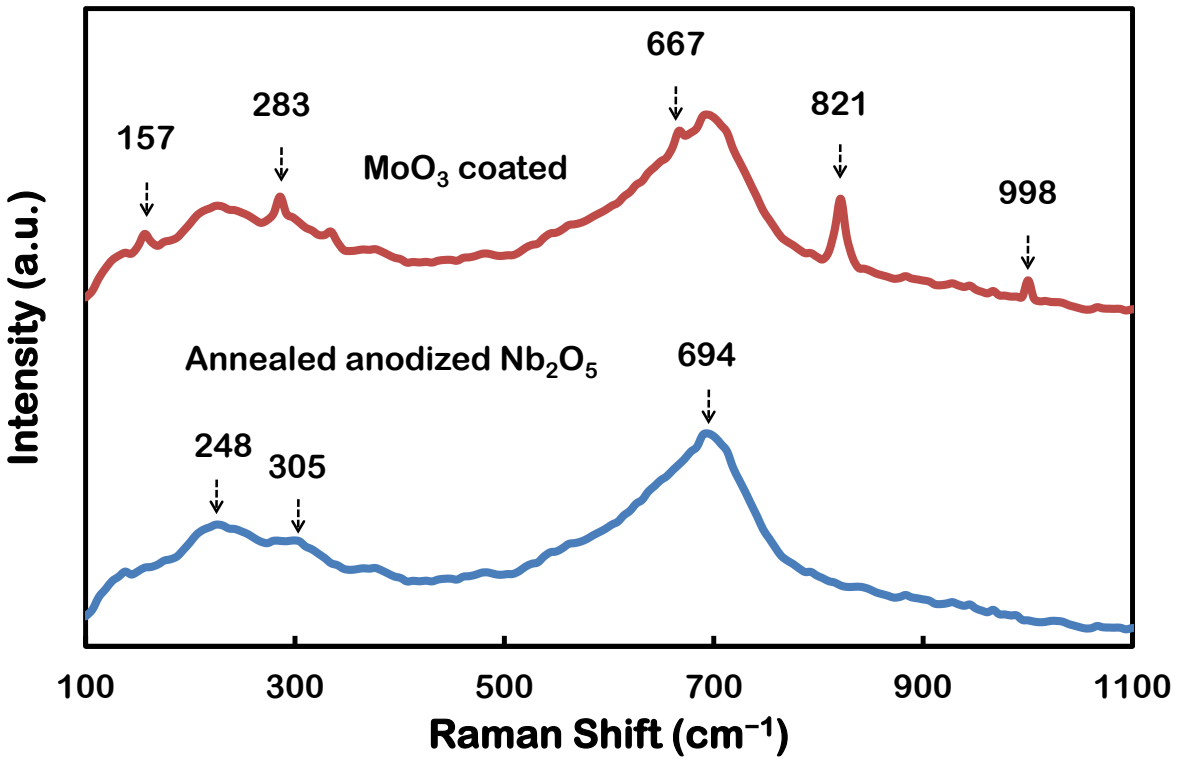

Figure 5.3 Raman spectra of the bare Nb_2O_5 film and MoO_3 coated Nb_2O_5.

The surface and cross sectional SEM images of bare and MoO_3 coated Nb_2O_5 films are presented in Figure 5.4. The bare Nb_2O_5 film (Figure 5.4(a)) appeared nanoporous on the surface with nanochannels running through the thickness of the film. Both the porosity of the surface and width of the nanochannel visibly diminish when a MoO_3 coating is deposited on to the Nb_2O_5 film as shown by the MoO_3 coating achieved after 40 cycles (Figure 5.4(b)). As the number of coating cycles reached 120 (Figure 5.4(c)), the SEM image reveals a complete blockage of the surface pores and the underlying nanochannel structures.

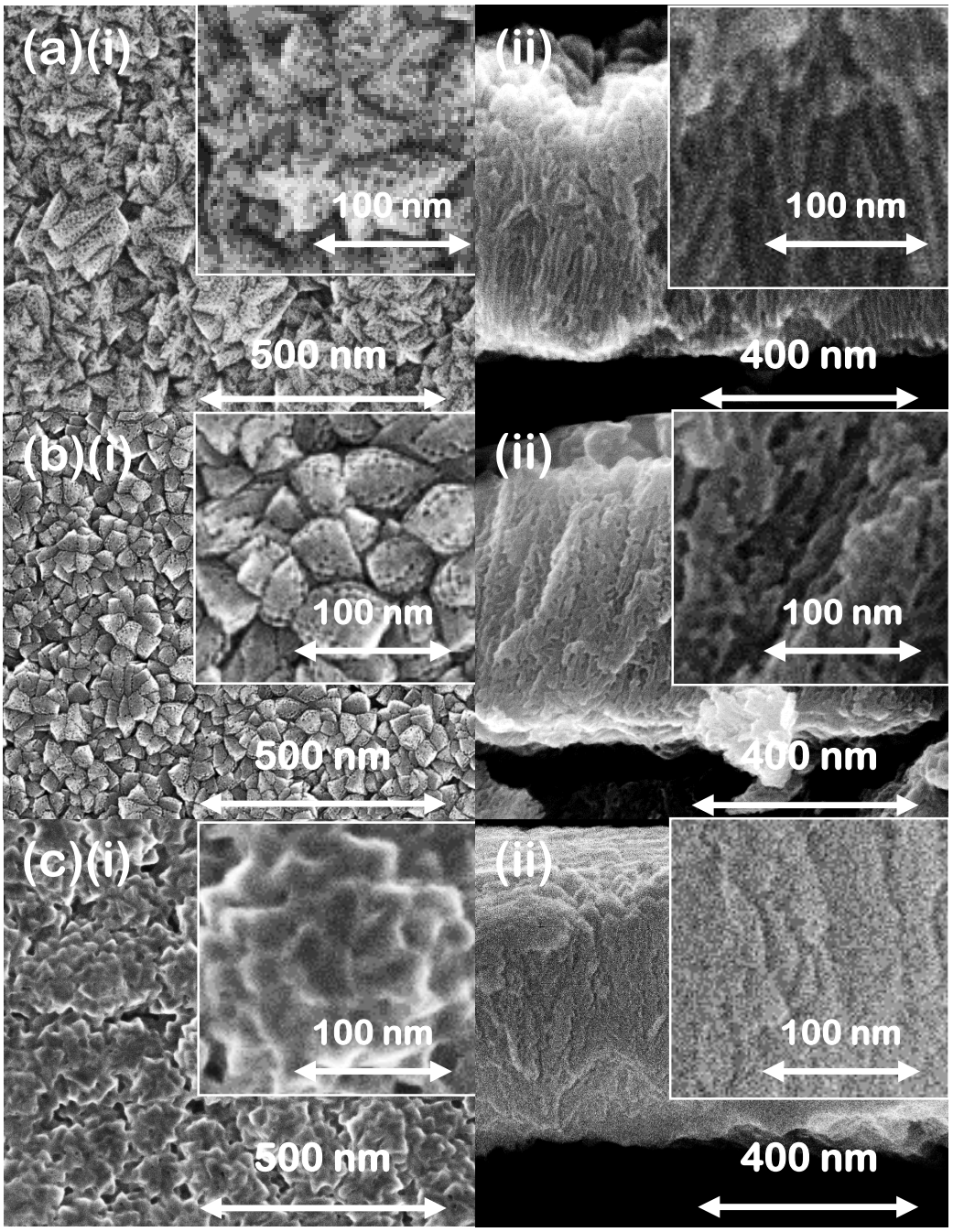

Figure 5.4 SEM images of (a) bare Nb_2O_5, MoO_3 coatings of (b) 40 cycles, (c) 120 cycles, with surface morphology (i) and cross sectional images (II)

5.3.2 EC investigations

The assessment of the coloration-bleaching kinetics and optical modulations are vital for the evaluation of the optical and electronic properties of the films. Therefore, *in situ* transmittance changes measured at an optical wavelength of 550 nm were carried out during the CA measurements (Figure 5.5). It is observed that the initial transmittance of all

coated samples, except the thickest MoO_3 coating exceeded 90%, which is comparable to the bare Nb_2O_5 sample or previously reported Nb_2O_5 samples fabricated for EC devices.[113] As can be seen for coloration, potentials of −0.25, −0.5, −0.75 and −1 V were applied against the reference electrode for 60 s and for bleaching, 0.25, 0.5, 0.75 and 1 V were applied.

Throughout the *in situ* measurements the samples (excluding 120 cycle coating) maintained its cyclic stability. Transmission in the bleached state for the 120 cycle MoO_3 coated sample continuously dropped upon repeated measurements. This is due to the thicker MoO_3 coating that covered the entire Nb_2O_5 film surface, which blocked all the pores and filled the nanochannels, as evidenced in the SEM images, which increases the chance of trapping of the intercalating ions.

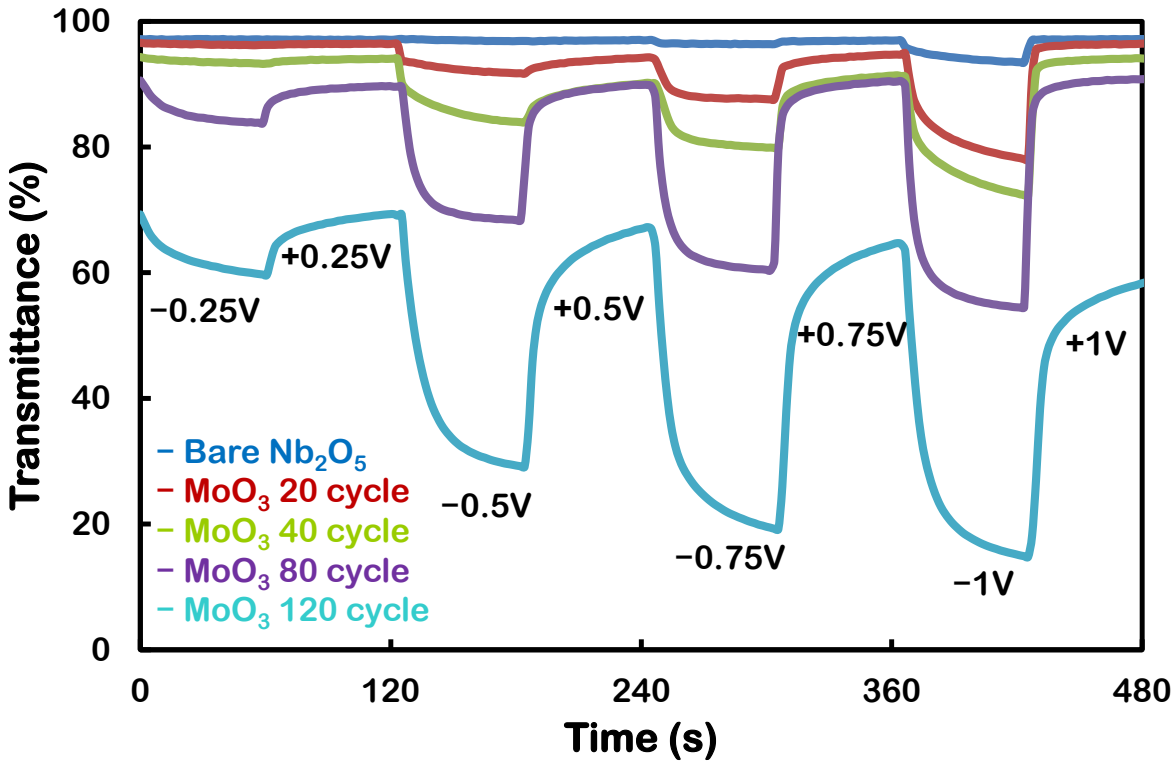

Figure 5.5 In situ transmittance of the bare and coated samples

The CE of an EC material is a critical factor for demonstrating its performance. The CE is defined as the change in optical density (ΔOD) per unit of the intercalated ionic charge (ΔQ) into an EC layer. CE and ΔOD can be obtained from the following equations:[3]

$$\mathrm{CE} = \frac{\Delta OD}{\Delta Q} \qquad (1)$$

$$\Delta OD = \log\left(\frac{T_b}{T_c}\right) \qquad (2)$$

where T_b and T_c refer to the transmittance of the layer in its bleached and colored states, respectively. The CE values for the four coatings of increasing thicknesses (20, 40, 80 and 120 cycles) at low applied potentials (–0.25, –0.5, –0.75 and –1 V) are presented in Figure 5.6. The calculated CE values for 20 cycles are 14.75, 27.35, 36.45 and 17.95 $cm^2\ C^{-1}$ at −0.25, −0.5, −0.75 and −1 V respectively. As the MoO_3 coating increased in thickness after 40 cycles, the calculated CEs were 11.7, 30.32, 24.03 and 20.49 $cm^2\ C^{-1}$, and then 35.41, 46.15, 46.73 and 39.33 $cm^2\ C^{-1}$ for 80 cycles coating and lastly 91.85, 149.64, 129.42 and 69.28 $cm^2\ C^{-1}$ for 120 cycles coating at −0.25, −0.5, −0.75 and −1 V, respectively.

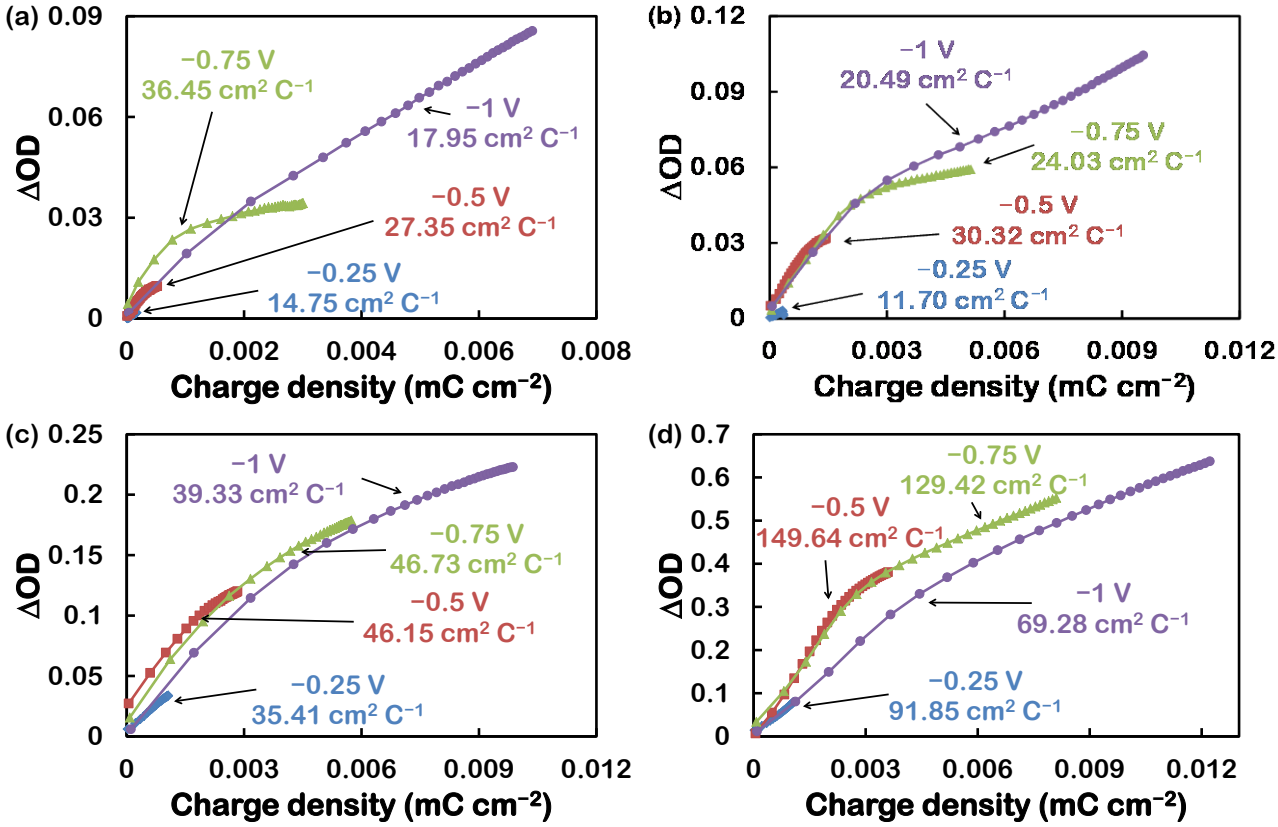

Figure 5.6. CEs of the Nb_2O_5 samples with MoO_3 coating of (a) 20 cycle, (b) 40 cycle, (c) 80 cycle and (d) 120 cycle. The values for bare Nb_2O_5 can be found in work by Yao et al.[113]

It is evident that the existence of the MoO_3 coating on the Nb_2O_5 nanochanneled structure considerably increased the device's EC performance. Additionally, the MoO_3 coated films demonstrate significantly stronger chromic responses at low potentials compared to the bare Nb_2O_5 sample, and as the number of deposition cycles increased the resultant optical modulation also increases. As we demonstrated using XRD and Raman spectroscopy analysis the coated MoO_3 is in the α-phase. It is known that this crystal phase of MoO_3 can accommodate a large number of ions into its stratified structure and as such it is regularly used for EC and battery storage applications.[13, 16] As a result, the MoO_3 coating on the Nb_2O_5 film increases the film's capability to accommodate more intercalated charges in comparison to the bare Nb_2O_5 sample. Additionally, it is also important to remember that both Nb_2O_5 nanochaneled structures and the α-MoO_3 lamellar coating provide directional and low impurity pathways for charge transfer.[28, 107]

As presented in Figure 5.7, cyclic voltammetric measurements were carried out at a sweep rate of 0.1 Vs^{-1} between -1 and 1 V in 0.1 M $LiClO_4$ to demonstrate the increased capacity of the MoO_3 coated samples for intercalating Li^+ ions. It is seen that the MoO_3 coating induced larger amount of Li^+ intercalation during the negative potential cycle as shown by the larger cathodic current peak and area. Moreover, the onset potential of the cathodic current peak was observed to shift towards more positive potentials as additional MoO_3 coatings (up to 80 cycles) are deposited. This indicates reduced interfacial charge transfer resistance, a larger volume for accommodating the ions and potentially altered ionization affinity energy of the bare Nb_2O_5 platform. The positive maxima (defined as the anodic peak) of each coated sample are also larger than the bare Nb_2O_5 sample, which indicates higher electron and Li^+ de-intercalation during the reverse potential sweep. Finally, it is observed that the anodic peaks for the coated samples are shifted to more positive potentials as more MoO_3 coatings are deposited, which indirectly reflects a change in each of the coated films' band edges. To confirm this observation, a UV-Vis analysis was conducted.

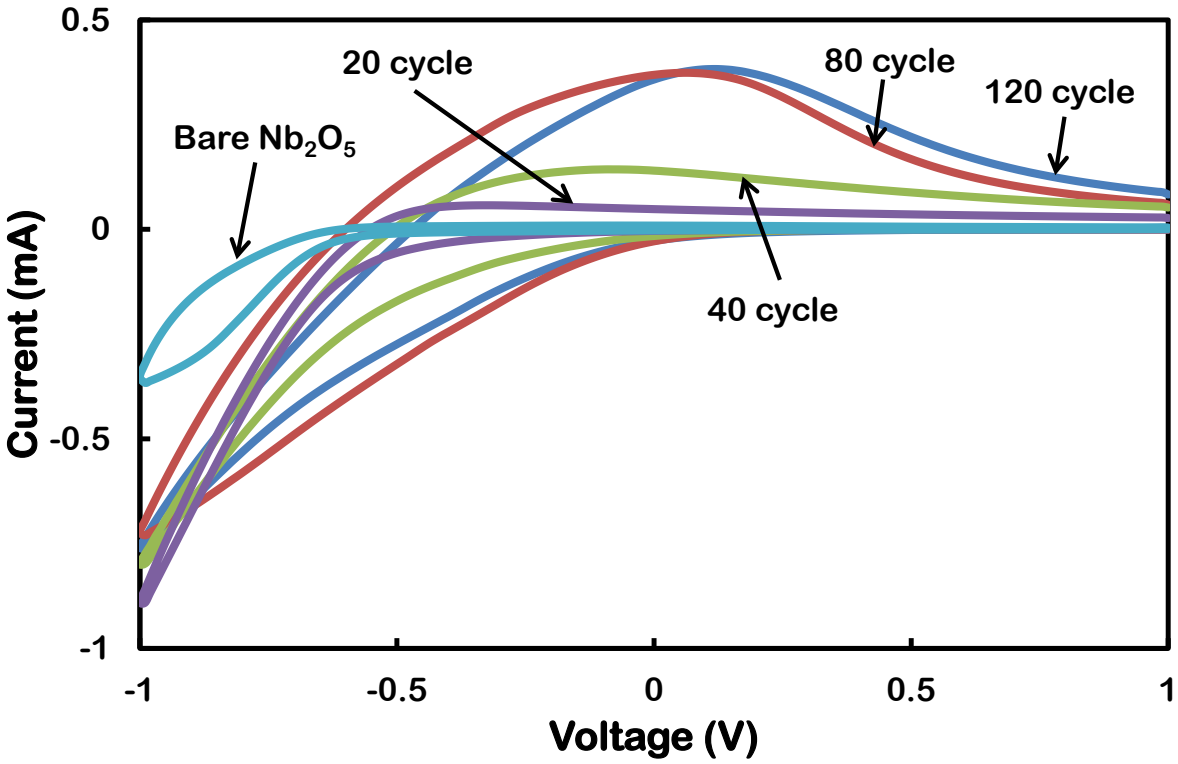

Figure 5.7. Cyclic voltammetric measurements recorded at 0.1 V $s^{-1}$of bare Nb_2O_5 and MoO_3 coated Nb_2O_5 samples in 0.1 M $LiClO_4$.

In order to investigate the band-structure properties of the bare Nb_2O_5 and MoO_3 coated Nb_2O_5 samples, Tauc plots of the samples were obtained by extracting their UV-Vis absorbance spectra and their bandgap energies were estimated (Figure 5.8). From the Tauc plots, it is observed that the bare Nb_2O_5 film bandgap was measured at 3.8 eV as previously reported.[87] The MoO_3 coating induced a drastic alteration on the original band gap. As MoO_3 coatings are deposited the band gap was reduced which was closer to that of pure MoO_3. With 20 cycles of MoO_3 deposited, the band gap reduced to 3.59 eV and then further to 3.57, 3.43 and finally 3.27 eV for 40, 80 and 120 cycles, respectively. The relatively large bandgap of the Nb_2O_5 sample is probably the main reason that it failed to demonstrate any electrochromism at low applied potentials (–0.25 and –0.5 V) and exhibited poor optical modulation at even higher voltages (–0.75 and –1 V) during the EC measurements, whereas the MoO_3 coated samples performed significantly better in both aspects.

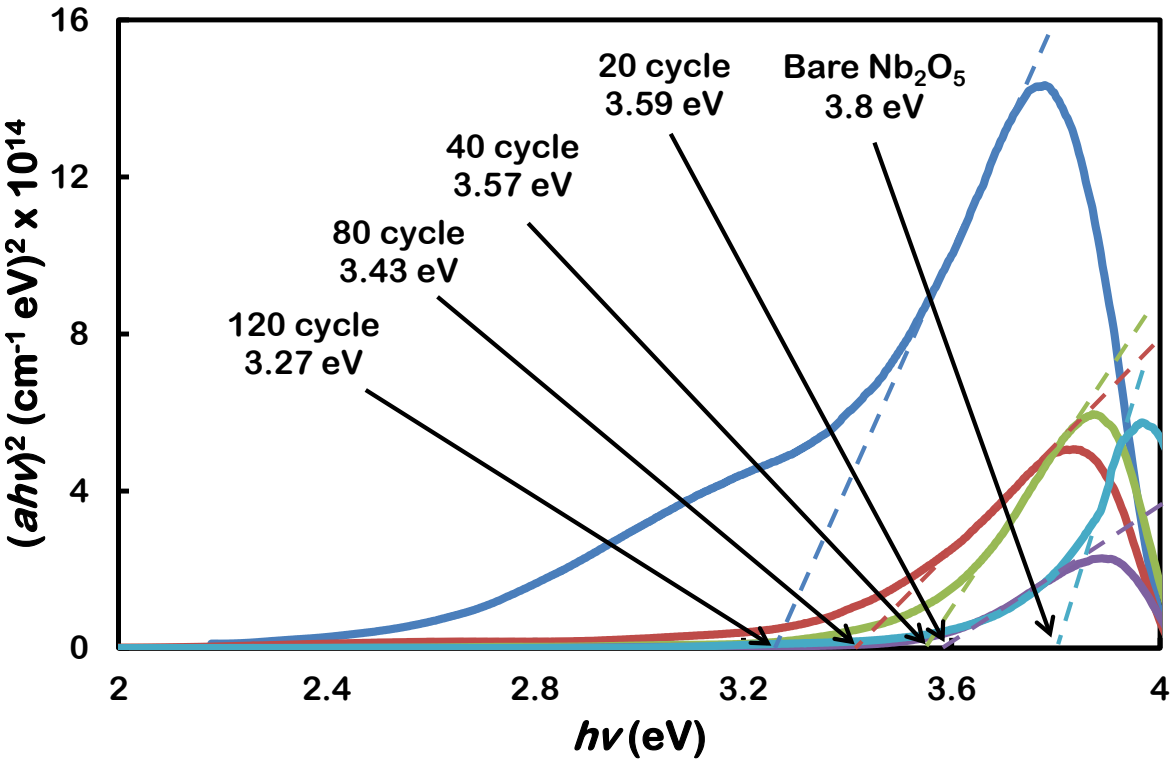

Figure 5.8. Tauc plots and calculated bandgap for bare and MoO_3 coated Nb_2O_5 samples

The 120 cycle MoO_3 coated sample demonstrated an extraordinarily high calculated CE of 149.64 $cm^2\ C^{-1}$, which far exceeded any previously reported values for either Nb_2O_5 or MoO_3 (47.0 and 54.0 $cm^2\ C^{-1}$ respectively). In addition, it is not a purely additive effect and a significant synergism is observed. Furthermore, the anodized Nb_2O_5 with MoO_3 coating demonstrates stronger CE performance in comparison to other EC TMO compounds fabricated using anodization methods (25 $cm^2\ C^{-1}$ at 550 nm for TiO_2[120] and 141.5 $cm^2\ C^{-1}$ at 750 nm for WO_3[3]).

5.4 Summary

In this chapter, the author fabricated highly ordered, low impurity Nb_2O_5 nanochanneled films of 500 nm thickness on FTO substrates by using a combination of RF sputtering and electrochemical anodization methods. Subsequently, he demonstrated α-phase MoO_3

coatings onto the Nb_2O_5 platform using a facile electrodeposition technique. The MoO_3 coated Nb_2O_5 binary films showed superior EC that was attributed to a reduced bandgap, enhanced charge transfer, enhanced ion capacity and large surface to volume ratio of the binary structure. The systems operated at low voltages as small as –0.25 V and showed remarkable optical modulations. The CE of 149.0 cm^2 C^{-1} was achieved for the sample made with a MoO_3 coating using 120 cycles, which is higher than any other EC Nb_2O_5 and MoO_3 based devices previously reported. The proposed method offers a viable process for developing future EC TMO devices.

In the next chapter the author will present a summary of his PhD thesis and discusses future works related to his PhD research project.

References

1. Ou, J. Z.; Rani, R. A.; Ham, M. H.; Field, M. R.; Zhang, Y.; Zheng, H.; Reece, P.; Zhuiykov, S.; Sriram, S.; Bhaskaran, M.; Kanee, R. B.; Kalantar-Zadeh, K., Elevated Temperature Anodized Nb_2O_5: A Photoanode Material with Exceptionally Large Photoconversion Efficiencies. *ACS Nano* 2012, *6*, 4045-4053.

2. Rani, R. A.; Zoolfakar, A. S.; Ou, J. Z.; Ab. Kadir, R.; Nili, H.; Latham, K.; Sriram, S.; Bhaskaran, M.; Zhuiykov, S.; Kaner, R. B.; Kalantar-zadeh, K., Reduced Impurity-Driven Defect States in Anodized Nanoporous Nb_2O_5: The Possibility of Improving Performance of Photoanodes. *Chem. Commun.* 2013, *49*, 6349-6351.

3. Yao, D. D.; Rani, R. A.; O'Mullane, A. P.; Kalantar-zadeh, K.; Ou, J. Z., High Performance Electrochromic Devices Based on Anodized Nanoporous Nb_2O_5. *J. Phys. Chem. C* 2013.

4. Zheng, H. D.; Sadek, A. Z.; Breedon, M.; Yao, D.; Latham, K.; du Plessis, J.; Kalantar-Zadeh, K., Fast Formation of Thick and Transparent Titania Nanotubular Films from Sputtered Ti. *Electrochem. Commun.* 2009, *11*, 1308-1311.

5. Yao, D. D.; Ou, J. Z.; Latham, K.; Zhuiykov, S.; O'Mullane, A. P.; Kalantar-zadeh, K., Electrodeposited α- and β-Phase Moo3 Films and Investigation of Their Gasochromic Properties. *Cryst. Growth Des.* 2012, *12*, 1865-1870.

6. O'Neill, S. A.; Parkin, I. P.; Clark, R. J. H.; Mills, A.; Elliott, N., Atmospheric Pressure Chemical Vapour Deposition of Thin Films of Nb_2O_5 on Glass. *J. Mater. Chem.* 2003, *13*, 2952-2956.

7. Yao, D. D.; Field, M. R.; O'Mullane, A. P.; Kalantar-zadeh, K.; Ou, J. Z., Electrochromic Properties of TiO_2 Nanotubes Coated with Electrodeposited MoO_3. *Nanoscale* 2013, *21,* 10353-10359.

8. Le Viet, A.; Jose, R.; Reddy, M. V.; Chowdari, B. V. R.; Ramakrishna, S., Nb_2O_5 Photoelectrodes for Dye-Sensitized Solar Cells: Choice of the Polymorph. *J. Phys. Chem. C* 2010, *114*, 21795-21800.

9. Özer, N.; Chen, D.-G.; Lampert, C. M., Preparation and Properties of Spin-Coated Nb_2O_5 Films by the Sol-Gel Process for Electrochromic Applications. *Thin Solid Films* 1996, *277*, 162-168.

10. Ou, J. Z.; Balendhran, S.; Field, M. R.; McCulloch, D. G.; Zoolfakar, A. S.; Rani, R. A.; Zhuiykov, S.; O'Mullane, A. P.; Kalantar-zadeh, K., The Anodized Crystalline WO_3 Nanoporous Network with Enhanced Electrochromic Properties. *Nanoscale* 2012, *4*, 5980-5988.

11. Wang, Z.; Madhavi, S.; Lou, X. W., Ultralong α-MoO_3 Nanobelts: Synthesis and Effect of Binder Choice on Their Lithium Storage Properties. *The Journal of Physical Chemistry C* 2012, *116*, 12508-12513.

12. Zhou, L.; Wu, H. B.; Wang, Z.; Lou, X. W., Interconnected MoO_2 Nanocrystals with Carbon Nanocoating as High-Capacity Anode Materials for Lithium-Ion Batteries. *ACS Appl. Mater. Interfaces* 2011, *3*, 4853-4857.

13. Liu, J.; Xue, D. F.; Li, K. Y., Single-Crystalline Nanoporous Nb_2O_5 Nanotubes. *Nanoscale Research Letters* 2011, *DOI:10.1186/1556-276X-6-138.*

14. Sorar, I.; Pehlivan, E.; Niklasson, G. A.; Granqvist, C. G., Electrochromism of Dc Magnetron Sputtered TiO_2 Thin Films: Role of Deposition Parameters. *Sol. Energy Mater. Sol. Cells* 2013, *115*, 172-180.

Chapter 6

Conclusions and future works

The author's vision for this PhD research involved electric field driven syntheses and investigating the characteristics of selected chromic materials to improve the operation efficiency by overcoming the materials' inherited limitations. The author's vision was realised by developing anodized and electrodeposited nanostructured transition metal oxides (TMOs) and their binary chromic systems in highly ordered thin film geometries. Specially, the combination of complimentary TMOs turned out to elevate the merits of both incorporated TMOs in the binary system, resulting in relatively high transparency, large optical modulation and strong coloration efficiency (CE).

In the course of carrying out this research, the author investigated numerous reports on existing chromic TMOs such as TiO_2, MoO_3, WO_3, Nb_2O_5 and V_2O_5. However, upon a thorough review and analysis of the past data, it was found that other than WO_3, the remaining TMOs did not perform nearly as satisfactory for practical chromic applications. Therefore, the author launched a comprehensive investigation into fully understanding the qualities and limitations experienced by other chromic TMOs. Various TMOs' optical and electronic properties, morphologies, stoichiometry, doping effect, obtainable nanostructures and fabrication methods were examined to assess and formulate a practical and effective method in synthesising chromic devices with desirable performance.

The investigations conducted by the author identified several existing chromic TMOs including MoO_3, TiO_2 and Nb_2O_5 with known limitations even though with great potentials to stretch their performance to exceed the current values reported. As such, the author's research was organised and carried out so as to overcome the identified the research gaps and key parameters that affect and augment their performance.

In the first stage of this PhD project, the author demonstrated chromic devices based on electrodeposited α- and β-MoO_3. α-MoO_3 was specially targeted for its intrinsically stratified structure to accommodate a large number of intercalated ion. However, the adhesion to the substrate was insufficient to test them for electrochromic (EC) performance, so the focused remain on gasochromic measurements. These measurements revealed the α-MoO_3's high accommodation of H^+ ions together with the directional paths for injected electrons are the main reasons for its excellent gasochromic properties. Subsequently, in the second stage, the author developed a binary EC devices based on anodized ordered TiO_2 nanotube templates with electrodeposited α-MoO_3. The template gave the system required durability for EC and α-MoO the enhanced chromic performance. The research demonstrated the MoO_3 coated TiO_2 EC device performance can exceed that of the bare TiO_2 EC device. The MoO_3 coating existed as an effective EC interface with enhanced charge carrier transfer to the ordered TiO_2 nanotube template and also increased the capacity of the ionic intercalation. In the third stage, the author synthesised EC devices based on anodized ordered nanoporous Nb_2O_5 with the highest obtained CE value for Nb_2O_5 at the time. However the relatively large bandgap inherited by Nb_2O_5 thwarted higher EC performance by limiting the operation to high applied voltages. Finally, in the fourth stage, prompted by the enhanced augmentation of the MoO_3 coating on TiO_2 template, the author applied a similar MoO_3 coating to the Nb_2O_5 template to obtain CE values comparative to the best chromic TMOs based on WO_3.

The major finding of each stage of this PhD research project are summarised as follows:

Stage 1

- In the first stage, the author demonstrated a facile and well controlled electrochemical synthesis process for the fabrication of both α and β-MoO_3. The cyclic voltametric electrodeposition process was shown to be carried out under

ambient conditions which made this process versatile and compatible with electronic device industry standards.

- In addition to the fine control of the experimental parameters, preferential growth of both α and β-MoO_3 crystal phases could be achieved by manipulating the applied potential limits and sweep rates under which the depositions were carried out.
- The author investigated the EC performance of both phases of MoO_3 and found that the films' adhesion to the substrate were poor so that the films did not remain intact during the EC measurements.
- The author further assessed the gasochromic performance of both phases of MoO_3 and found that the intrinsically stratified α-MoO_3 performed better than the β-MoO_3 due to the stratified structure and the possibility of direction passage of the free charges in α-MoO_3.

Stage 2

- In this stage, the author developed EC devices with a binary system of TMOs with complimentary properties. The author electrodeposited α-MoO_3 coating over anodized ordered TiO_2 nanotube arrays. This binary system of MoO_3 interface with TiO_2 template overcame the adhesion issue experienced by bare electrodeposited MoO_3 in stage 1 and the performance of bare TiO_2 devices.
- Highly ordered TiO_2 nanotube arrays of 1 μm thickness with 70 and 95 nm inner and outer diameters, respectively, were synthesised on FTO substrates employing the anodization method. The author demonstrated uniform α-MoO_3 coatings from 5 to 15 nm on the TNT platform by employing a facile electrodeposition technique. It was found that the coating was the α-phase of MoO_3 which deposited parallel to the surface of the highly ordered TiO2 nanotubular platform in a highly homogenous manner.
- UV-Vis and EC measurements of these coated films demonstrated a reduction in the bandgap and shifting of the band edges of the overall system which resulted in

superior charge transfer performance. The author found that these alterations gave rise to significant improvements in the electrochromic properties of the MoO_3 coated TiO_2 nanotubular platform in comparison to bare TiO_2 platform in terms of both optical density and repeatability.

Stage 3

- In this stage, the author developed EC devices using anodized ordered nanoporuos Nb_2O_5 and demonstrated the highest obtained CE value at the time. The author showed that the ordered nanostructure greatly enhanced the EC performance by the devices in comparison to random aligned nanostructures or bulk material. However the relatively large bandgap inherited by Nb_2O_5 existed as a hurdle to higher performance EC devices by not allowing operation at relatively low applied voltages.
- The author synthesized compact three dimensional (3D) Nb_2O_5 nanoporous networks with thicknesses of 500 nm, 750 nm and 1 µm by employing a combination of RF sputtering and electrochemical anodization methods. It was revealed that the as-synthesized Nb_2O_5 films, obtained in 0.1 M $LiClO_4$ electrolyte at low applied potentials, exhibited extraordinary EC performances.
- The author found that the compact 3D nanoporous networks with high active surface areas demonstrated an excellent coloration efficiency (500 nm thick sample achieved 47.0 $cm^2\ C^{-1}$ at 550 nm) that exceeded any previously reported Nb_2O_5 EC system. The author demonstrated that coupling these merits with high bleached state transparency, large optical modulation, and consistent cyclic stability make Nb_2O_5 a suitable choice for EC devices.
- The author hypothesis a combination of Nb_2O_5 with low bandgap EC materials such as MoO_3 or WO_3 would potentially improve its EC performance and efficiency, which were presented in stage 4.

Stage 4

- In this final stage, the author continued fabrication of binary TMO EC devices based on α-MoO_3 and Nb_2O_5. It was observed that the coating of the relatively low bandgap MoO_3 brought the overall system's bandgap to values closer to that of MoO_3, which overcame the bandgap limitations experienced by the bare Nb_2O_5 template in stage 3. As a result, the binary device with complimentary TMOs incorporating Nb_2O_5 demonstrated comparative EC performance to the best WO_3 based EC devices.
- The author synthesized highly ordered Nb_2O_5 nano-channelled films of 500 nm thickness on FTO substrates by using a combination of RF sputtering and electrochemical anodization methods. He demonstrated the formation of homogeneous α-MoO_3 coatings on the Nb_2O_5 platform using a facile electrodeposition technique.
- It was found that the α-MoO_3 coating augmented Nb_2O_5 film demonstrated significant improvements in EC performance in comparison to both MoO_3 or Nb_2O_5 in terms of low voltage applications and coloration efficiency (20 cycle coating at 550 nm optical wavelength achieved 149.0 $cm^2\ C^{-1}$, which is higher than any MoO_3 or Nb_2O_5 device previously reported) These results indicate that coating of Nb_2O_5 nano-channels with MoO_3 offers a viable method for the fabrication of efficient EC devices.

  In conclusion, this PhD research project has successfully improved and overcame the performance limitations of the some of the known nanostructured chromic materials that were formed using electronic driven methods. By using the binary systems he created EC devices with performance comparative with the best EC material. As such the outcomes of this PhD research added significant values to the body of knowledge of the field of EC materials and as a result published in

prestigious peer reviewed scientific journals. A complete list of publications by the author since the beginning of this PhD research project, is as follows:

Journal publications:

- Yao, D. D.; Ou, J. Z.; Latham, K.; Zhuiykov, S.; O'Mullane, A. P.; Kalantar-zadeh, K., "Electrodeposited α- and β-Phase MoO_3 Films and Investigation of Their Gasochromic Properties*." Crystal Growth & Design* 4, 1865 (2012).
- Yao, D. D.; Field, M. R.; O'Mullane, A.P.; Kalantar-zadeh, K.; Ou, J.Z., "Electrochromic properties of TiO_2 nanotubes coated with electrodeposited MoO_3*." Nanoscale* (2013).
- Yao, D. D.; Rani, R. A.; O'Mullane, A. P.; Kalantar-zadeh, K.; Ou, J. Z., "High Performance Electrochromic Devices Based on Anodized Nanoporous Nb2o5." *The Journal of Physical Chemistry C* 118, 476 (2013).
- Yao, D. D.; Rani, R. A.; O'Mullane, A. P.; Kalantar-zadeh, K.; Ou, J. Z., "Enhanced Coloration Efficiency for Electrochromic Devices based on Anodized Nb_2O_5 / Electrodeposited MoO_3 Binary Systems," *The Journal of Physical Chemistry C* (under review).
- Zheng, H. D.; Sadek, A. Z.; Breedon, M.; Yao, D. D.; Latham, K.; du Plessis, J.; Kalantar-zadeh, K., "Fast formation of thick and transparent titania nanotubular films from sputtered Ti*." Electrochemistry Communications* 12, 1308 (2009).
- Ou, J. Z.; Campbell, J. L.; Yao, D. D.; Wlodarski, W.; Kalantar-zadeh, K., "In Situ Raman spectroscopy of H_2 gas interaction with layered MoO3.' *American Chemical Society* 115, 10757 (2011)
- Walia, S.; Weber, R.; Balendhran, S.; Yao, D. D.; Abrahamson, J.T.; Zhuiykov, S.; Bhaskaran, M.; Sriram, S.; Strano, M.S. and Kalantar-zadeh, K.; "ZnO based thermopower wave sources," *Chemical Communications* 48, 7462 (2012).

- Walia, S.; Balendhran, S.; Yi, P.; Yao, D. D.; Zhuiykov, S.; Pannirselvam, M.; Weber, R.; Strano, M. S.; Bhaskaran, M.; Sriram S.; and Kalantar-zadeh, K.; "MnO_2 in thermopower wave sources with exceptionally large output voltages," *Journal of Physical Chemistry C 117,* 9137 (2013).
- Wang, YC.; Ou, JZ.; Balendhran, S.; Chrimes, AF.; Mortazavi, M.; Yao, DD.; Field, MR.; Latham, K.; Bansal, V.; Friend, JR.; Zhuiykov, S.; Medhekar, NV.; Strano, MS.; and Kalantar-zadeh, K.; "Electrochemical Control of Photoluminescence in Two-Dimensional MoS2 Nanoflakes," *ACS Nano 7,* 10083-10092 (2013).
- Zhang, W.; Ou, JZ.; Tang, SY.; Sivan, V. Yao, DD.; Latham, K.; Khoshmanesh, K.; Mitchell, A.; O'Mullane, AP and Kalantar-zadeh K.; "Liquid Metal/Metal Oxide Frameworks," *Advanced Function Materials, DOI*.

Recommendations for future works

Significant advancement in the field of EC materials have been achieved during the course of this PhD project, however the author feels that there still exists many opportunities for continuing research in alignment with those presented in this thesis, and recommends the following as future works:

- The binary systems of complimentary TMOs require further investigation into the theory and practice of chromic materials, their selection and fabrication. This includes optimised TMO thicknesses and their morphologies as well as their crystalline structures. Improving charge carrier transfer between different TMO within the system and interconnecting structures are other issues that should be addressed.
- The author showed that the coating of anodized TiO_2 and Nb_2O_5 templates with thin layers of α-MoO_3 offered a viable method for the fabrication of efficient EC devices. Other molybdenum oxide compounds such as MoO_2 can also exhibit

potentials as complimentary material for nanoscale coatings and should be investigated.

- It is possible to expand the binary system to other TMOs as well as systems with more than two TMOs. Such binary and multiple TMO systems can be employed to combine the merits and potentially enhance the EC performance even further.
- Existing chromic devices are restricted by their colour schemes, and although Nb_2O_5 have shown to exist in multiple colours, however the majority of the chromic devices are only able to exist in a bleach and coloured state transition. Such multi coloured systems should be investigated.
- Investigations into the intercalation of ions and charge carrier transfer stimulus in layered TMOs should be extended to understand and exploit their numerous possibilities.